1969

Optical radar observations of the stratosphere and mesosphere

Douglas Parker Woodman
College of William & Mary - Arts & Sciences

69-22,082

WOODMAN, Douglas Parker, 1942-
OPTICAL RADAR OBSERVATIONS OF THE STRATOSPHERE AND MESOSPHERE.

The College of William and Mary in Virginia, Ph.D., 1969
Physics, general

University Microfilms, Inc., Ann Arbor, Michigan

OPTICAL RADAR OBSERVATIONS OF THE STRATOSPHERE AND MESOSPHERE

A Dissertation

Presented to

The Faculty of the Department of Physics

The College of William and Mary in Virginia

In Partial Fulfillment

of the Requirements for the Degree of

Doctor of Philosophy

By

Douglas P. Woodman

1969

APPROVAL SHEET

This dissertation is submitted in partial fulfillment of

the requirements for the degree of

Doctor of Philosophy

Douglas Parker Woodman

Douglas Parker Woodman

Approved, May 1969

James D. Lawrence, Jr.

Rolf G. Winter

Frederic R. Crownfield, Jr.

Kenneth F. Bick

Roy L. Champion

Lynn D. Doverspike

Arden Sher

ACKNOWLEDGEMENTS

I wish to express my appreciation to Dr. James D. Lawrence, Jr., who initially suggested this research, for his guidance and support over the last five years. I am also indebted to Dr. Frederic R. Crownfield, Jr. for assuming the duties of principal investigator of the research grant in 1967 and for his helpful suggestions.

Without the assistance and cooperation of the personnel of NASA, Wallops Island, Va., this experiment would not have been possible. I am grateful to Mr. Bob Carr for allowing me to use the NASA facilities and to Mr. Jack Hartman for his assistance in matters pertaining to the RT-2 research telescope.

I also thank Mr. Torrey Froscher and Mr. Thomas Morgan for their invaluable assistance in conducting the experiment during the summer of 1968.

The constant cooperation and expert craftsmanship of the machine shop personnel contributed significantly to the success of this experiment. Thanks are extended to Mr. Stanley Hummel and the William and Mary Machine Shop staff.

I wish to thank Drs. Kenneth F. Bick, Roy L. Champion, Frederic R. Crownfield, Jr., Lynn D. Doverspike, James D. Lawrence, Jr., Arden Sher and Rolf G. Winter for their helpful criticism of this manuscript.

Finally, I wish to thank my wife, Susan, for her patience and encouragement and for typing this thesis.

This work has been supported by NASA Grant NGR-47-006-011.

ABSTRACT

A sensitive optical radar system developed at the College of William and Mary is described, and measurements of the molecular and particulate content of the atmosphere made at Wallops Island, Virginia are presented. The backscattered signal from vertically directed laser pulses has been measured using both analog and digital photomultiplier current measurements. These measurements have permitted a calculation of the relative volume backscatter cross section of the atmosphere at altitudes from 10 km to 80 km on September 15/16, 1968. The data has been fitted to a curve based on the U. S. Standard Atmosphere Supplements, 1966, which represents the scattering from a pure molecular atmosphere. Data points which fall appreciably above the molecular scattering curve are interpreted as evidence of aerosol or particulate scattering. The excellent fit of the data to a molecular scattering curve in the 30 - 55 km region suggests that the scattering is predominantly molecular in this region. By assuming that molecular scattering is dominant at 50 km, estimates of the volume backscatter cross section of scattering layers in the 70 - 80 km region have been made. No statistically significant deviations from the average background count were observed during the time interval corresponding to the altitude range of 80 - 180 km.

Measurements of backscatter from meteorological phenomena are presented, including cirrus cloud records and an aerosol scattering feature at 6 km. Effective filtering of scattered sunlight has per-

mitted operation of the optical radar system under daytime sky background conditions. Measurements of backscatter from cirrostratus clouds obtained 2:00 p.m. on May 8, 1968 are included.

Douglas Parker Woodman,

Department of Physics,

The College of William and Mary in Virginia

TABLE OF CONTENTS

LIST OF FIGURES

OPTICAL RADAR OBSERVATIONS OF THE STRATOSPHERE AND MESOSPHERE

I. INTRODUCTION

The least explored region of the earth's atmosphere lies between 50 and 150 km. Complex physical processes exist at these altitudes, and our understanding of the physics of this region of the atmosphere is far from complete. Some of the phenomena common to this region such as noctilucent clouds, auroras and meteors are visible to the unaided eye. It is also well known that the upper atmosphere contains dust layers, a sodium layer and regions of ionization.

Aerosol particles, although relatively few in number, play an important role in atmospheric processes. Cloud formation and smog are often a direct result of the presence of aerosols. It has been suggested that meteoric debris may be responsible for noctilucent clouds and the sodium layer (Gadsden, 1966). Bowen (1953) has reported a correlation between periods of high meteoric activity and world rainfall. Particles are also important constituents in determining the radiation balance of the atmosphere, and Volz and Goody (1962) suggest that they may be important as catalysts in recombination processes, affecting both the chemical and electrical properties of the upper atmosphere. Measurement of the vertical distribution of aerosols has permitted estimates to be made of the eddy diffusion coefficient in the 20 - 25 km region (Newkirk and Eddy, 1964) and the rate of accretion of extra-terrestrial material by the earth (Newkirk and Eddy, 1964; Dubin and McCracken, 1962; Dubin,1960; LaGow and Alexander, 1960; Whipple, 1961; Rosen, 1965).

Both direct sampling and remote sensing techniques have been used to study the particulate content of the atmosphere. Satellites have been effective in providing measurements above 150 km, and the lower atmosphere can be investigated using instruments carried by balloons and small meteorological rockets. The intermediate region can be probed by larger and more expensive research rockets, but data collection is limited by cost and lack of suitable measuring techniques. Rocket probe and satellite measurements have established the average cumulative mass distribution for dust particles in the vicinity of the earth (Alexander et al., 1963), and samples of meteoric debris have been recovered and analyzed (Soberman, 1965; Greenman and Gilpin, 1965). Although detectors are available for particles with masses as small as 10^{-13}g, the bulk of the rocket data includes only particles with masses greater than 10^{-9}g. With exception of Mikirov's work (1963), the rocket measurements have yielded very little data on the vertical distribution of dust. Mikirov's work was unique in that he measured sky brightness with a rocket-borne photometer, and was in effect sampling a large number of scatterers. Mikirov measured sky brightness in two spectral regions as a function of altitude from 70 - 450 km and found that the sky brightness above 100 km was dominated aerosol scattering.

Indirect light scattering methods have many advantages over direct sampling techniques, but supporting information is often needed to make definitive measurements because scattering is dependent on the particle concentration, size, index of refraction, and shape. Among the pre-laser methods which have provided information about the concentration and size

distribution of the particulate matter in the atmosphere are measurements of the twilight sky, balloon-borne coronograph measurements of scattered solar radiation and searchlight probe experiments. E. K. Bigg (1956) interpreted discontinuities in the scattered sunlight during twilight in terms of the interaction of the edge of the earth's shadow with regions of dust particles in the atmosphere. Subsequent experiments by other investigators have yielded more quantitative information on the aerosol content of the stratosphere. Volz and Goody (1962) measured the twilight intensity at 20° elevation and obtained turbidity profiles to a height of 65 km. They observed a maximum in the scattering profile near 20 km, and found that the dust mixing ratio above 30 km was constant at 25 percent of the 15 km value. Newkirk and Eddy (1964) measured the spectral distribution of skylight from 0.37 μ to 0.79 μ at a scattering angle of 2°4' and the angular distribution at $\lambda = 0.44$ μ from 1°7' to 58° using a balloon-borne coronograph. They also found a broad maximum in particle concentration at 20 km and observed evidence of very thin laminae of scattering particles in the stratosphere. Newkirk and Eddy concluded that Volz and Goody's estimate of the overall atmosphere turbidity above 25 km is about 10 times too large. G. V. Rosenberg (1960) carried out both twilight and searchlight experiments, concluding that aerosols are chiefly responsible for the scattering of light at all altitudes to 80 or 90 km. This view conflicts with that of L. Elterman (1954, 1964, 1966) who found that aerosol attenuation above 35 km in the stratosphere is sufficiently small that it can be neglected. N. B. Davari (1964) has reported, on the basis of twilight sky measure-

ments, that the ratio of the brightness of the aerosol component to the brightness of the molecular component is constant from 40 - 70 km and close to unity. Thus, it is evident that there is substantial disagreement among investigators using different techniques concerning the extent of aerosol scattering in the 30 - 70 km region. The twilight measurements of Volz and Goody, Davari, and Rosenberg indicate a higher turbidity of the 40 - 70 km region than the searchlight methods of Elterman and the coronograph experiments of Newkirk and Eddy. It is generally recognized that the analysis of twilight data requires assumptions which are difficult to justify. There appears to be considerable uncertainty in the method of dealing with the effect of clouds at the sunset point, and multiple scattering effects have not been treated at all. The searchlight and coronograph experiments, which are amenable to relatively straightforward analyses, probably yield more accurate results than the twilight experiments.

As a result of the development of lasers which are capable of emitting short (of the order of 10^{-8} sec) pulses of highly collimated, nearly monochromatic radiation, a new method of remotely sensing the molecular and aerosol content of the atmosphere has become feasible. The scattering properties of the atmosphere can be observed by measuring the radiation backscattered from a laser pulse as it passes through the atmosphere. The systems which generate the transmitted laser pulse and measure the backscattered radiation are called optical radar systems.

The purpose of the present investigation was to develop a high

sensitivity optical radar system and measure the relative volume backscatter cross section of the atmosphere over the range of 10 - 80 km. It was anticipated that the results of the experiment would help to determine the importance of aerosol scattering in the stratosphere and mesosphere.

Optical radar systems can be considered an outgrowth of the searchlight probe technique which was first suggested by Synge (1930). L. Elterman developed the technique using a searchlight transmitter and a searchlight receiver separated by 30 km. The transmitter consisted of a 36 inch searchlight fitted with a modulated shutter and a high intensity lamp at its focal point. The receiver was a searchlight with a photomultiplier at its focal point. Profiles of the atmospheric scattering were obtained by causing the receiver field of view to intersect the transmitter beam and then scanning up the searchlight beam. In 1956 Friedland, Katzenstein and Zatzick described a pulsed searchlight system operated from a single site (the transmitter and receiver were actually separated by 0.5 km). The elapsed time between the transmitted and received signal was used for altitude determination instead of the triangulation method used with previous systems. Friedland's work demonstrated the feasibility of an optical radar system, but the technique was not fully developed because of the lack of a suitable light source.

With the advent of the ruby laser, a realization of the inherent advantages of a pulsed system became possible. The high energy, monochromaticity, and narrow beam divergence of the laser permits very

effective discrimination against sky background noise. The first results using the optical radar techniques were reported by Fiocco and Smullin (1963); they reported the detection of aerosol layers at heights up to 140 km, but several investigators have questioned the existence of these layers because of unsatisfactory features in the published data. Sandford (1967) concluded, "It is thus felt that there is no reliable optical radar evidence for aerosol scattering above 90 km." Other workers include McCormick et al. (1966), Collis and Ligda (1966), Bain and Sandford (1966, 1966a) and Kent, Clemesha and Wright (1967, 1967a). Bain and Sandford measured a scattering enhancement at 71 km equal to 2.5 times the expected molecular scattering. P. D. McCormick et al. (1966) detected a scattering layer near 80 km. Kent, Clemesha and Wright (1967), however, found no appreciable scattering enhancements in the 40 - 90 km region. On April 1, 1968 the relative volume backscatter cross section of the atmosphere was measured with the William and Mary optical radar system over the range of 30 - 55 km, and no scattering layers were observed. On September 16, 1968 measurements over the range of 30 - 80 km revealed scattering layers near 71 km and 76 km.

Fiocco and Smullin's optical radar was also used to probe the atmosphere below 30 km. During 1964 and 1965, Fiocco and Grams studied the temporal characteristics of the "20 km layer." The presence of this layer of particulate matter in the lower stratosphere was deduced by Gruner and Kleinert (1927) and has been verified by both direct particle sampling and indirect light scattering experiments. Extensive

measurements using various techniques have shown this layer to be a worldwide feature of the stratosphere. The work of Fiocco and Grams (1967), and Rosen (1964, 1966, 1967) indicates that the total dust associated with the "20 km layer" may be decreasing. G. G. Goyer and R. D. Watson (1968) have compared their measurements of the scattering ratio (observed backscatter cross section/molecular backscatter cross section) of the layer with those of Fiocco and Grams (1967), Clemesha, et al. (1966) and Elterman (1964). Measurements of the scattering ratio of the "20 km layer" made with the William and Mary optical radar agree approximately with the results of other workers, but accurate comparisons of the existing data cannot be made because the differences must be attributed in part to the temporal fluctuations of the layer.

II. THEORETICAL SECTION

A. Scattering Theory

Radiation passing through the atmosphere is attenuated by scattering and absorption by molecules and particles. In this paper, aerosols are defined as particles of terrestrial, extraterrestrial, or atmospheric origin suspended in the gaseous medium. These aerosols range in size from approximately 0.01 μ to 20 μ. Aerosols smaller than 0.01 μ coalesce rapidly with other particles (Twomey and Severynse, 1964), and those larger than 20 μ are removed by gravitational settling. Mie theory, which describes the scattering by spherical particles of any size, has been applied to aerosol scattering. In applying the Mie theory, it is assumed that the scattering pattern caused by reflection from a large number of randomly oriented particles is identical with the scattering pattern produced by a group of spheres of equivalent size (Van de Hulst, 1957). The value $n = 1.50$ has been used by many investigators as the mean refractive index of atmospheric aerosols, but it is likely that a small imaginary part should be added. Molecular absorption can be neglected when the ruby laser is temperature controlled to prevent a shift of the laser wavelength into the water vapor absorption line at 6943.8Å.

The characteristics of the atmosphere and the optical radar system permit simplification of the scattering problem. The scattering theory which is applicable to atmospheric optics problems may be classified as independent scattering. Because of the random positions of scatterers

in a gas, the scattered intensities are added without regard to phase. In addition, the optical depth of the atmosphere permits the analysis of optical radar backscatter on the basis of single scattering under most conditions. Exceptions include dense cloud scattering and backscatter from extremely high altitudes (>100 km). The following discussion is also restricted to scattering in which the frequency of the incident light is preserved.

If the differential scattering cross section for an individual scatterer is $d\sigma(\theta)/d\Omega$ and independent, single scattering assumed, the volume differential scattering cross section is given by

$$\sum N_i \frac{d\sigma_i(\theta)}{d\Omega} \tag{1}$$

where N = number density of scatterers of type i. The fraction of light backscattered into the solid angle ω subtended by the receiver is

$$\int_{\omega} \sum N_i \frac{d\sigma_i(\theta)}{d\Omega} d\Omega = \sum N_i \frac{d\sigma_i(\pi)}{d\Omega} \omega = \sigma\omega \tag{2}$$

where σ = volume backscatter cross section since $\omega < 10^{-7}$ for $z > 2$km. For atmospheric scattering, $\sigma = \sigma_R + \sigma_M$ where σ_R and σ_M are the volume scattering cross sections for molecules and large particles, respectively. The volume scattering coefficient is given by

$$\beta = \int_{\Omega} \sum N_i \frac{d\sigma_i(\theta)}{d\Omega} d\Omega \tag{3}$$

If absorption is neglected, the attenuation of a light beam is described by the equation

$$q(x) = \frac{I}{I_o} = \exp\left[-\int_o^x \beta dx\right] \tag{4}$$

where

$q(x)$ = transmissivity

I = transmitted intensity

I_o = intensity at $x = 0$

The optical depth of the scattering medium is T where

$$T = \int_o^x \beta dx \tag{5}$$

For the scattering geometry shown in Fig. 1, the backscattered power at the receiver is given by

$$P_R = Fq(\sigma_R + \sigma_{Mie})\Delta V\omega \tag{6}$$

where

F = flux incident upon scattering volume

q = transmission factor from ground level to scattering volume

σ_R = volume backscatter cross section for molecules

σ_M = volume backscatter cross section for aerosols

ΔV = scattering volume

ω = solid angle subtended by the detector.

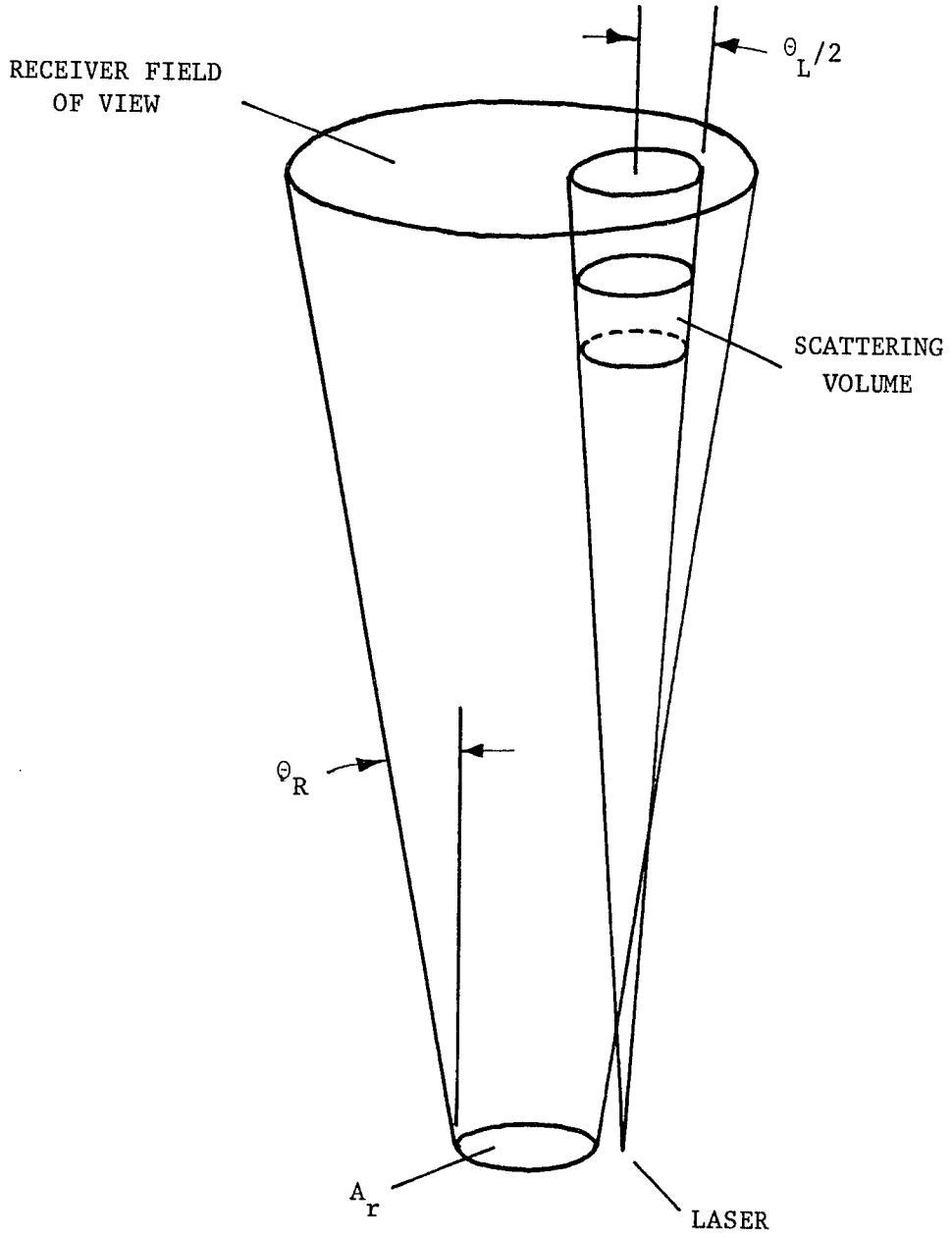

Fig. 1 Scattering geometry of the optical radar system.

The flux incident on the scattering volume is

$$F = \frac{q\bar{P}_L}{\pi/4(z\Theta_L)^2} \tag{7}$$

where

$\bar{P}_L$ = average laser power

Θ_L = laser beam divergence (full angle)

Scattered light will be received simultaneously from a height range $c\gamma/s$, and the scattering volume, therefore, is given by

$$\Delta V = \frac{\pi}{8}(z\Theta_L)^2 c\gamma \tag{8}$$

where γ is the laser pulse duration. Since the laser beam diameter and pulse length are small compared to the altitude, the solid angle subtended by the receiver is given by

$$\omega = \frac{A_r}{z^2} \tag{9}$$

where A_r is the area of the receiver. The power at the receiver is then given by

$$P_R = \frac{q^2 cPtA_r(\sigma_R+\sigma_M)}{2z^2} = \frac{q^2 cEA_r(\sigma_R+\sigma_M)}{2z^2} \tag{10}$$

where E is the laser energy.

In a form which is more convenient for single photoelectron counting data, the photon flux at the receiver is

$$\frac{cN_o A_r q^2 (\sigma_R + \sigma_{Mie})}{2z^2} \quad \text{photons/sec} \tag{11}$$

where N_o is the number of photons per laser pulse. The number of scattered photons counted in time interval τ, where $\tau >> \gamma$, corresponds to the number scattered in a height interval $\Delta z = c\tau/2$. The number of counts received from a height interval between z_1 and z_2 is, therefore,

$$S = \varepsilon N_o A_r q^2 \int_{z_1}^{z_2} \frac{\sigma_R + \sigma_{Mie}}{z^2} \, dz \tag{12}$$

where ε is the receiver efficiency. If $z_2 - z_1$ is small, the integrand of equation (12) may be considered constant over the interval, and the equation can be written

$$S = \frac{\varepsilon N_o A_r q^2 \Delta z (\sigma_R + \sigma_{Mie})}{z^2} \tag{13}$$

1. Rayleigh Scattering

The region of the atmosphere in which a constant ratio of molecular oxygen and nitrogen concentrations is maintained is called the homosphere. Large scale atmospheric circulations produce eddies which keep this region well mixed, preventing diffusive separation of molecular oxygen and nitrogen. Numerous direct measurements and calculations of the atmospheric composition have established that the homosphere extends to at least 85 km (Ratcliffe, 1960). The average polarizability of air is therefore

not a function of altitude below 85 km. Since independent and single scattering are assumed, the volume backscatter cross section of the atmosphere at height z is n(z) times the average backscatter cross section of an atmospheric molecule, where n(z) is the number density of molecules.

The volume backscatter cross section for molecular scattering is

$$\sigma_R = k^4 \bar{\alpha}^2 N_R(z) f \tag{14}$$

where

$k = \frac{2\pi}{\lambda}$ = wave number of incident radiation

$\bar{\alpha}$ = average polarizability of air

$N_R(z)$ = molecular number density

and

$$f = \frac{3(2 + \Delta)}{6 - 7\Delta} \tag{15}$$

The factor f, which accounts for the depolarization caused by anistropy of the molecules, equals 1.054 for atmospheric air (G. de Vaucouleurs, 1951). The expression

$$\bar{\alpha} = \frac{n^2 - 1}{4\pi N} \tag{16}$$

where

n = index of refraction

N = number of scatterers per unit volume

yields a value $\bar{\alpha} = 1.73 \times 10^{-30}$ m^3 for the average polarizability of air. The volume backscatter cross section for scattering of ruby laser light by the aerosol free atmosphere is, therefore,

$$\sigma_R = 2.11 \times 10^{-32} N_R(z) \text{ m}^{-1} \text{ sr}^{-1} \tag{17}$$

2. Mie Scattering

Aerosols ranging in size from 0.1 μ to 10 μ scatter visible radiation effectively and are likely to have appreciable residence times in the atmosphere. The analysis of scattering from these aerosols is complex because the scattered light is composed of light originating from various parts of the particle. For particles with diameters greater than 20 times the wavelength of the incident light, geometrical optics can be applied, and scattered light can be analyzed in terms of the portions resulting from reflection, refraction and diffraction. When the particle size is of the order of the incident wavelength, however, approximation methods cannot be applied, and Mie's theory of scattering of electromagnetic waves from a spherical boundary of arbitrary radius and index of refraction must be used (G. Mie, 1908). The exact solution for the scattered amplitude is an infinite series of products of Bessel functions of the particle radius and refractive index, and Legendre polynomials which are functions of the scattering angle.

The differential scattering cross section for a spherical particle illuminated by a beam of linearly polarized light (Chu and Churchill, 1955) is

$$\frac{d\sigma_M}{dr} = \frac{\lambda^2}{4\pi^2}[i_1(\alpha,n,\Theta)\cos^2\Phi + i_2(\alpha,n,\Theta)\sin^2\Phi] \quad (18)$$

where

n = index of refraction

Θ = scattering angle

α = size parameter ($2\pi r/\lambda$)

$i_{1,2}$ = the Mie intensity function for light polarized parallel and perpendicular to the direction of the electric vector of the incident wave, respectively

Φ = the azimuthal angle between the electric vector of the incident light and the direction of scattering.

The literature contains numerous tabulations of the intensity functions for spherical particles of homogeneous index of refraction (e.g., Penndorf, 1961, 1962; Giese, 1959).

Because the atmospheric aerosol is a highly variable mixture of particles of different size, shape, and index of refraction, it is important to know the effect of these parameters on the scattering. Fig. 2 shows the efficiency factor (scattering cross section/geometrical cross section) versus size parameter α. A maximum occurs at $\alpha = 4$ when $n = 1.5$, and the efficiency factor approaches 2 for large α. The scattering cross section for a large sphere is, therefore, twice the geometrical cross section, an expected result because the incident light is both scattered, in the normal sense, and diffracted by the sphere. Fig. 3 shows the backscatter intensity function [$i(\alpha,1.5,180°)$] over a wide range of sizes for a particle of index of refraction $n = 1.5$.

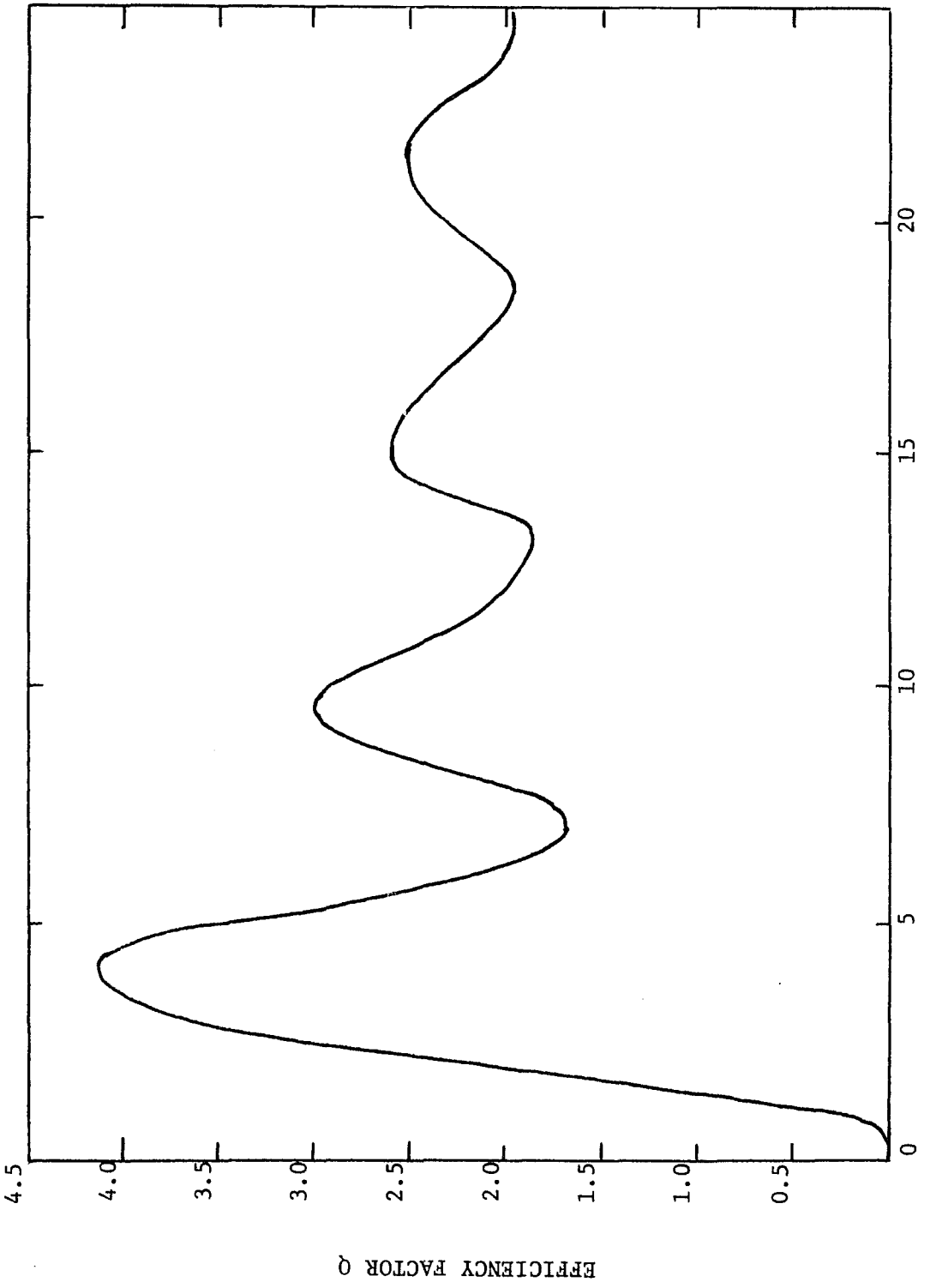

Fig. 2 Efficiency factor versus size parameter for scattering by a spherical particle of index of refraction n = 1.5.

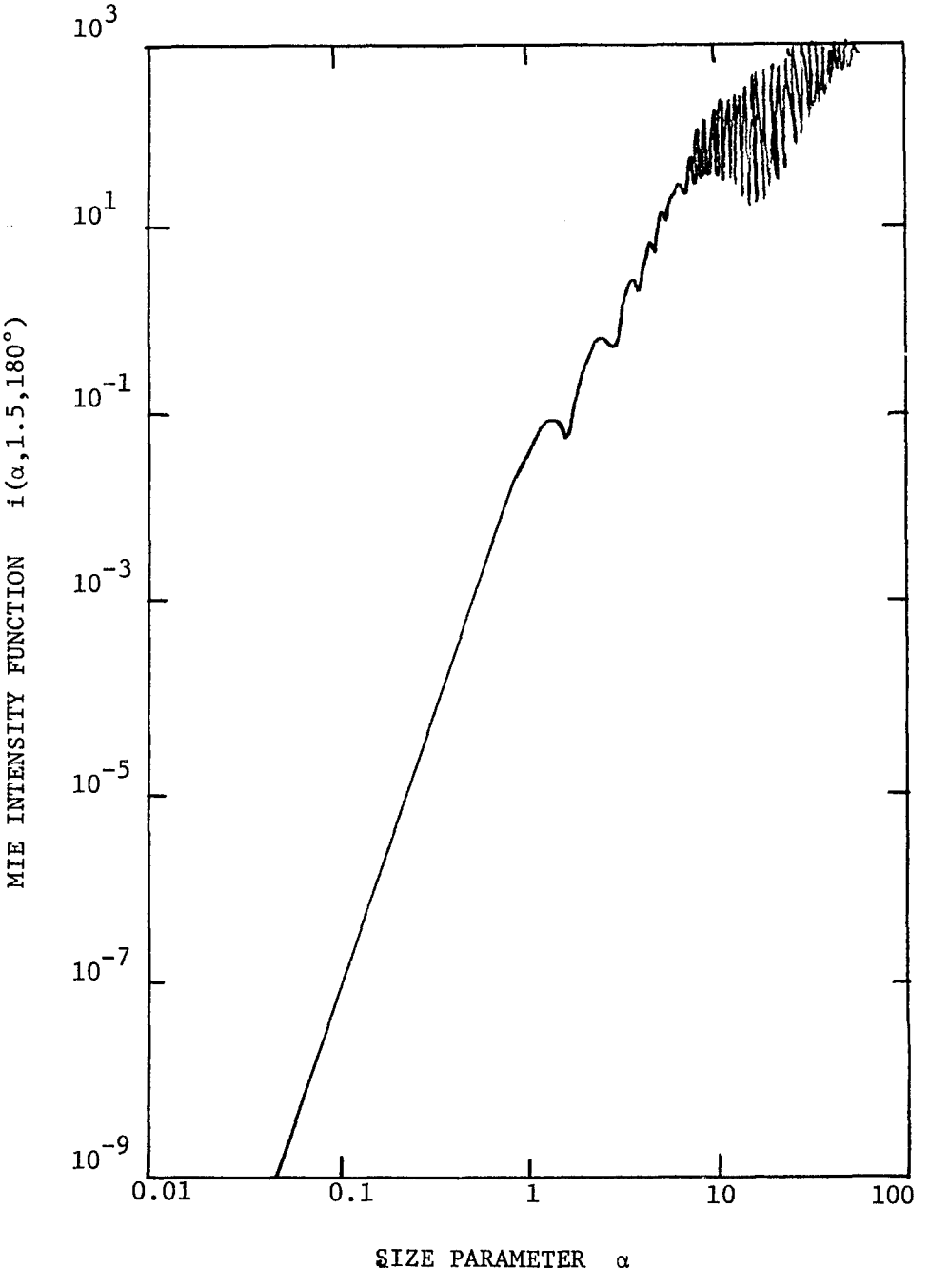

Fig. 3 Mie intensity function i(α,1.5,180°) versus size parameter for backscatter from a spherical particle of index of refraction n = 1.5.

The curve demonstrates the rapid decrease in scattered intensity for small size parameter and the rapid oscillation (represented approximately by the shaded portion of the curve) of the backscattered intensity values that results from interference of reflected and refracted rays for large size parameter.

In the analysis of atmospheric scattering, one is concerned with a polydisperse mixture of aerosols. If the scattering properties of individual particles and the total number density and size distribution of the aerosols are known, the scattering properties of an atmospheric air volume can be determined. Junge (1961) has shown that, on the average, the size distribution of aerosols in the troposphere is described by the equation

$$dN_M(r)/d\log r = Cr^{-\nu} \tag{19}$$

where $dN_M(r)/dr$ is the particle concentration, r is the particle radius, C is a parameter dependent upon the total number of particles. The size distribution parameter ν can range from 2.5 to 4.0 and averages 3 for large (0.1 - 1.0 μ) aerosols near the ground. This size distribution is not applicable near the mesopause because the meteorology of the upper atmosphere differs significantly from that of the troposphere.

The volume differential scattering cross section for Mie scattering is

$$\frac{\lambda^2}{4\pi^2} \sum [i_1(\alpha,n,\Theta)\cos^2\Phi + i_2(\alpha,n,\Theta)\sin^2\Phi]N_M(r) \tag{20}$$

where $N_M(r)$ is the number density of particles of radius r. The volume backscatter cross section is

$$\sigma_M = \frac{\lambda^2}{4\pi^2} \sum i(\alpha,n,180°)N_M(r) \tag{21}$$

where $i \doteq i_1 = i_2$ for $\Theta = 180°$. Equation (19) can be written

$$dN_M(r) = Cr^{-(\nu + 1)}dr \tag{22}$$

For a Junge distribution of particle sizes, equation (21) can be written

$$\sigma_M = C \int_{r_1}^{r_2} \frac{i(\alpha,n,180°)}{\alpha^2 r^{(\nu - 1)}} dr \tag{23}$$

or, changing variables

$$\sigma_M = C\left(\frac{2\pi}{\lambda}\right)^{(\nu - 2)} \int_{\alpha_1}^{\alpha_2} \frac{i(\alpha,n,180°)}{\alpha^{(\nu + 1)}} d\alpha \tag{24}$$

Tables of the average differential backscatter and total cross sections per particle for Junge aerosol distributions may be found in the literature (McCormick, Lawrence and Crownfield, 1968). The calculations were performed for four laser wavelengths and various combinations of size distribution parameter and particle size limits.

The volume backscatter cross section of an atmosphere containing both molecules and aerosol particles may therefore be calculated if ν, α_1, α_2, n, $N_R(z)$ and $N_M(z)$ are known. Equation (17) with $N_R(z)$

given by the U. S. Standard Atmosphere Supplements, 1966 predicts the molecular component of the scattering with sufficient accuracy for measurements of the aerosol content of the atmosphere. Aerosol scattering is highly dependent on ν, α_1, n and $N_M(z)$. These parameters have been measured, but the measurements usually represent an average over a wide range of atmospheric conditions. Long term averages of optical radar data should agree with a model of atmospheric scattering based on published values of ν, α_1, α_2, n, $N_M(z)$, if these parameters actually represent average atmospheric conditions. In analyzing optical radar data accumulated over short time periods, however, one must ask the extent to which published values of ν, α_1, α_2, n, $N_M(r)$ represent atmospheric conditions at the time and location of the optical radar measurements. It is clear that if quantitative measurements of the properties of atmospheric aerosols are to be inferred from optical radar measurements, supporting information such as an independent measurement of ν, α_1 or $N_M(z)$ will be needed.

B. Noise Sources

In this paper the term "noise" refers to any measured signal other than backscattered laser radiation. Noise sources which are important in this experiment exist within, and external to, the receiver electronics. External noise sources are scattered fluorescence and flashlamp radiation, RF noise generated by system electronics, fluctuation of the sky background signal, and Cerenkov light flashes caused by cosmic rays entering the photomultiplier faceplate. The only internal noise source of appreciable magnitude, compared to other noise sources, is the photomultiplier dark current.

The effects of sky background and scattered flashlamp radiation are minimized by using narrow bandpass optical filters. Fluorescence radiation, which is the same wavelength as the laser radiation, and flashlamp radiation are eliminated by a synchronized rotating shutter that closes off the laser cavity after the Q-switched laser pulse is emitted. This shutter is essential when measuring weak signals scattered from high altitudes because near-field scattering of fluorescence radiation, which is emitted by the laser for one to two milliseconds after the emission of the Q-switched pulse, can cause an intolerable background level. At ground level, the background count caused by cosmic rays is negligible compared to other sources. System generated RF noise is controlled by proper shielding and filtering of the detector and the noise source. The external noise sources that cannot be eliminated are, therefore, sky background and statistical noise in

the signal. Finally, the photomultiplier dark count rate, which is caused predominantly by thermionic electrons emitted by the photocathode, can be reduced below the sky background count rate by cooling.

Under most operating conditions, the fluctuation of the sky background is the most troublesome noise source. Stars in the field of view of the telescope and scattered moonlight can increase the sky background by one or two orders of magnitude over that expected from airglow considerations. The sky background level caused by scattered sunlight is 10^4 to 10^6 times the nighttime level.

C. Estimation of Maximum Accessible Altitude Based on a Molecular Scattering Model

The most recent data on seasonal and latitudinal variations of atmospheric molecular number density are tabulated in the U. S. Standard Atmosphere Supplements, 1966. Because the minimum atmosphere scattering is purely molecular, calculations of expected laser backscatter from an atmosphere free from aerosols provide a useful indication of the possible altitudes which can be probed with the optical radar system. Obviously, much higher altitudes would be accessible if dust and other particles, which scatter more effectively than molecules, are present.

The capability of the optical radar system for high altitude backscatter measurements was analyzed in terms of the statistical properties of the received signal and noise. The standard deviation of the number of signal counts is

$$\delta_S = (\delta_{S+B}^2 + \delta_B^2)^{\frac{1}{2}} \tag{25}$$

where

δ_S = standard deviation of the number of signal counts

δ_{S+B} = standard deviation of the total number of counts

δ_B = standard deviation of the number of background counts.

The background count rate is measured independently over a long period of time such that $\delta_B << \delta_{S+B}$. δ_S is, therefore, practically identical with δ_{S+B}. The maximum accessible altitude for molecular backscatter is defined as that altitude at which the signal-to-noise ratio equals 2, or

$$n_S/\delta_S = 2 \quad \text{or} \quad n_S = 2(n_{S+B})^{\frac{1}{2}} \tag{26}$$

where

n_{S+B} = total counts

n_S = number of signal counts.

In a form more useful for treatment of data,

$$2[(C_S + C_B)N\tau]^{\frac{1}{2}} = C_S N\tau \tag{27}$$

where

C_S = backscattered signal counting rate

C_B = background counting rate

N = number of laser shots

τ = counting time bin width.

The signal counting rate versus altitude for a pure molecular atmosphere can be determined from equation (10) where $\sigma_M = 0$. The signal counting rate decreases very rapidly with altitude because of the rapid decrease of the factor σ_R/z^2 in equation (10). The variation of σ_R/z^2 with altitude is shown in Table I.

The photon flux χ caused by airglow in the 6938Å to 6948Å wavelength range and the astronomical contribution is estimated to be 1.2×10^{10} photons m^{-2} sec^{-1} (Broadfoot and Kendall, 1968). The count rate produced by sky background, in the absence of scattered moonlight is then

$$C_B = \chi \Omega_R A_r B q \varepsilon / 4\pi \tag{28}$$

where

Ω_R = receiver solid angle

B = optical filter bandwidth

ε = receiver efficiency.

For the optical radar receiver telescope with $\Omega_R = 2.3 \times 10^{-5}$sr, equation (28) yields a value for C_B of 1240 counts/sec. Using equations (13) and (27), the maximum accessible altitude for molecular backscatter versus number of laser shots has been calculated. The q^2 factor of equation (13) is highly dependent upon the meteorological conditions of the lowest three kilometers of the atmosphere even on "clear," cloudless days. Attenuation by aerosols at 1 km altitude is an order of magnitude larger than the molecular attenuation. It is obvious,

TABLE I VARIATION OF σ_R/z^2 WITH ALTITUDE

Altitude (km)	σ_R/z^2 (m^{-3} sr^{-1})
10	1.70×10^{-15}
30	8.30×10^{-18}
50	1.90×10^{-19}
70	7.50×10^{-21}
90	1.78×10^{-22}

therefore, that the attenuation of a vertically directed laser pulse will vary according to the local meteorological conditions such as aerosol number density and size distribution, index of refraction, humidity, etc. The best available data on the attenuation characteristics of the "clear standard atmosphere" (an atmosphere characterized by molecular, aerosol and ozone attenuation) is contained in "Atmospheric Attenuation Model, 1964, in the Ultraviolet, Visible, and Infrared Regions for Altitudes to 50 km" (Elterman, 1964). The zenith transmission factor for the entire atmosphere predicted by Elterman's model for $\lambda = 0.7\ \mu$ is 0.67. The atmospheric turbidity decreases rapidly with increasing altitude and less than two percent of the total attenuation of the laser pulse occurs above 10 km. In this analysis of stratospheric and mesospheric scattering, therefore, the variation of q^2 with altitude is neglected. Other system parameters are as follows:

Receiver area A_r	$= 0.4556\ m^2$
Counting time bin width τ	$= 11.0\ \mu sec$
Receiver efficiency ε	$= 0.01$
Number of transmitted photons N_o	$= 2.55 \times 10^{18}$
Laser energy E	= 0.73 joule.

Fig. 4 shows the signal counting rate versus altitude for a pure molecular atmosphere, and Fig. 5 shows the maximum accessible altitude for the assumed system parameters including a background level of 1240 counts/sec. The graph indicates that measurements of scattering from

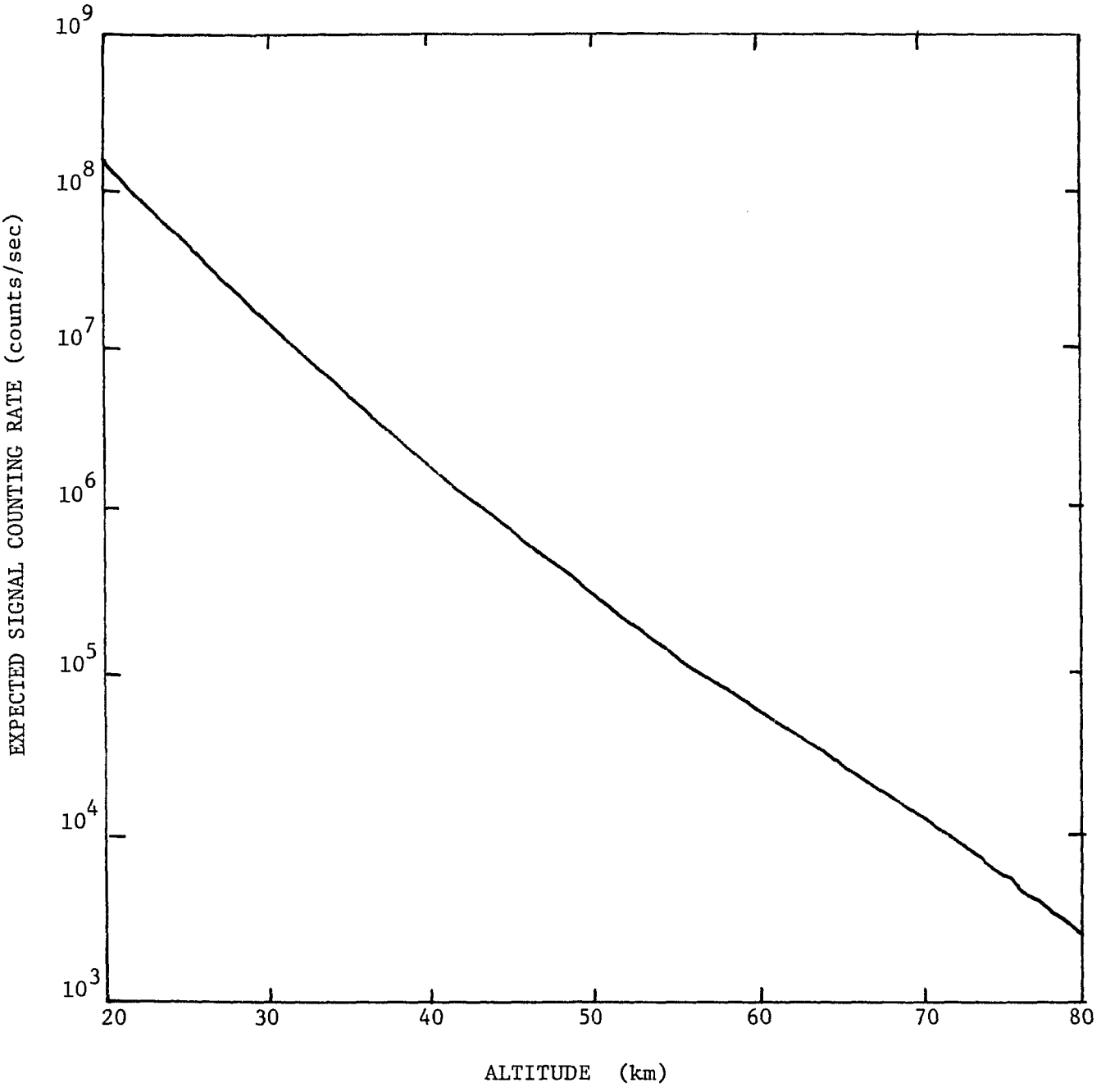

Fig. 4 Expected signal counting rate versus altitude for laser backscatter from an aerosol free atmosphere.

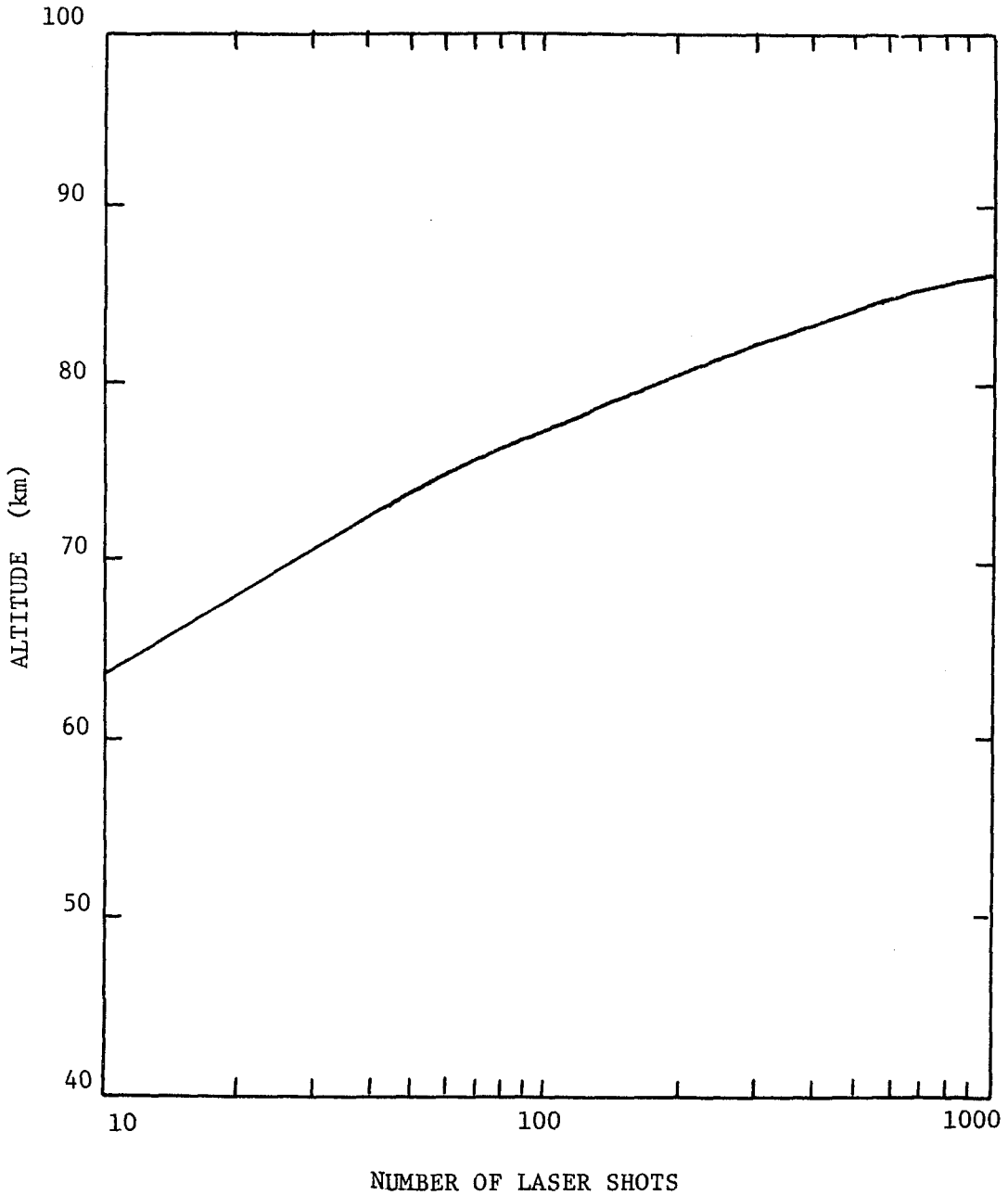

Fig. 5 Maximum accessible altitude for molecular backscatter versus number of laser pulses. The background level $C_B = 1.24 \times 10^3$ counts/sec.

the mesopause should be possible using data accumulated during a single night.

The performance of an optical radar system can be strongly dependent upon the level of background radiation. At night the sky background can be dominated by scattered moonlight, and daytime operation can involve a 10^4 to 10^6 increase of the background power incident on the receiver. Under daytime sky background conditions the counting rate produced by background alone could be 10^8 counts/sec. In order to avoid saturation of the counting circuitry, the power incident on the photomultiplier would have to be attenuated by a factor of 10^3. Under these conditions, the maximum accessible altitude for molecular backscatter versus number of laser shots is shown in Fig. 6.

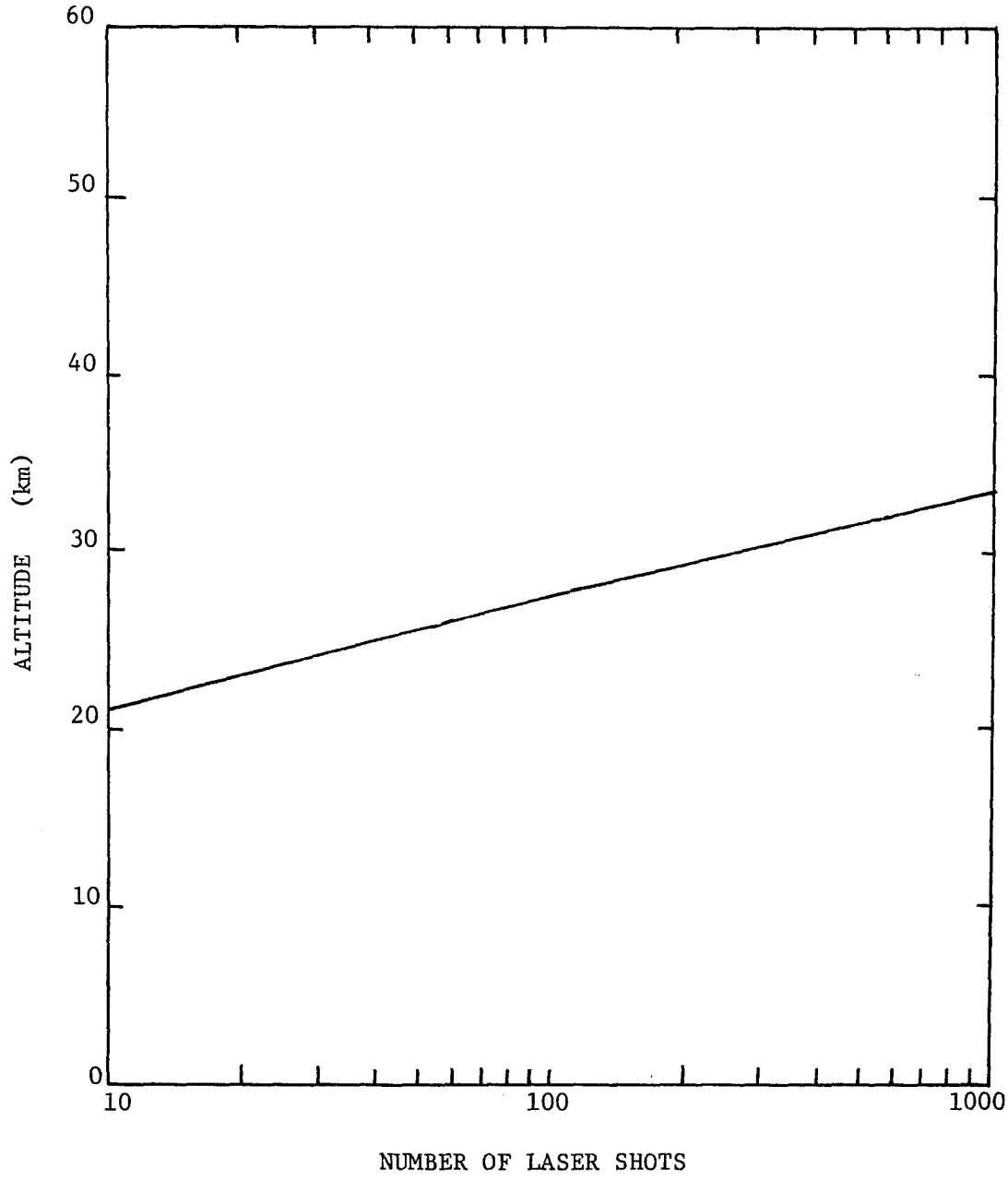

Fig. 6 Maximum accessible altitude for molecular backscatter versus number of laser pulses. The background level $C_B = 10^5$ after attenuation of the received power by 10^3.

III. EXPERIMENTAL EQUIPMENT

The optical radar system consists of a laser transmitter, a receiver and associated electronics equipment. The transmitter utilizes a Korad K-1-QP laser with auxiliary external optics for collimation of the laser beam. The RT-2 telescope at NASA, Wallops Island, has been modified for use as a receiver. The focal plane of the telescope has been fitted with an instrumentation platform which can accomodate electronic and optical equipment for either analog or digital measurement of the backscattered signal. The transmitter is attached to the telescope on a steerable mount with the axis of the laser parallel to the axis of the primary telescope mirror. A photograph of the RT-2 telescope after modification for use as an optical radar system is shown in Fig. 7.

A. Laser Transmitter

A diagram of the laser transmitter, a term which refers to the laser head and associated mechanical and optical equipment, is shown in Fig. 8. Included in the laser transmitter are a laser, a mechanical shutter, an energy monitor, and collimation optics.

1. Laser

The Korad K-1-QP ruby laser, which is the basic element of the laser transmitter, nominally produces one joule, 20 nsec pulses, at a rate of one pulse per minute. A Pockel's Cell Q-switch assures single pulses and

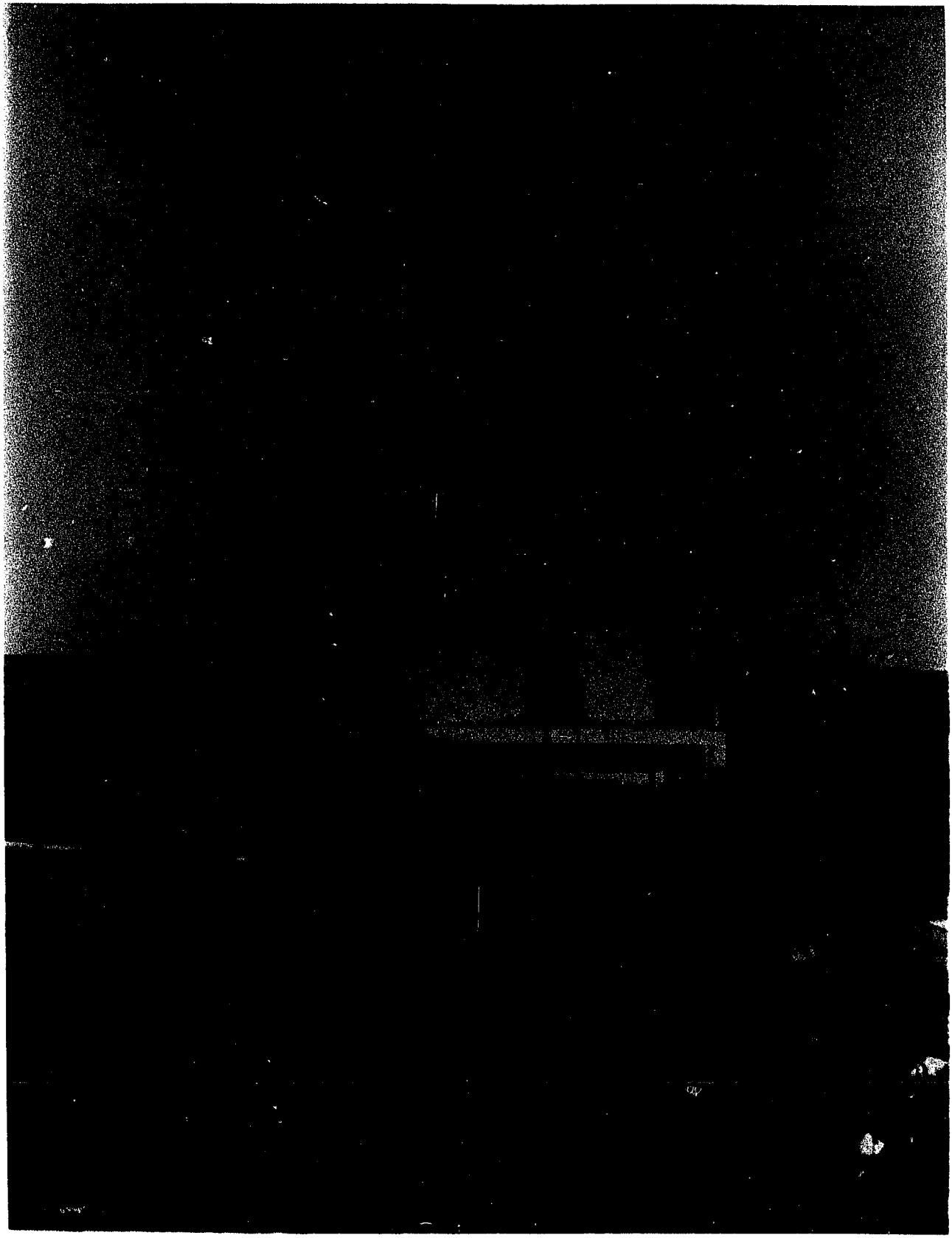

Fig. 7 The RT-2 telescope at NASA, Wallops Island after modification for use as an optical radar.

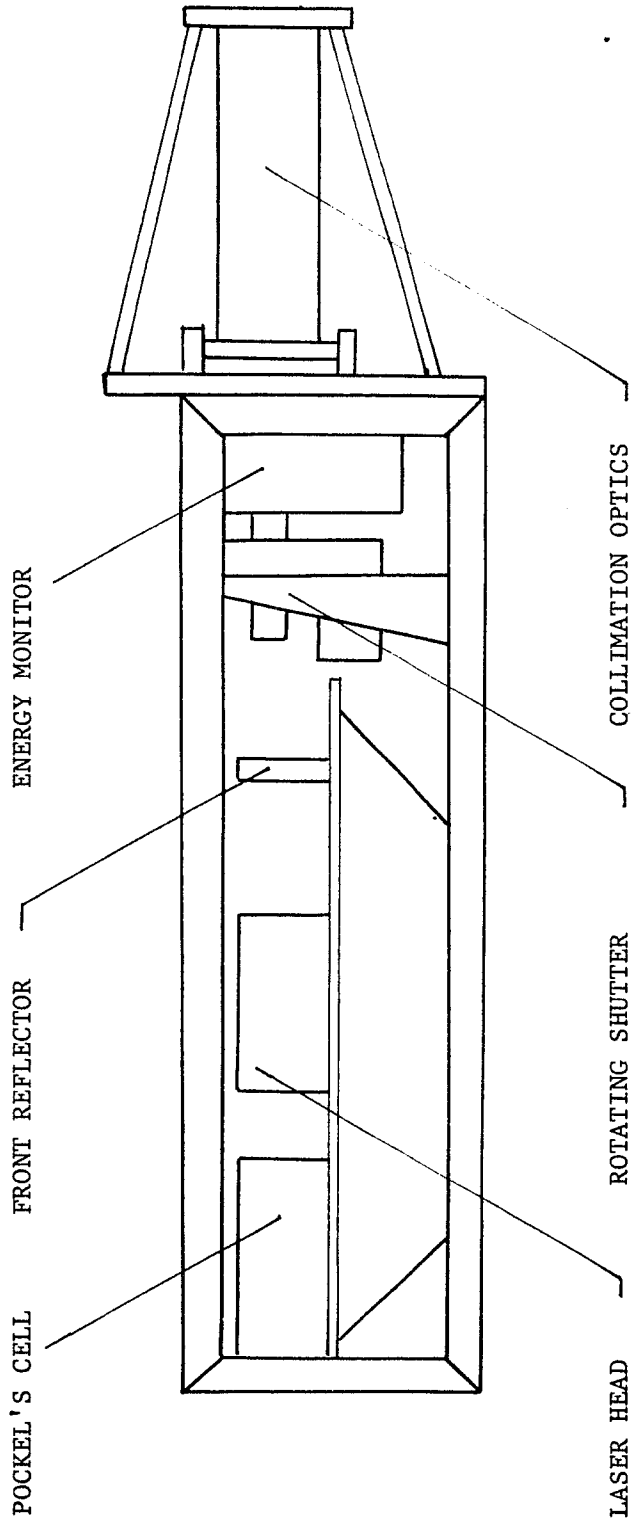

Fig. 8 Components of the laser transmitter

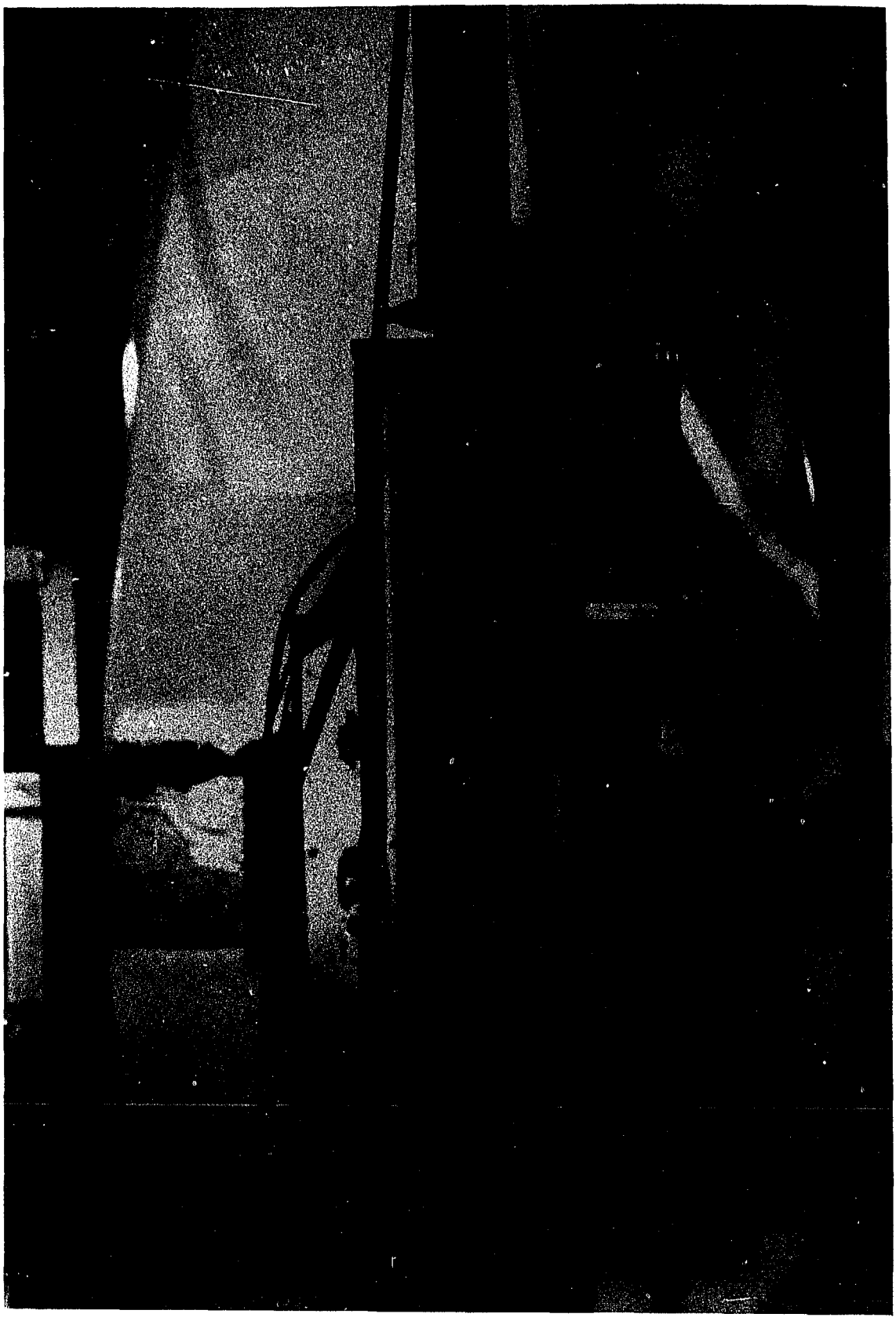

Fig. 9 Photograph off the laser transmitter mounted on the telescope. The top cover is removed.

provides accurate laser pulse timing with respect to the mechanical shutters. The 4 inch by 9/16 inch laser rod was selected to meet a low beam divergence specification of 2.8 mr (half angle, half power).

During the course of the experiment, the laser transmitter was operated over a wide range of ambient temperatures. To prevent a shift of the laser wavelength into a region of water vapor absorption, the temperature of the laser head is maintained at 70° ± 0.5° F. Dry nitrogen was piped across the front and rear surfaces of the ruby rod during warm humid conditions to prevent condensation of moisture on the optical surfaces.

2. Fluorescence Shutter

For a period of one to two milliseconds after the emission of the Q-switched pulse, the laser emits fluorescence and flashlamp radiation. When measuring mesospheric backscatter, near field scattering of this radiation into the receiver can cause a high background level and seriously reduce the sensitivity of the system. At times corresponding to altitudes above 30 km, the flashlamp and fluorescence radiation is prevented from leaving the transmitter housing by a synchronized rotating shutter which completely closes off the laser cavity in less than 180 μsec after the emission of the Q-switched pulse. The aluminum rotor of the shutter is driven at 13,200 rpm and timed so that the laser fires through one of two diametrically opposed holes. Synchronization of the shutter is accomplished by triggering the laser with a delayed pulse derived from the shutter. The timing pulse is generated by an electromagnetic pickup which senses the rotation of a set screw in the rotor drive pulley.

3. Energy Monitor

After emerging from the shutter, the laser pulse then passes through a Lear Siegler energy monitor. A beam splitter in this device directs 7 percent of the beam towards a calibrated SD-100 photodiode. The energy of each pulse is recorded, and the laser pulse shape and peak power are checked periodically.

4. Laser Beam Collimator

The final element of the laser transmitter is the laser beam collimator. The positive and negative lens system closely resembles the configuration of a Galilean telescope; the lenses, however, are not achromats. A computer ray trace program was written and used to determine the proper lens shapes for minimum spherical aberration of the two-element lens system (other aberrations can be neglected in this application). The results of the spherical aberration calculations for the corrected lens system at λ = 6943Å are shown in Fig. 11. The collimator has a magnification of 5:1 and will reduce the laser beam divergence to approximately 0.5 mr (1/2 angle, 1/2 power). The lenses were fabricated from Suprasil I grade quartz because of its high purity and low coefficient of expansion. All lens surfaces were coated for minimum reflection at 6943Å (less than 0.1%).

All of the components of the laser transmitter are mounted in a light-proof enclosure. Since flashlamp and fluorescence light can escape only along the laser beam axis, the shutter ensures the elimination of spurious light from the laser.

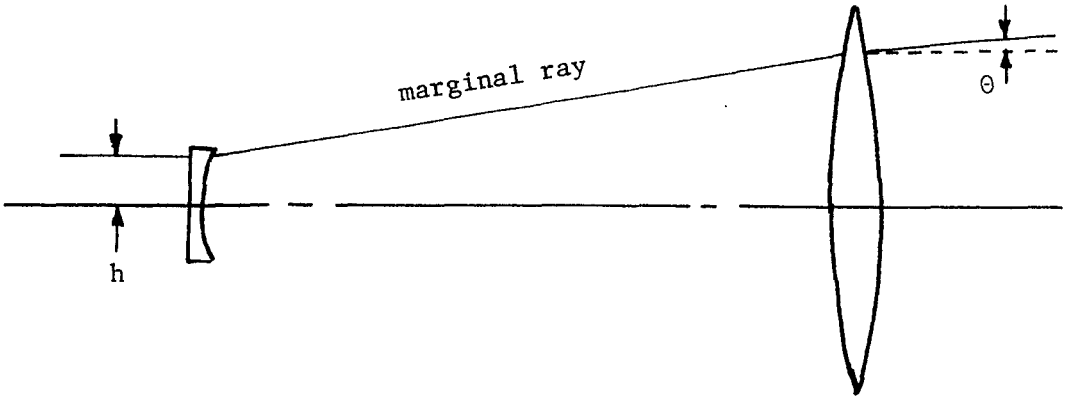

Fig. 10 Ray trace geometry for spherical aberration computer program.

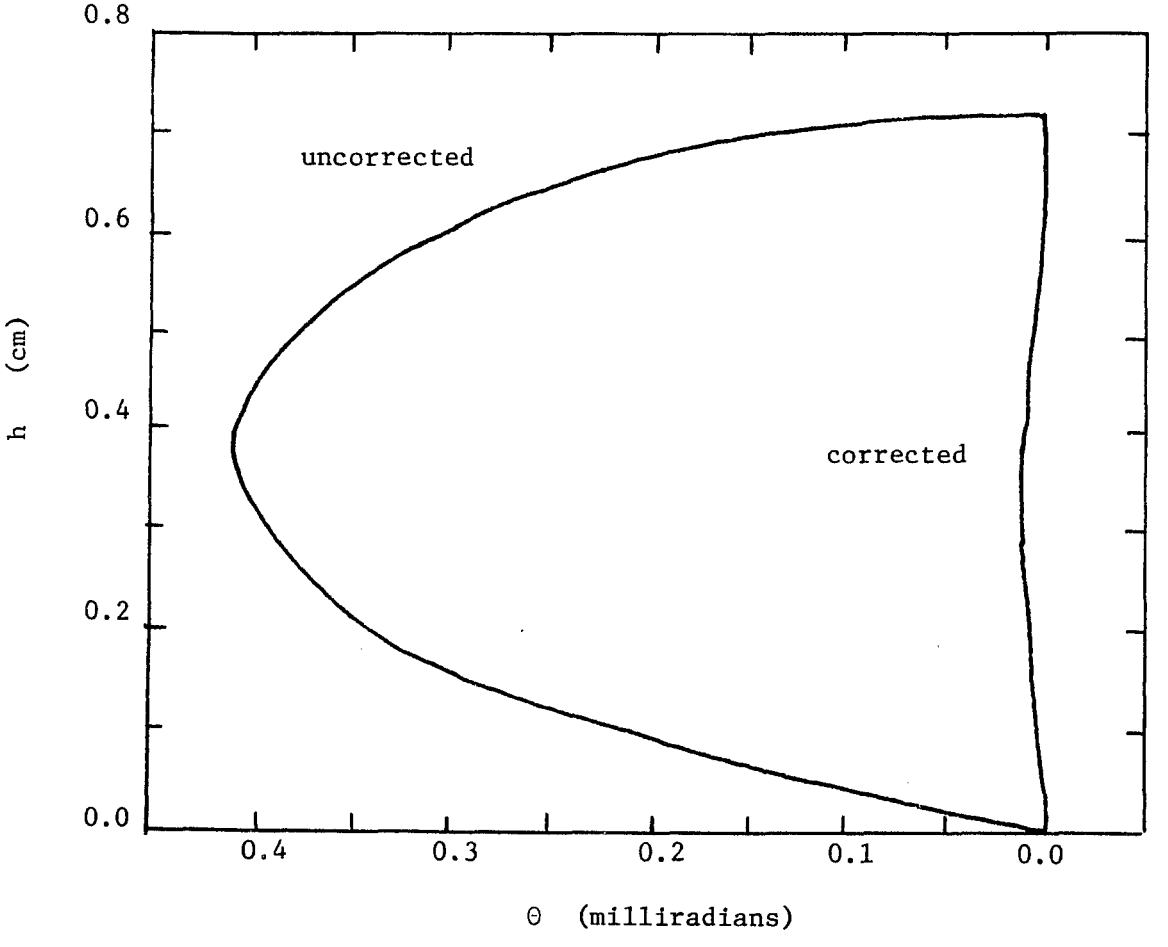

Fig. 11 Residual spherical aberration of corrected laser beam collimator. The spherical aberration of a collimator composed of equiconcave and equiconvex lenses (uncorrected) is shown for comparison.

B. Receiver

The RT-2 telescope is a scaled up version of the Baker-Reflector-Corrector Camera which is corrected for aberration from 3600Å through the visible portion of the spectrum. The system consists of an objective corrector plate, a primary mirror of 31 inch aperture, a field flattener and a secondary mirror to focus the light at the Newtonian focus. The equivalent focal length is 108 inches with a field of view of 6 degrees (105 milliradians).

The telescope has been modified in several ways to make the instrument suitable for use as an optical radar receiver. The objective corrector plate and field flattener were removed because they are unnecessary for narrow field operation. This makes the focal length of the telescope the same as the focal length of the primary mirror (140 inches). An instrument platform supporting the photomultiplier tube and associated optical and mechanical equipment was installed near the focal plane of the telescope.

The backscattered signal can be measured using analog or single photoelectron counting techniques; the particular measurement method is dependent upon the altitude range under investigation. For sufficiently low light levels, the backscattered power is proportional to the count rate of pulses at the anode of the photomultiplier. A discriminator generates a standardized pulse for each amplified anode pulse which exceeds a specified threshold. The count rate is sampled as the laser pulse passes through the atmosphere. The measuring time (1.5 msec or an

equivalent altitude range of 230 km) is divided into short time bins, during each of which the received photons are counted. The number of counts in each successive bin is stored in a delay line memory, and this information is printed out after each laser shot. At altitude below 30 km, the backscattered power is proportional to the voltage across the phototube load resistor. In this case the return signal is displayed on a Tektronix 555 oscilloscope and photographed. Voltage readings are taken from enlargements of the photographs at 0.6 km intervals.

1. Digital Receiver Configuration

A schematic diagram and a photograph of the digital receiver instrumentation are shown in Fig. 12 and Fig. 13, respectively. The backscattered laser radiation, focussed by the primary mirror, passes through a field stop, a mechanical shutter and then a collimation lens. The light, which is now collimated to within ± 4.8°, passes through an interference filter and impinges upon the photocathode of the cooled photomultiplier. An evacuated glass cell is epoxied to the phototube window to prevent condensation.

The single photoelectron counting instrumentation is shown in Fig. 14. Anode pulses resulting from single photoelectrons ejected from the photocathode are amplified by a Chronetics Model 106 dual Nanoamp and then standardized by an EG&G T101/N discriminator. The discriminator generates a 2 volt, 25 nsec wide pulse for each input pulse of amplitude which exceeds a specified threshold. The optimum threshold level depends strongly on the photomultiplier gain, and the level must be determined for each photomultiplier tube used. Satisfactory performance will be obtained for most tubes when

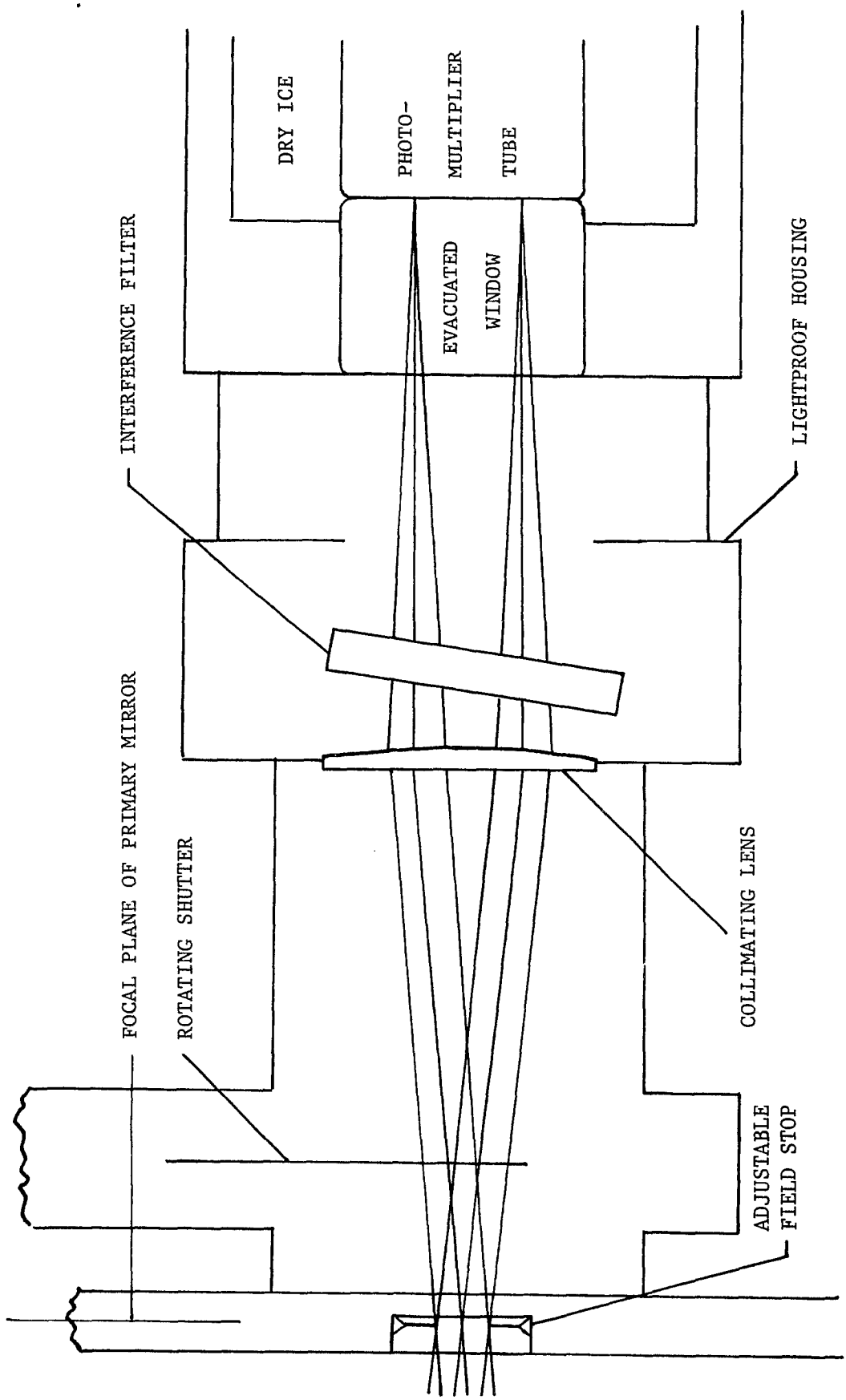

Fig. 12 Schematic diagram of digital receiver optics.

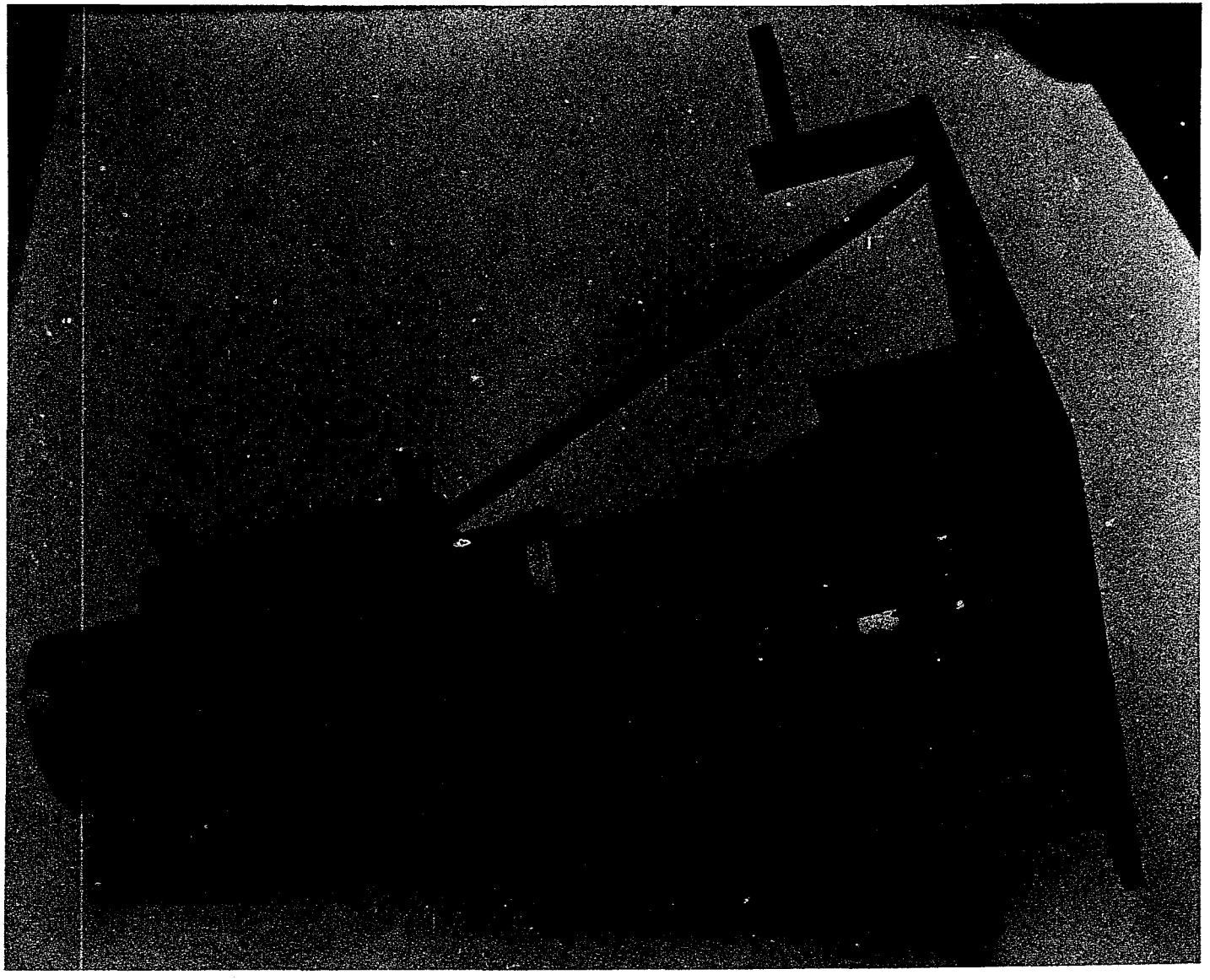

Fig. 13 Photograph of the receiver optical instrumentation used in the single photoelectron counting mode of operation.

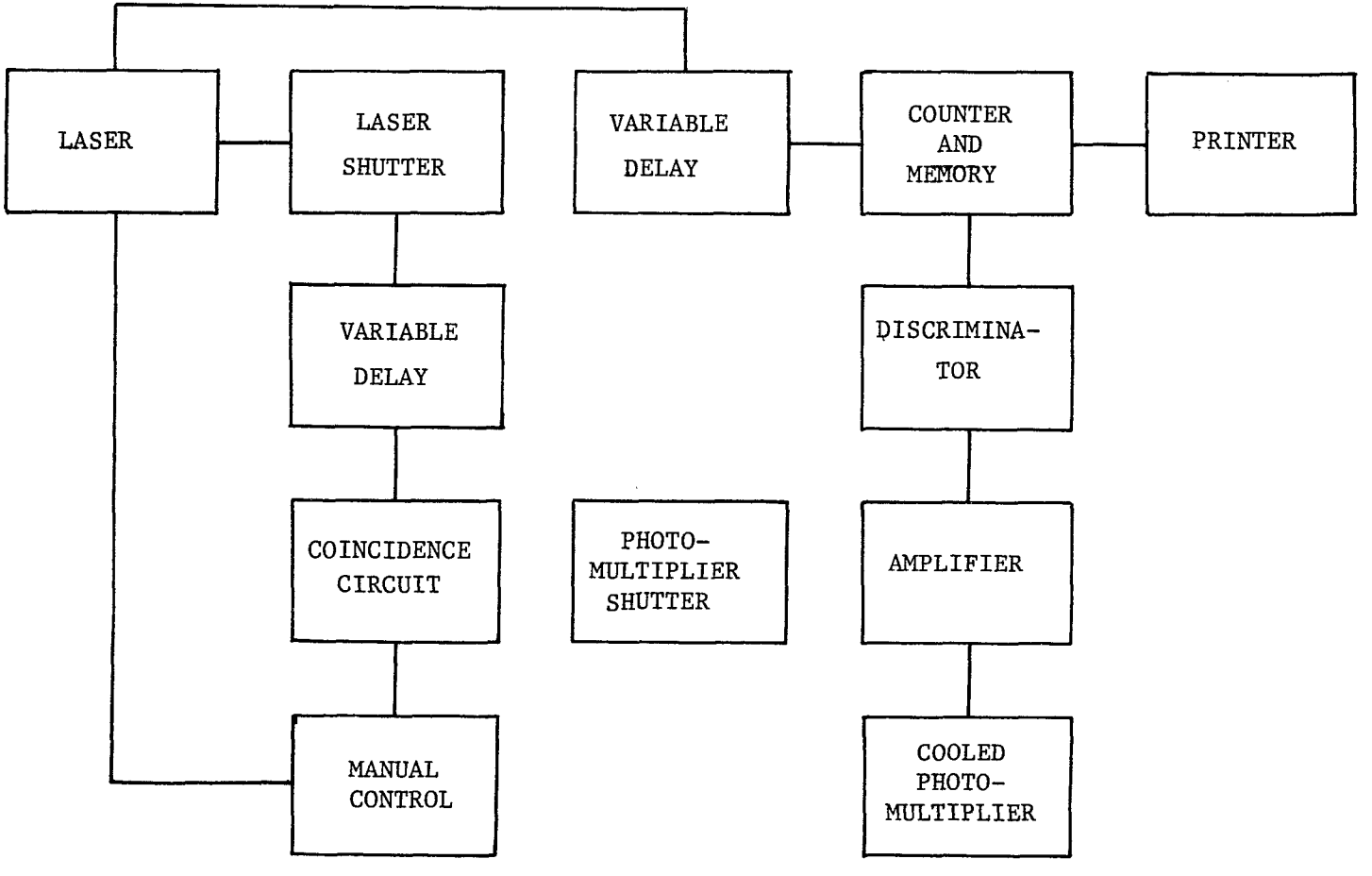

Fig. 14 Block diagram of single photoelectron counting instrumentation.

the level is set at 20% of the average pulse height. The standardized pulses from the discriminator are counted and summed over 11 μsec (1.66 km) intervals. The total counting time is 1.5 msec, or an equivalent altitude range of 230 km. The total counts in each 11 μsec time bin are stored in a delay line memory and then read out by means of a Hewlett Packard printer after each laser shot.

2. Analog Receiver Configuration

The analog receiver optics differ depending on the level of sky background. For daytime operation the optics are the same as the digital receiver optics with the 15 A filter replaced by a 3 1/2 A filter. During nighttime operation the optimum signal-to-noise ratio is achieved using the configuration shown in Fig. 15. The Wratten filter has the advantage of a 95% transmission at 6943Å and does not require collimated light. Although the effective bandpass of the photomultiplier and filter combination is 700 Å, the sky background current is still less than 1/10 of the signal current at 30 km. The increased transmission of the Wratten 70 filter, therefore, has the effect of increasing the signal-to-noise ratio of the system under nighttime sky background conditions. A block diagram of the analog receiver instrumentation is shown in Fig. 17. A trigger pulse, which is generated simultaneously with the laser pulse emission, serves as a start pulse for the system electronics. After a specified delay, (typically 60 μsec) the pulse triggers a photomultiplier focus gate and Time Base A of the Tektronix 555 dual beam oscilloscope. The focus gate switches the focus potential of the RCA 7265 dynode circuit from negative bias to 280 volts positive with respect to the photocathode.

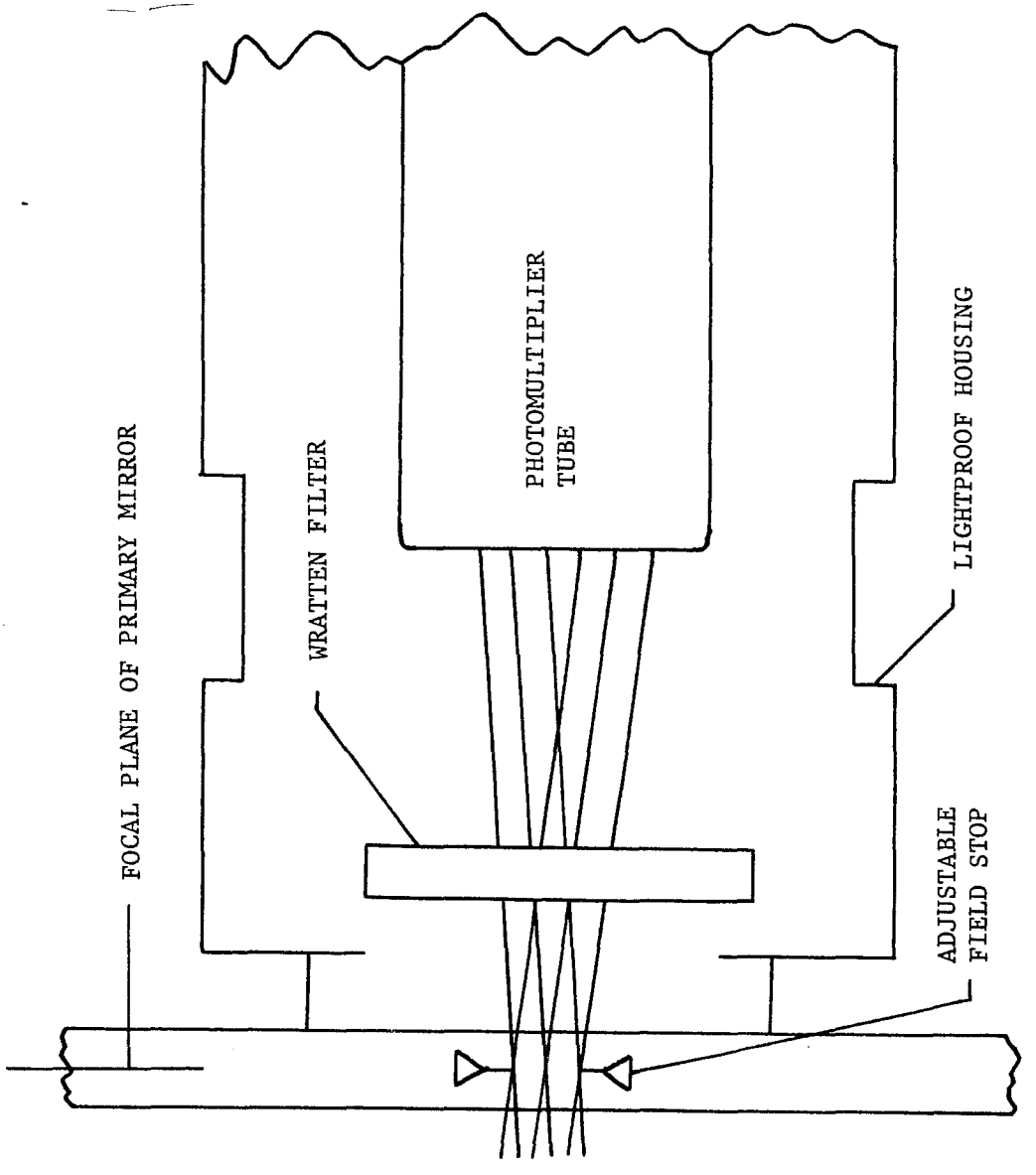

Fig. 15 Schematic diagram of analog receiver optics.

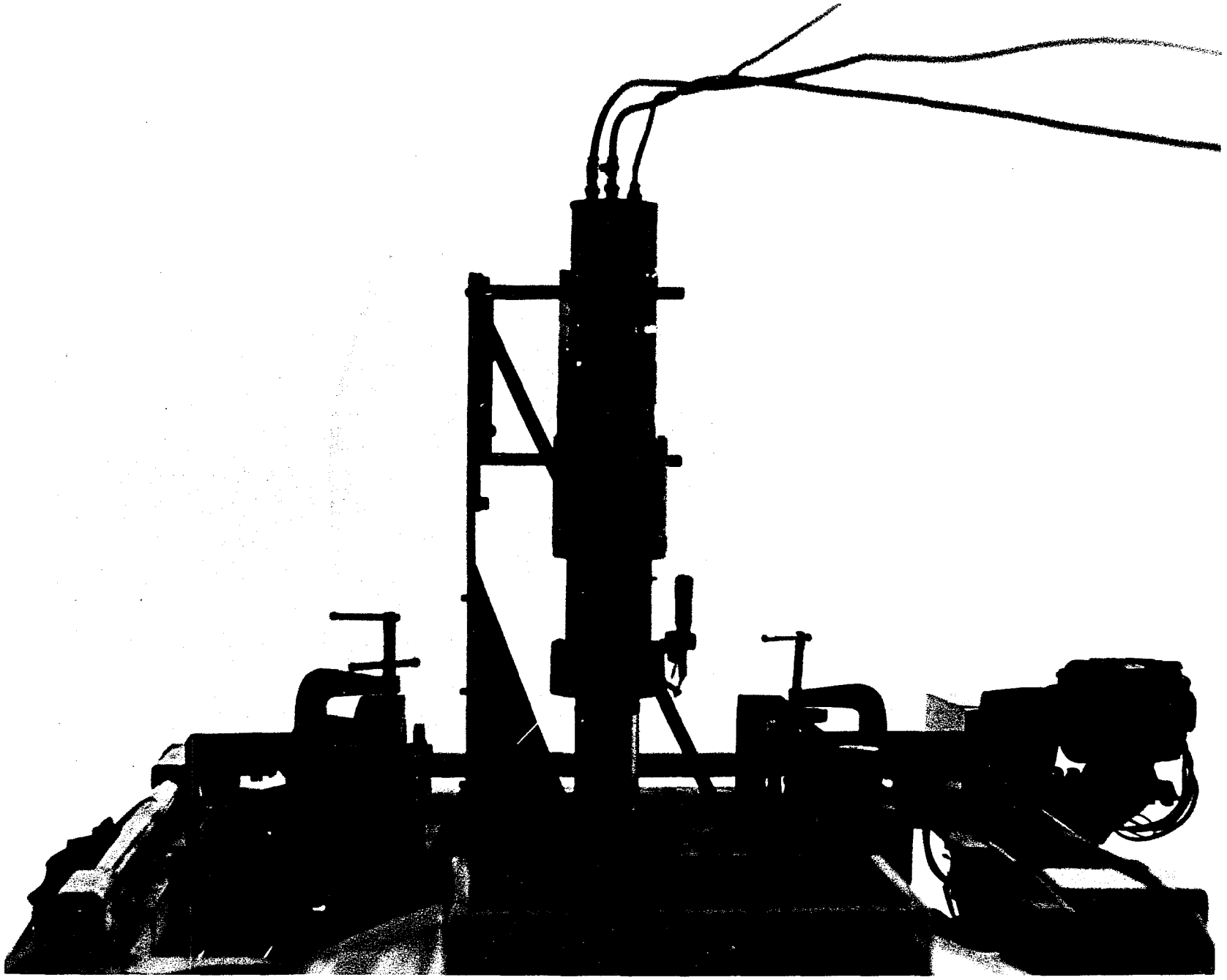

Fig. 16 Photograph of analog receiver instrumentation.

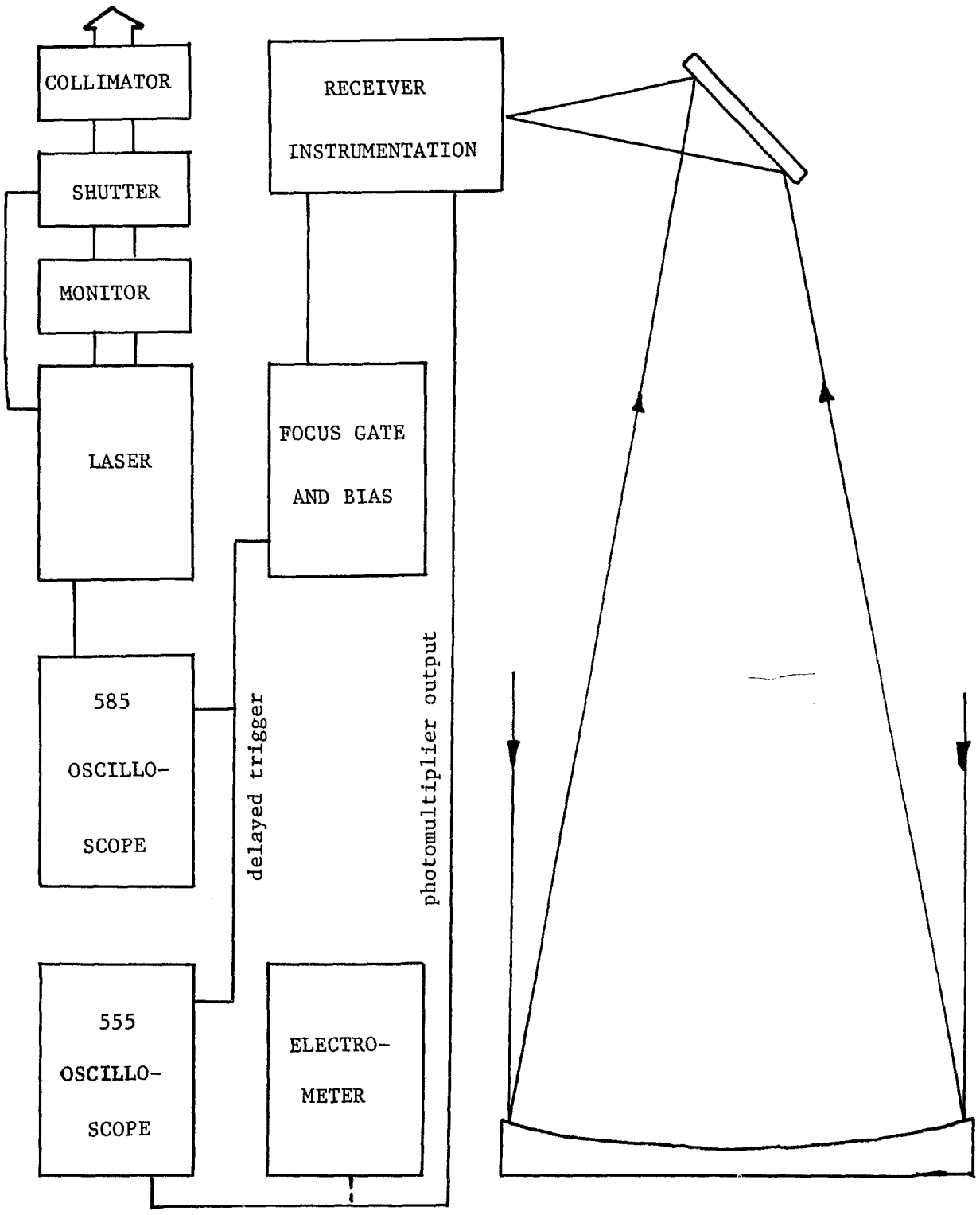

Fig. 17 Block diagram of analog receiver instrumentation

The initial negative bias effectively turns off the tube during the intense return from low altitudes and prevents nonlinear phototube response. The voltage across the photomultiplier load resistor is displayed on the upper and lower beams of the oscilloscope. The lower beam is used to display the 15 - 30 km return signal at high gain.

C. Alignment Procedures

The achievement of an optimum signal-to-noise ratio for the optical radar system required the development of accurate alignment techniques for the laser and receiver axes was critical because of the narrow field of view of the receiver. Since the eyepiece was available for the receiver telescope, it appeared that the alignment could be accomplished by sighting both the receiver telescope and the laser on a star (Polaris is bright and affected little by the earth's rotation). A sighting telescope was mounted on the laser transmitter and aligned parallel to the laser beam axis. This was accomplished in the laboratory using a gas laser reflected from the ruby laser front reflector to indicate the laser beam axis. The complete laser transmitter assembly (laser, shutter, energy monitor, collimation optics and sighting telescope) was then attached to the telescope on an adjustable mounting platform. In the course of the alignment attempts, it was found that the flexing of the transmitter frame was causing an alignment change of up to 2 milliradians when the telescope was moved from a horizontal position to the vertical. This alignment technique had another drawback; realignment of the system (often necessary after alignment of the laser) involved the formidable task of removing the transmitter from the

telescope. For these and other reasons, the sighting telescope method was abandoned. In order to avoid alignment problems associated with flexing of the transmitter frame, a technique was devised which allowed the laser and receiver axes to be aligned while remaining in the vertical position. The photomultiplier current resulting from the backscattered signal from the 25 - 30 km region was observed while the laser-receiver alignment was changed. With the receiver field of view matched to the laser beam divergence, the laser transmitter alignment was adjusted to maximize the backscattered signal. The field stop diameter was then increased slightly to allow for small changes in the laser transmitter alignment.

IV. EXPERIMENTAL RESULTS

In the following section, plots of the observed relative volume backscatter cross section of the atmosphere are fitted to a curve which represents the expected results for scattering from a pure molecular atmosphere. Scattering in excess of the predicted molecular scattering is attributed to the presence of aerosol particles at the altitude of the scattering enhancement. It is appropriate, therefore, to consider the limitations of the molecular scattering model.

As shown in equation (17), the volume backscatter cross section for molecular scattering is equal to a constant times the molecular number density. The molecular component of the laser backscattering can therefore be calculated if the molecular number density versus altitude is known. The U. S. Standard Atmosphere, 1962 provides information on the middle latitude, year-round mean characteristics of the molecular number density versus altitude. The U. S. Standard Atmosphere Supplements, 1966 includes separate tables of molecular density versus altitude for summer and winter seasons at latitudes of 30° N, 45° N, 60° N and 75° N. The supporting data for the various standard atmospheres to 80 km comprise radiosonde observations at stations to within a few degrees of latitudes 15°, 30°, 45°, 60° and 75° N and observations made from rockets and instruments released from rockets. The rockets were fired from eighteen different locations covering a range of latitudes from 8° N to 71° N, and the preponderance of available data was for North America.

The standard atmospheres for 30° N January, 30° N July and Mid-Latitude Spring/Fall should provide a sufficiently accurate representation of the molecular number density above Wallops Island (38° N). The seasonal standard atmospheres represent average conditions determined from the results of numerous rocket and balloon experiments. In interpreting optical radar measurements, which are often conducted over a period of several hours, it is important to know the range of fluctuation of the individual rocket measurements of the molecular number density. Fig. 18 shows the departure of the July and January standard atmosphere densities for 30° N from the annual and latitudinal average represented by U. S. Standard Atmosphere, 1962. The arrows include 95 percent of the observed profiles which were used to determine the average seasonal profile. The fact that 95 percent of the rocket density measurements deviated from the seasonal standard atmosphere values by less than 20 percent shows that the molecular scattering should be a relatively stable and predictable component of the total atmospheric scattering. The detection of aerosol layers in the atmosphere by fitting observed backscatter profiles to predicted molecular backscatter profiles would therefore seem to be a sound technique if the enhanced scattering exceeds the possible variations of the molecular scattering.

In February, 1967, arrangements were made with NASA Wallops Island for the use of the RT-2 research telescope as an optical radar receiver, and design and construction of the transmitter and receiver equipment was started. During the summer of 1967, the digital counting system was checked out, and preliminary laser backscatter measurements

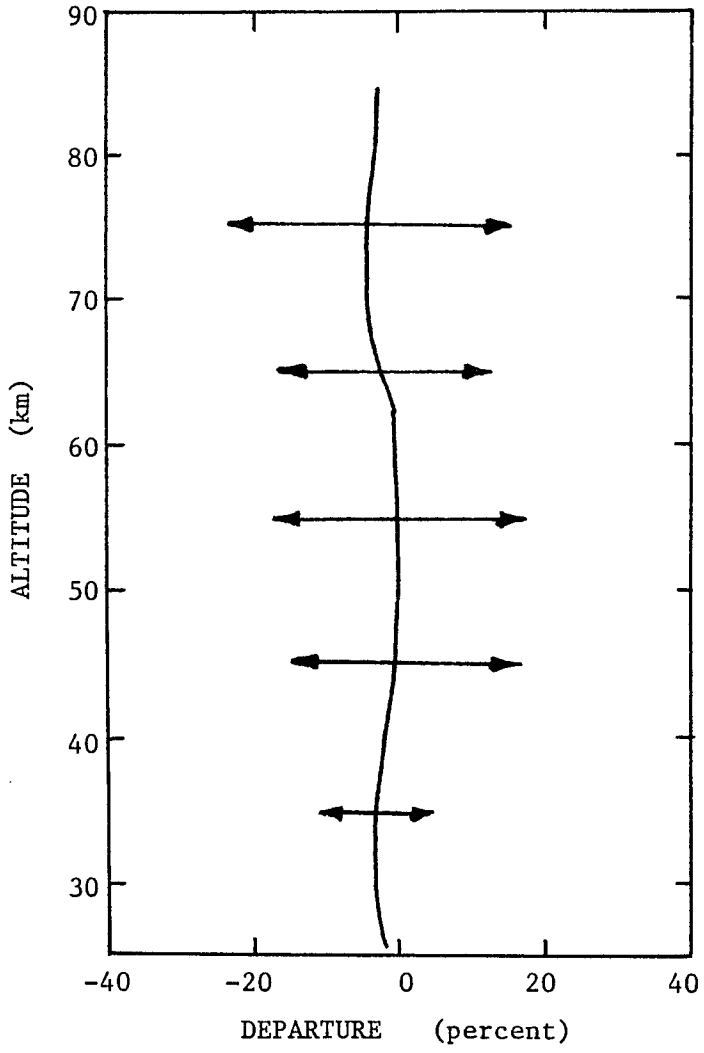

Fig. 18 Approximate 95 percent range of individual rocket density measurements for the July, 30° N., seasonal standard atmosphere. The solid line represents the departure of the seasonal standard atmosphere from the U. S. Standard Atmosphere, 1962.

were made at Williamsburg, Va. with a 12 inch Cassegrainian receiver telescope. By February 1968, modification of the RT-2 telescope at Wallops Island, Va. was complete. Techniques for alignment of the laser and receiver axes were developed, and the optical radar system was operational by April 1968.

On April 1, 1968 single photoelectron counting instrumentation was used to record the backscattered signal from a series of 33 vertically directed laser pulses. Fig. 19 shows the total counts received in each counting time interval. Curve A represents the predicted slope for a pure molecular atmosphere, and Curve B represents the average background counting rate. The observed counts from an atmosphere in which molecular scattering is dominant would be expected to fit Curve C. The received single photoelectron counts for each laser pulse were summed over 1.65 km altitude intervals (11 μsec counting intervals). Data was not analyzed below 33 km because the count rate exceeded the capability of the 10 Mhz counting circuitry. In the 30 - 55 km region, no variations from the molecular scattering curve of greater than two standard deviations were observed. The magnitude of the backscattered signal, however, was less than one tenth of the expected signal (see section II. C.). Inspection and testing of the transmitter and receiver revealed that the fluorescence shutter was partially obstructing the transmitted laser pulse, and that improper collimation of the receiver optics was also causing a loss of signal. Subsequent modifications of the transmitter and receiver increased the sensitivity of the system by a factor of five. During the summer of 1968, methods of recording

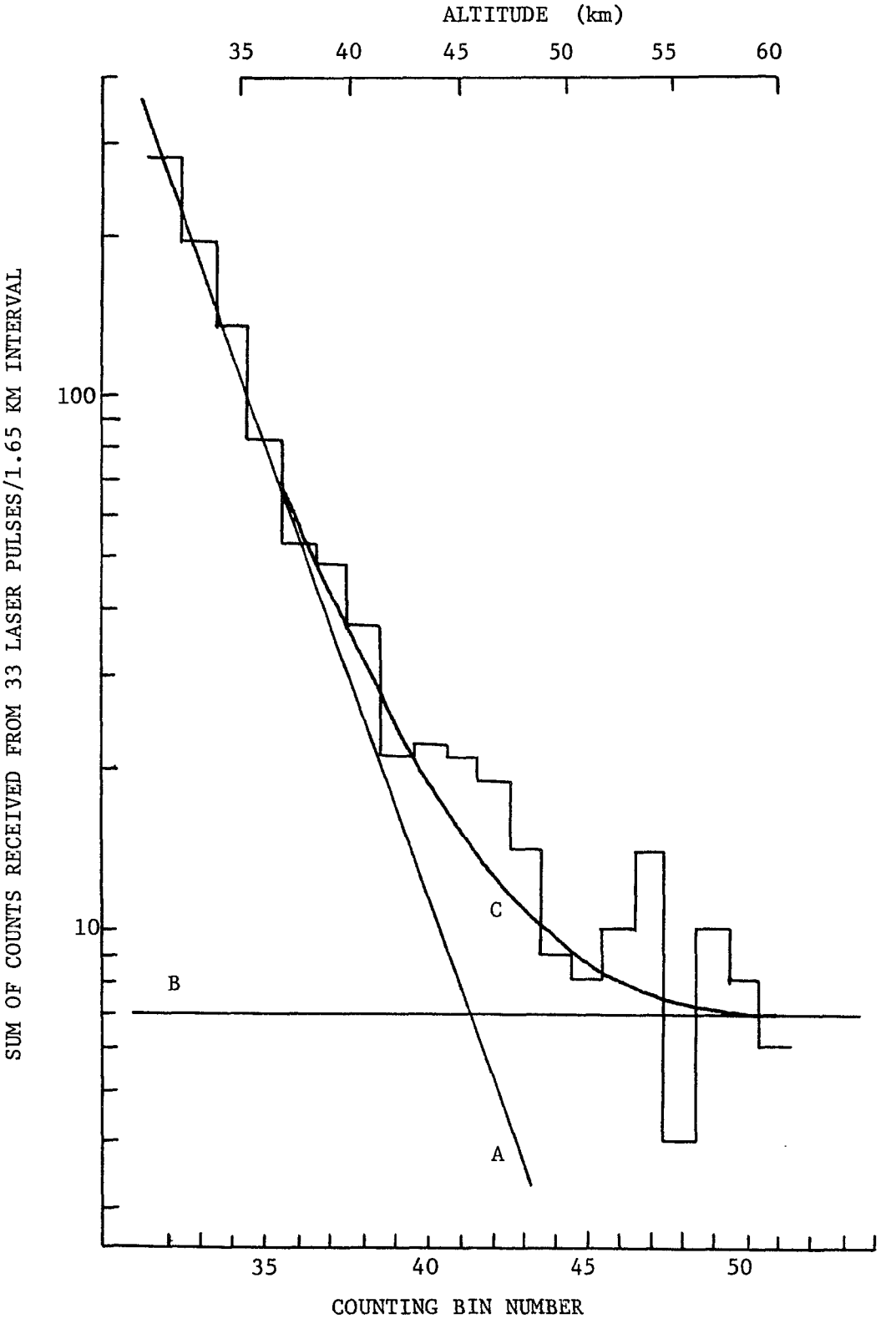

Fig. 19 Sum of counts received from 33 laser pulses per 1.65 km interval versus altitude. Data was accumulated on April 1, 1968.

low altitude backscatter and receiver calibration procedures were studied, since weather conditions and equipment failures prohibited high altitude observations.

On September 15/16, 1968, favorable weather conditions and properly functioning equipment permitted a particularly successful series of measurements. Using both analog and digital measurements of the backscattered signal from vertically directed laser pulses, the relative volume backscatter cross section of the atmosphere was measured from 10 km to 80 km.

Figs. 20 and 21 show data obtained for altitudes below 30 km. Voltage readings of the amplified photomultiplier signal were taken from these photographs at altitude increments of 0.6 km. As shown by equation (10), the volume backscatter cross section is equal to $Az^2P(z)/q^2$, where A is a constant which is dependent upon the laser energy, receiver size, and other system parameters. Elterman's attenuation model shows that the significant attenuation of the laser beam occurs in the first three kilometers of the atmosphere for a vertically directed beam. According to this model, which accounts for the effects of both aerosol and molecular scattering, the $q^2(z)$ term of equation (10) does not vary more than three percent over the range of 10 - 30 km. To simplify data reduction, therefore, the q^2 term will be considered to be a constant with altitude. The amplitudes of the oscilloscope traces shown in Figs. 20 and 21 are proportional to the backscattered power incident on the receiver. All of the backscatter records exhibited the same general form, but small differences were

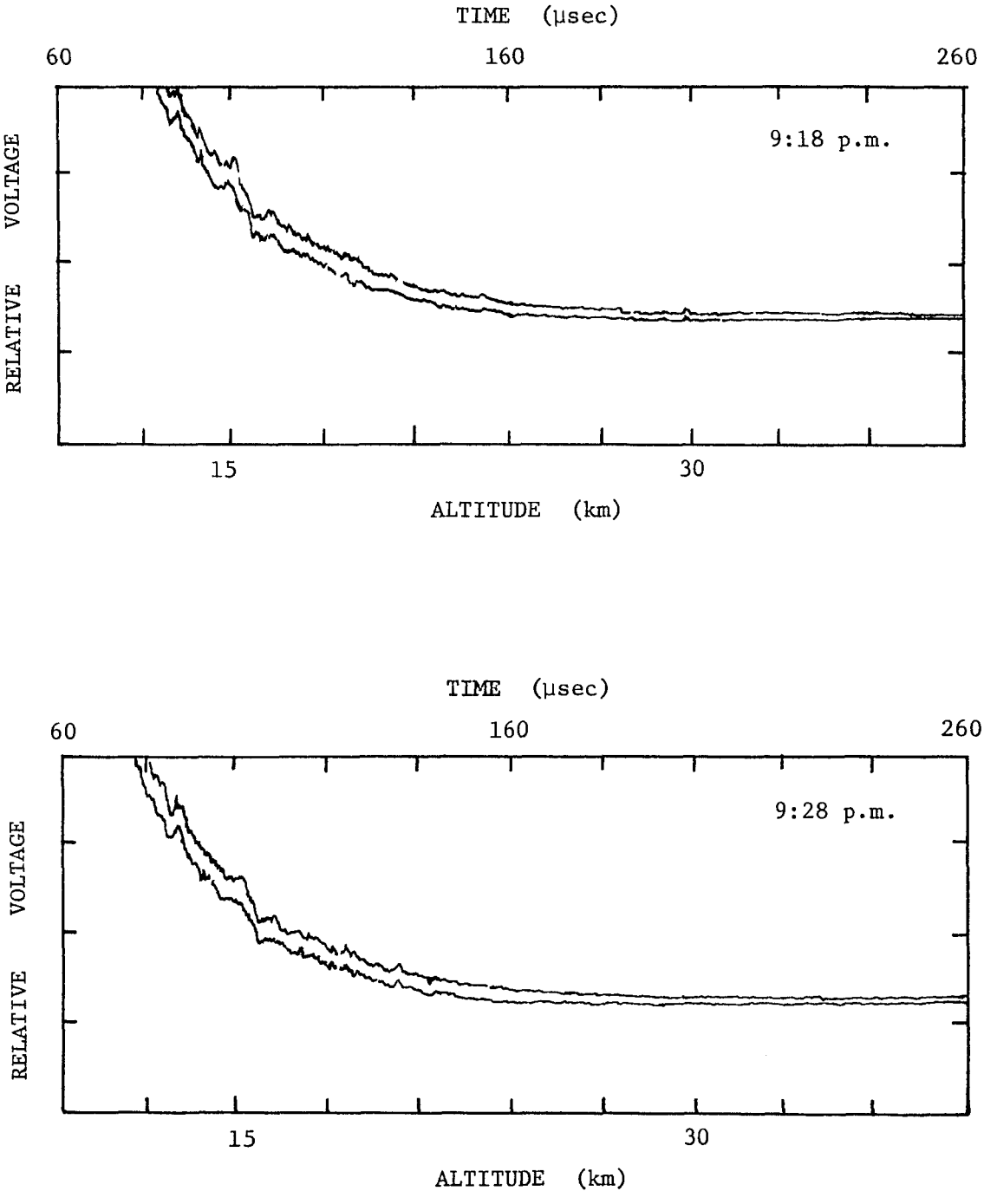

Fig. 20 Voltage across the photomultiplier load resistor versus altitude of the scattering volume. The photomultiplier was gated on 60 μsec after the emission of the laser pulse. The records were taken at 9:18 p.m. and 9:28 p.m. on September 15, 1968.

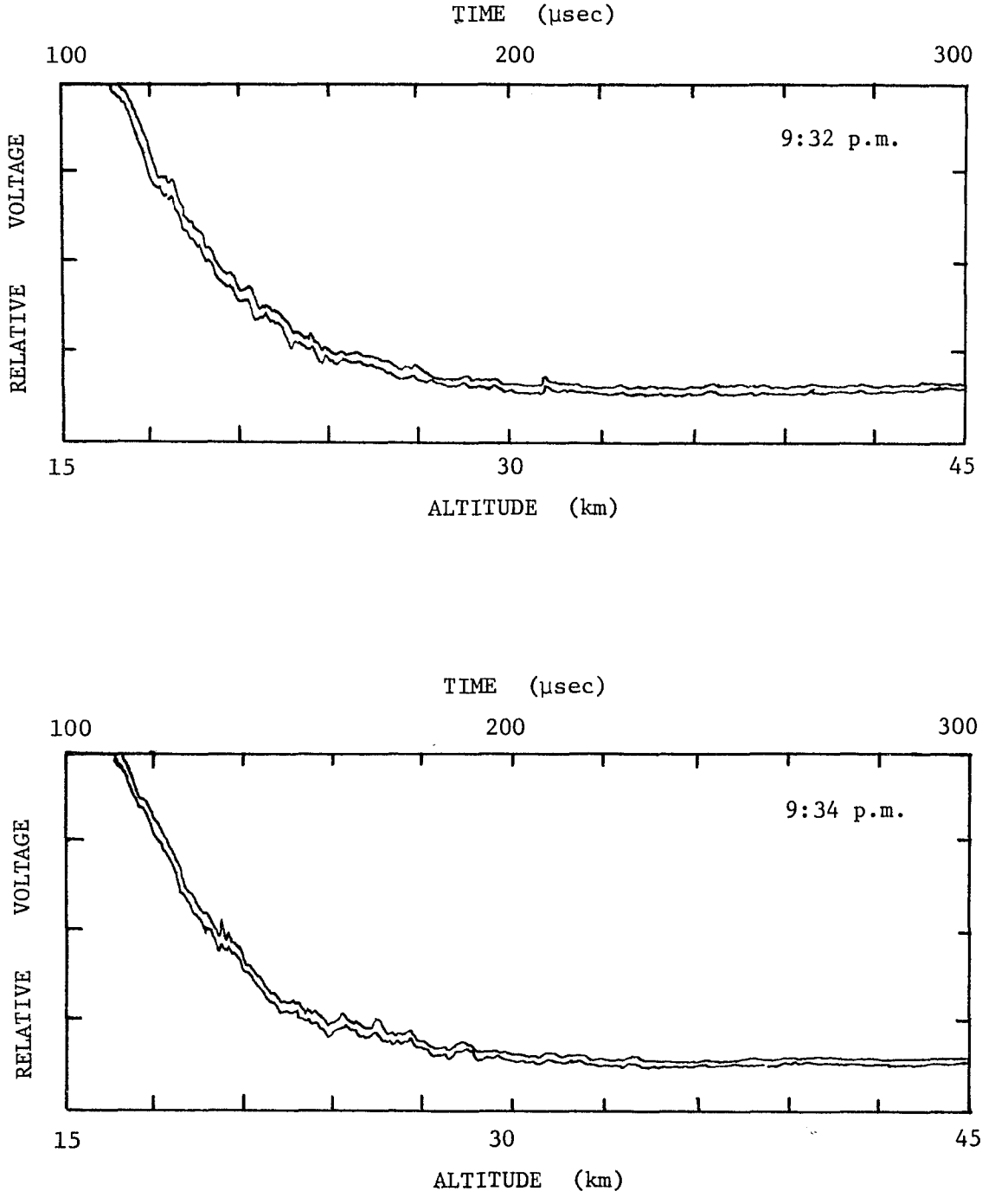

Fig. 21 Voltage across the photomultiplier load resistor versus altitude of the scattering volume. The photomultiplier was gated on 100 μsec after the emission of the laser pulse. The records were taken at 9:32 p.m. and 9:34 p.m. on September 15, 1968.

evident between individual backscatter records. In order to determine the average characteristics of the backscattered signal, a backscatter profile was constructed by summing the voltage readings from four laser pulses. These voltages were then used to construct the graph of the relative volume backscatter cross section versus altitude shown in Fig. 22. The solid line, which represents the slope expected for scattering from a molecular atmosphere, has been normalized to the observed curve at 28 km where it is generally accepted that aerosol scattering is negligible. A recent balloon borne particle sampling experiment (Rosen, 1969) confirms this assumption. In Fig. 23 the data is presented in the form of the scattering ratio (observed volume backscatter cross section/molecular volume backscatter cross section) versus altitude. The published results of other investigators using searchlight or optical radar techniques are also shown. Fiocco's curve, which represents an average of 66 daily scattering ratio profiles obtained during 1964 and 1965, indicates an average scattering ratio of 1.9. The rms fluctuation of the daily measurements from the average profile was 0.3. In view of the temporal fluctuations observed by Fiocco and the fact that measurements represented in Fig. 23 span a period of four years, it is obvious that differences in the curves cannot be attributed to spatial variations of the layer. The measurements do, however, demonstrate that the layer is not a transient or spatially localized feature of the atmosphere.

After the 10 - 30 km backscatter data was obtained, using the analog receiver instrumentation, the single photoelectron counting instru-

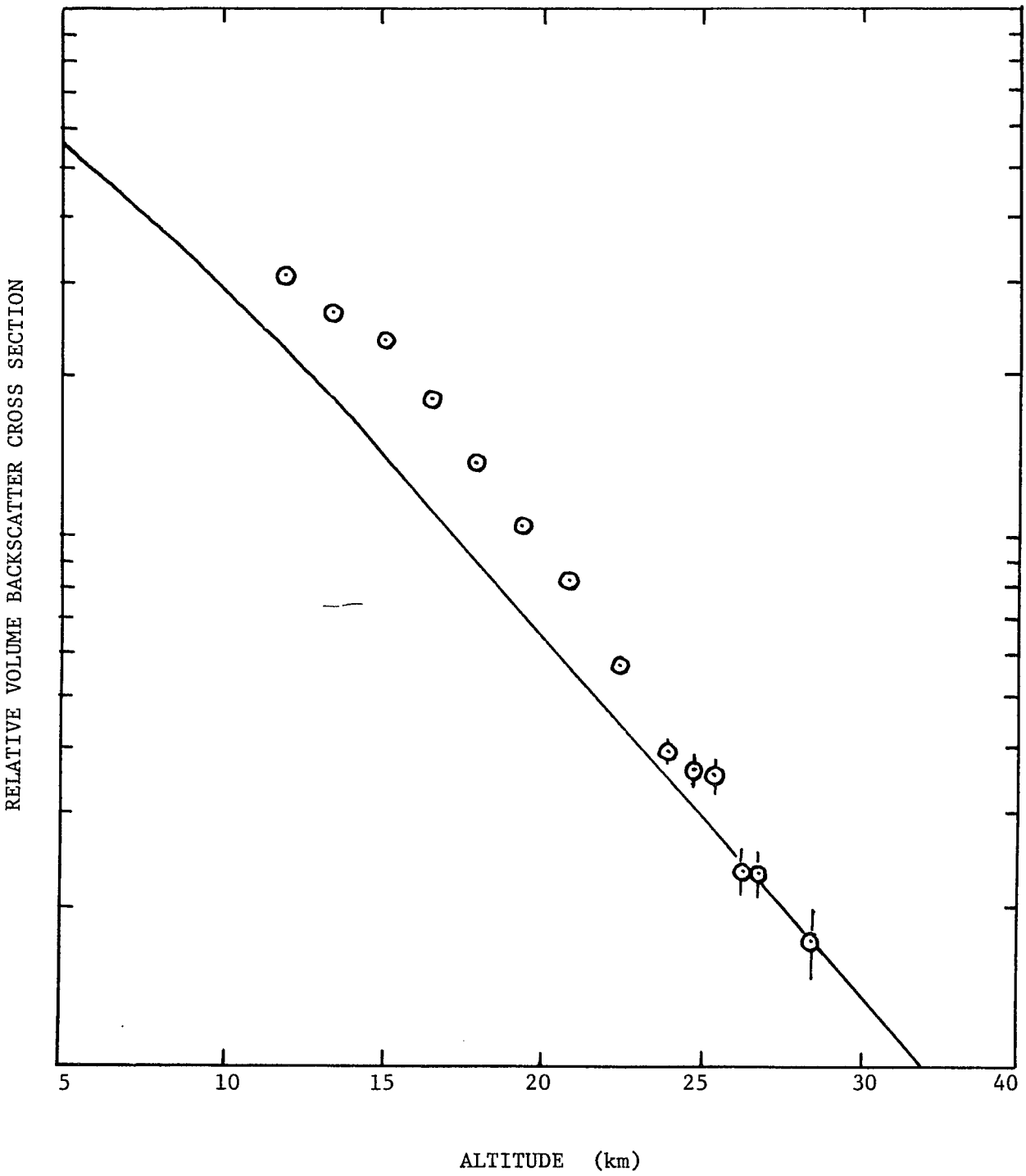

Fig. 22 Relative volume backscatter cross section (10-30 km) versus altitude for September 15, 1968. Average of four laser shots.

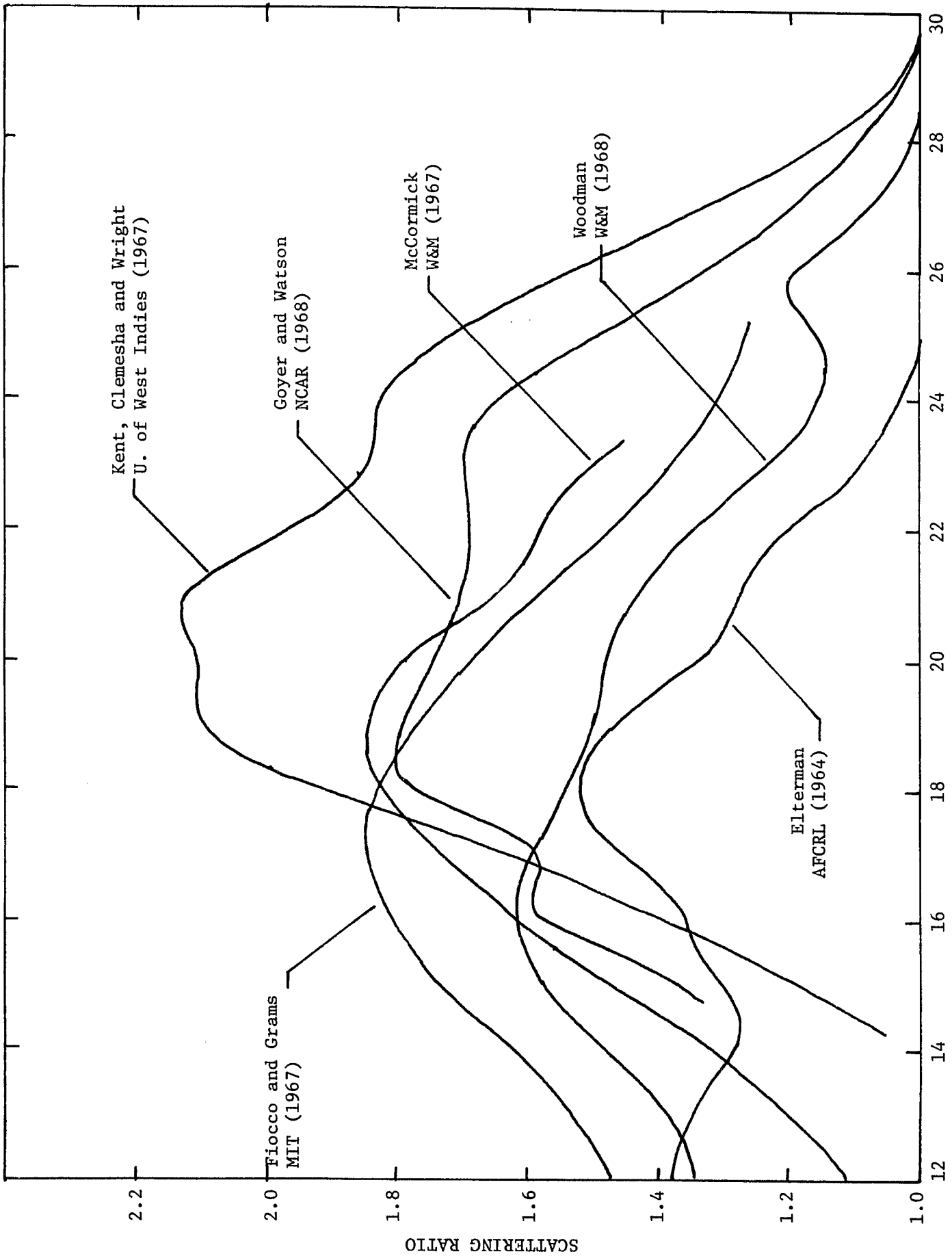

Fig. 23 Measurements of scattering ratio versus altitude.

mentation was installed in preparation for measurements of backscatter from the mesosphere and upper stratosphere. The system was operated in the single photoelectron counting mode from approximately 1:00a.m. to 3:00 a.m. on September 16, 1968, and backscatter data from 46 laser pulses was accumulated. Fig. 24 shows the sum of counts received from 46 laser pulses versus altitude. As in Fig. 19, Curve A represents the predicted slope for a pure molecular atmosphere, Curve B represents the average background counting rate, and Curve C is the sum of Curves A and B. Below 52.8 km, the received single photoelectron counts for each laser shot were summed over 1.66 km altitude intervals (11 μsec counting interval). Above this altitude, the received counts were averaged over a 3.3 km (22.0 μsec) interval.

It is useful to present the data in the form shown in Fig. 24. As shown by equation (13), the volume backscatter cross section, averaged over Δz, is equal to a constant times z^2S, where z is the altitude of the scattering volume, and S is the number of backscattered signal counts. The solid line in Fig. 25 represents the variation of the volume backscatter cross section with altitude for a molecular atmosphere and the data points represent the observed altitude dependence of the volume backscatter cross section for September 16, 1968. Because of the uncertainty of the factor q^2 in equation (13), absolute measurements were not possible, and the standard atmosphere was fitted to the observed data points.

The agreement of the observed scattering curve and the molecular scattering curve in Figs. 24 and 25 is good over the range of 30 - 55 km.

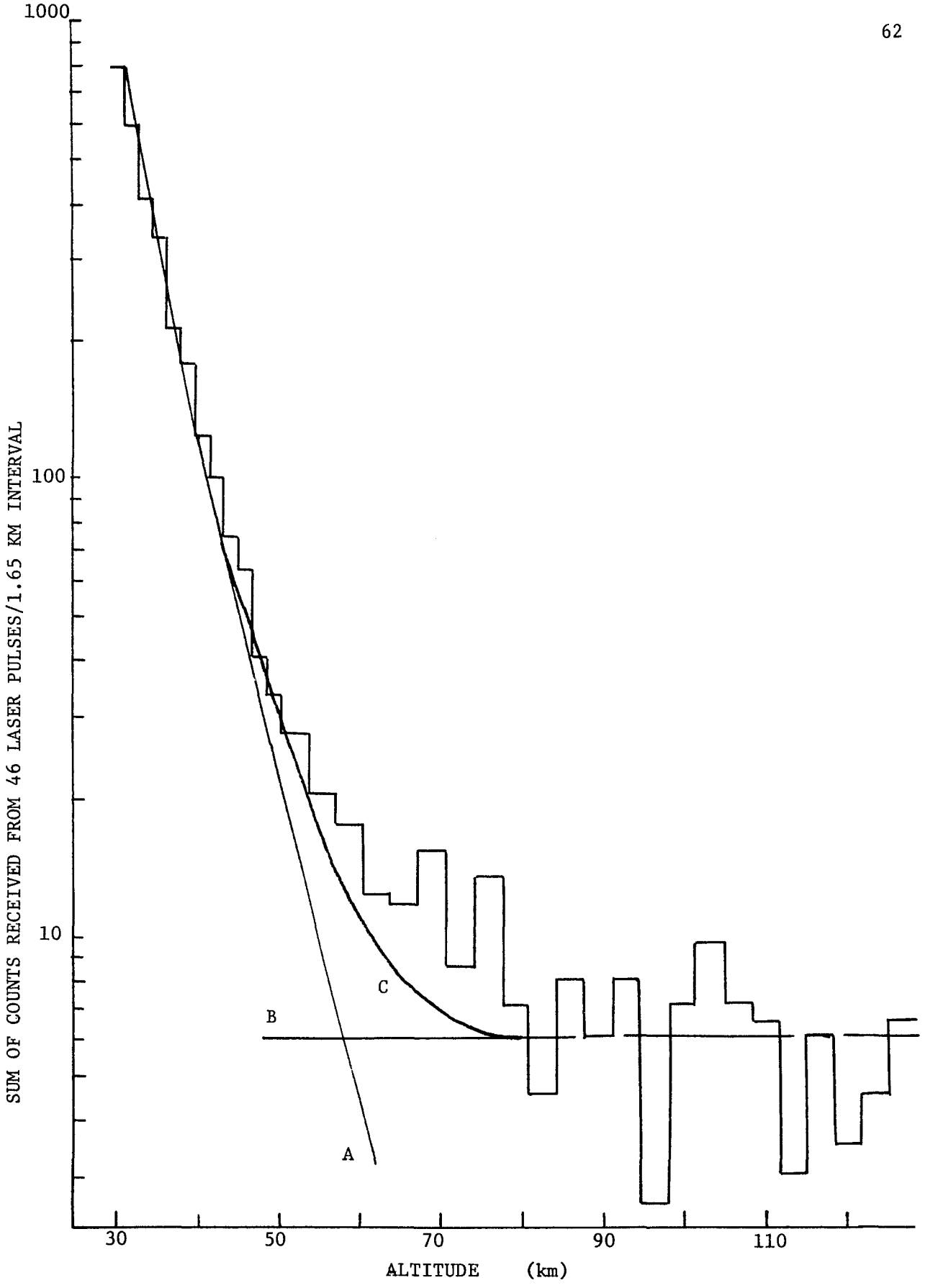

Fig. 24 Sum of counts received from 46 laser pulses per 1.65 km interval versus altitude. Data was accumulated on September 15/16, 1968.

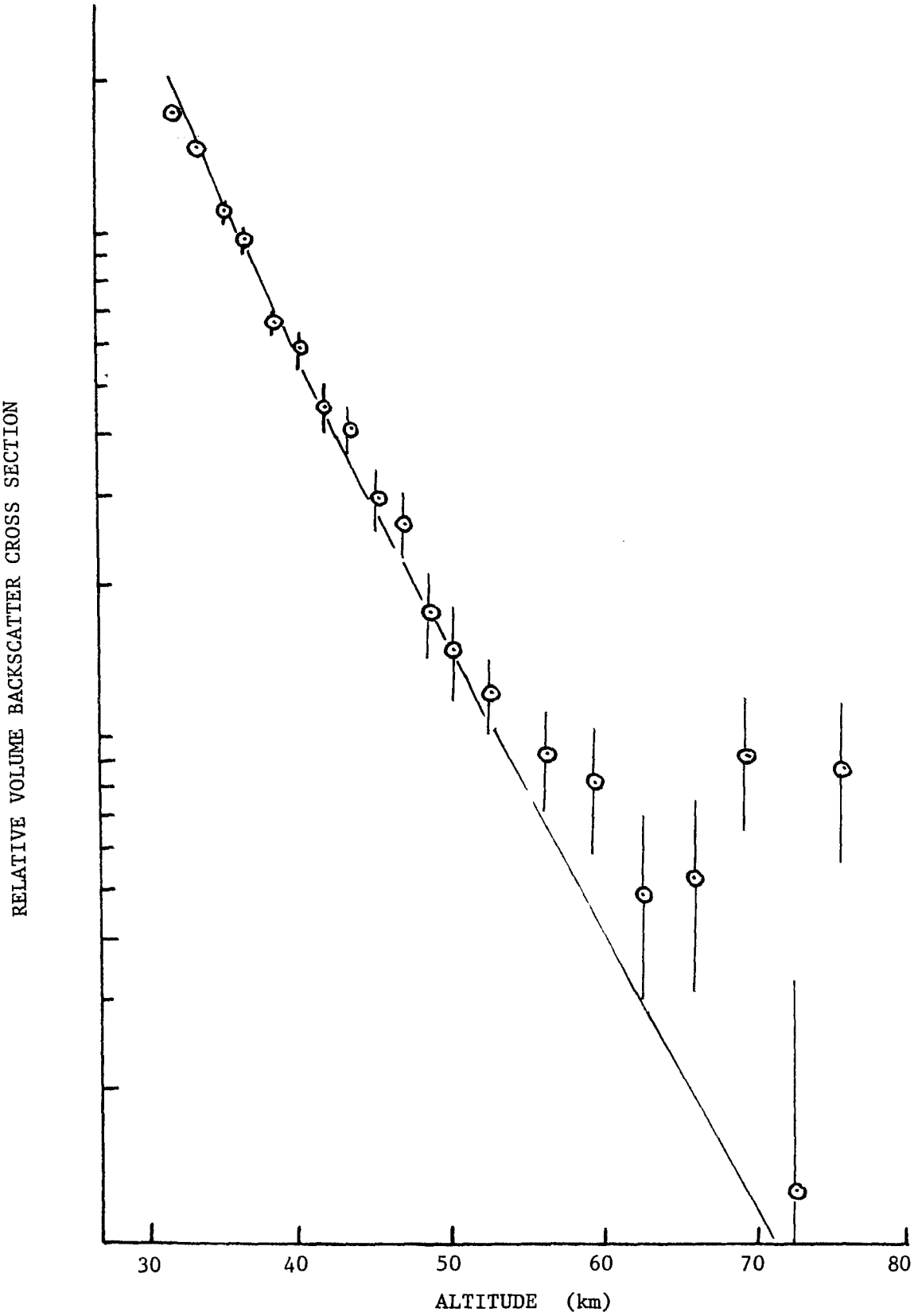

Fig. 25 Relative volume backscatter cross section versus altitude for September 16, 1968 (30 - 80 km).

When the observed counts were summed over the 57.75 - 77.55 km region, however, the total count exceeded the count expected on the basis of an aerosol free atmosphere by 5.6 standard deviations. The probability that the observed deviation could be the result of a statistical fluctuation of the molecular plus background count is negligible. It may be concluded, therefore, that the backscatter from the 57.75 - 77.55 km region of the atmosphere exceeded the possible molecular scattering. Concentrations of particles of extraterrestrial origin known to be present near 80 km could account for the additional scattering.

The number of counts received during the interval of time which corresponds to 67.65 - 70.95 km was 30. This count is 4.3 standard deviations above the count expected from the molecular and background components of the signal. The probability that the observed count resulted from a statistical fluctuation of the molecular plus background count, thereby causing a false detection of a scattering layer, is approximately 0.0063 percent. It is highly probable, therefore, that the scattered radiation from the 67.65 - 70.95 km region of the atmosphere resulted in 18 ± 5.5 counts (the average background count was 12). Similarly, from the 74.25 - 77.55 km region 15 ± 5.2 counts resulted from the backscattered signal, and the probability of a false detection is 0.0063.

Following the practice of Bain and Sandford (1966, 1966a) and Kent, Clemesha and Wright (1967), it will be assumed that the molecular scattering predominates in the 30 - 55 km region because of the excellent fit of this data to a molecular scattering curve. This assumption is supported

by the published results of Elterman (1964), and Newkirk and Eddy (1964), but verification by absolute optical radar measurements has not yet been accomplished. If the scattering near 50 km is assumed to be predominantly molecular and accurately described by equation (17) and the standard atmosphere number density tables, the constant $K = \varepsilon N_o A_r q^2$ of equation (13) can be evaluated. Equation (13), for $\sigma_M = 0$ and $z = 50.3$ km is

$$S(49.50 - 51.15) = \frac{K(1.65 \times 10^3)\sigma_R(50.3)}{(50.3 \times 10^3)^2}$$

where $K = \varepsilon N_o A_r q^2$. Equation (17) with $N_R(50.3) = 1.47 \times 10^{22}$ m^{-3} yields

$$\sigma_R(50.3) = 3.08 \times 10^{-10} \text{ m}^{-1} \text{ sr}^{-1}$$

Since $S(49.50 - 51.15) = 28$, the constant K is found to be 1.37×10^{17}, and equation (13) may be written

$$\sigma_R + \sigma_M = \frac{Sz^2}{1.37 \times 10^{17} \Delta z}$$

Evaluation of equation (13) for $S(67.65 - 70.95) = 18 \pm 5.5$ and $S(74.25 - 77.55) = 15 \pm 5.2$ yields $\sigma_R + \sigma_M = 1.90 \pm 0.58 \times 10^{-12}$ cm^{-1} sr^{-1} near 69.3 km and $1.92 \pm 0.66 \times 10^{-12}$ cm^{-1} sr^{-1} near 75.9 km. The counts received during the time interval from 0.53 ms (80 km) to 1.18 ms (180 km) after the emission of the laser pulse were summed over 22 μsec (3.3 km) intervals, and no deviations of greater than 2 standard deviations were observed.

B. Meteorological Scattering Features

Although the study of clouds has not been a major objective of this research, the prevalence of overcast sky conditions has resulted in the accumulation of several cloud backscatter records. Below approximately 6 km, clouds are composed of water droplets. High clouds (excluding nacreous and noctilucent clouds) are usually of the cirrus type and are composed of ice crystals. The size distribution of cloud water droplets varies according to cloud type. In general, however, cloud droplets range in size from 1 μ to 30 μ with most droplets falling in the 5 - 12 μ range (Cadle, 1966). The total concentration of droplets is of the order of 300 cm^{-3} (Carrier, Cato and von Essen, 1967). In contrast, a typical cirrostratus ice particle might be a prism 200 μ long, 30 μ wide and occurring in an average particle concentration of 0.5 cm^{-3} (Weickmann, 1949). Weickmann found that cirrus and cirrostratus clouds occurred most frequently in thin layers up to 300 m thick. Hall (1968) characterized a typical cirrus cloud as 200 m thick with a number density of ice particles of 0.5 cm^{-3}.

Figs. 26 - 30 show five oscilloscope photographs of the photomultiplier response to the backscattered signal from cirrostratus clouds. The cirrostratus cloud was identified by the characteristic halo which is produced when sunlight is transmitted through this type of cloud. Wallops Island radiosonde records show that the wind speed in the region of cirrostratus was approximately 30 knots. Laser backscatter records taken at one minute intervals correspond, therefore, to samplings of

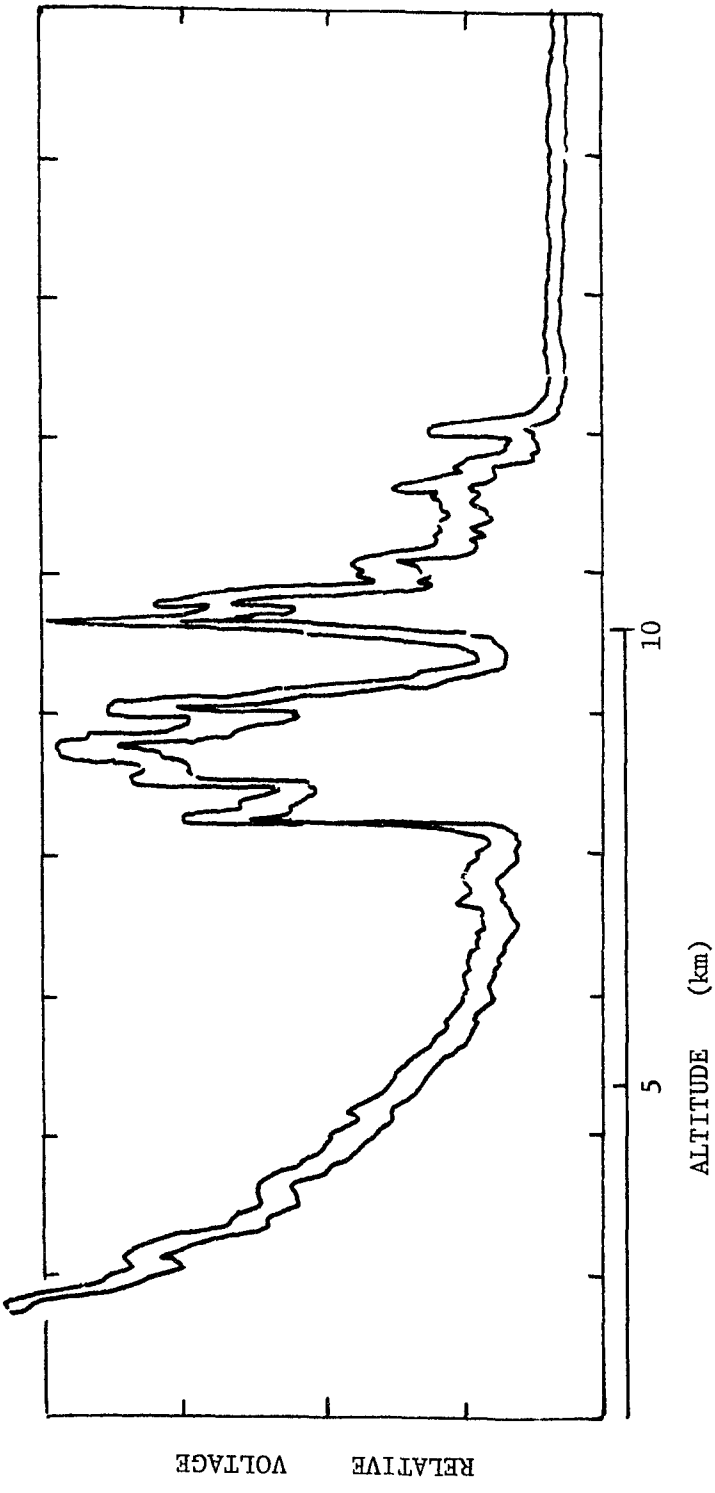

Fig. 26 Voltage across the photomultiplier load resistor versus altitude of scattering volume for backscatter from cirrostratus clouds on May 8, 1968 at 2:13 p.m.

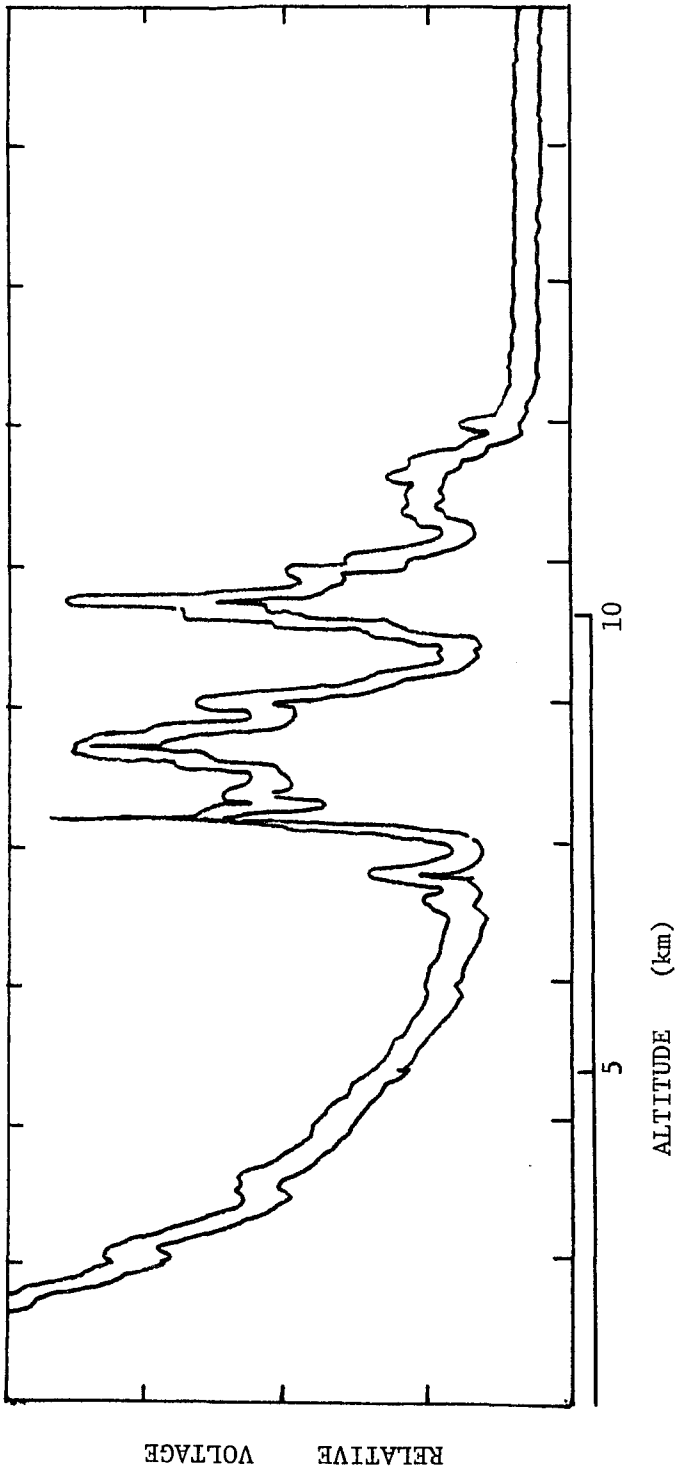

Fig. 27 Voltage across the photomultiplier load resistor versus altitude of scattering volume for backscatter from cirrostratus clouds on May 8, 1968 at 2:15 p.m.

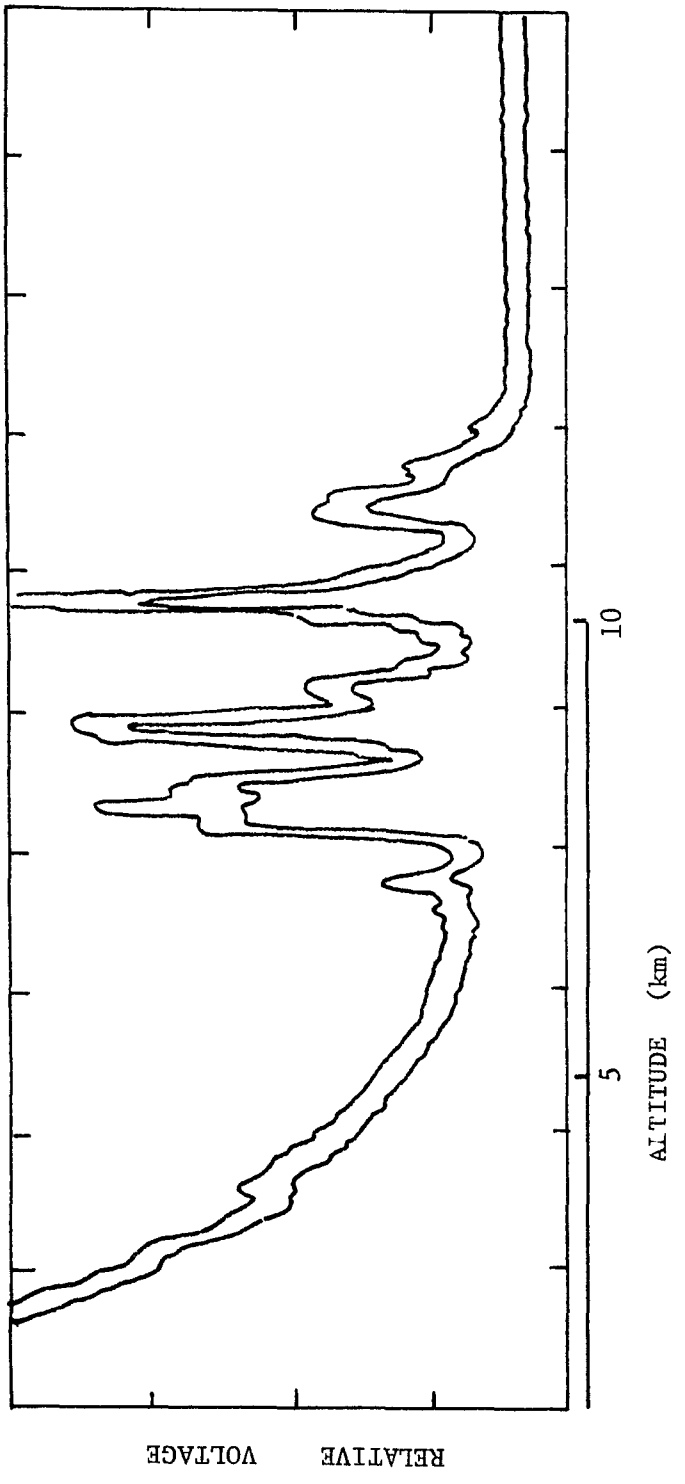

Fig. 28 Voltage across the photomultiplier load resistor versus altitude of scattering volume for backscatter from cirrostratus clouds on May 8, 1968 at 2:16 p.m.

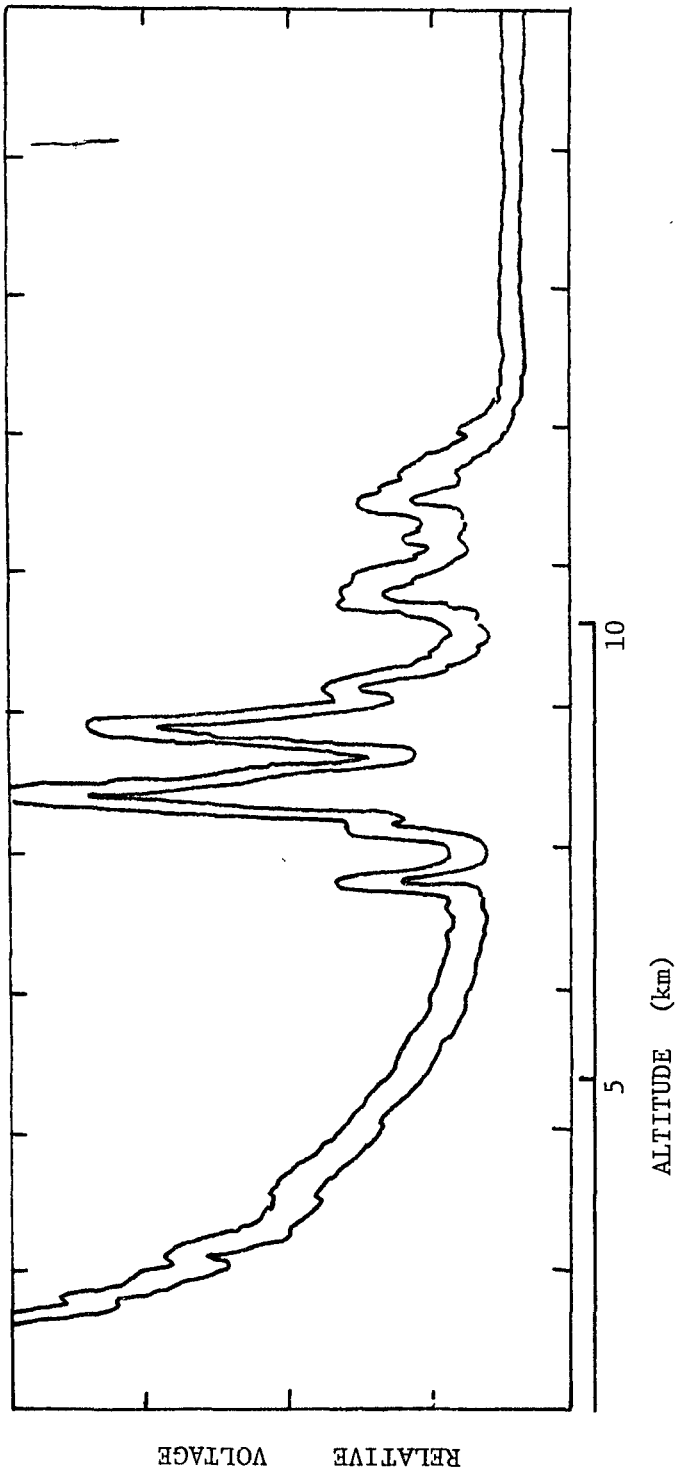

Fig. 29 Voltage across the photomultiplier load resistor versus altitude of scattering volume for backscatter from cirrostratus clouds on May 8, 1968 at 2:17 p.m.

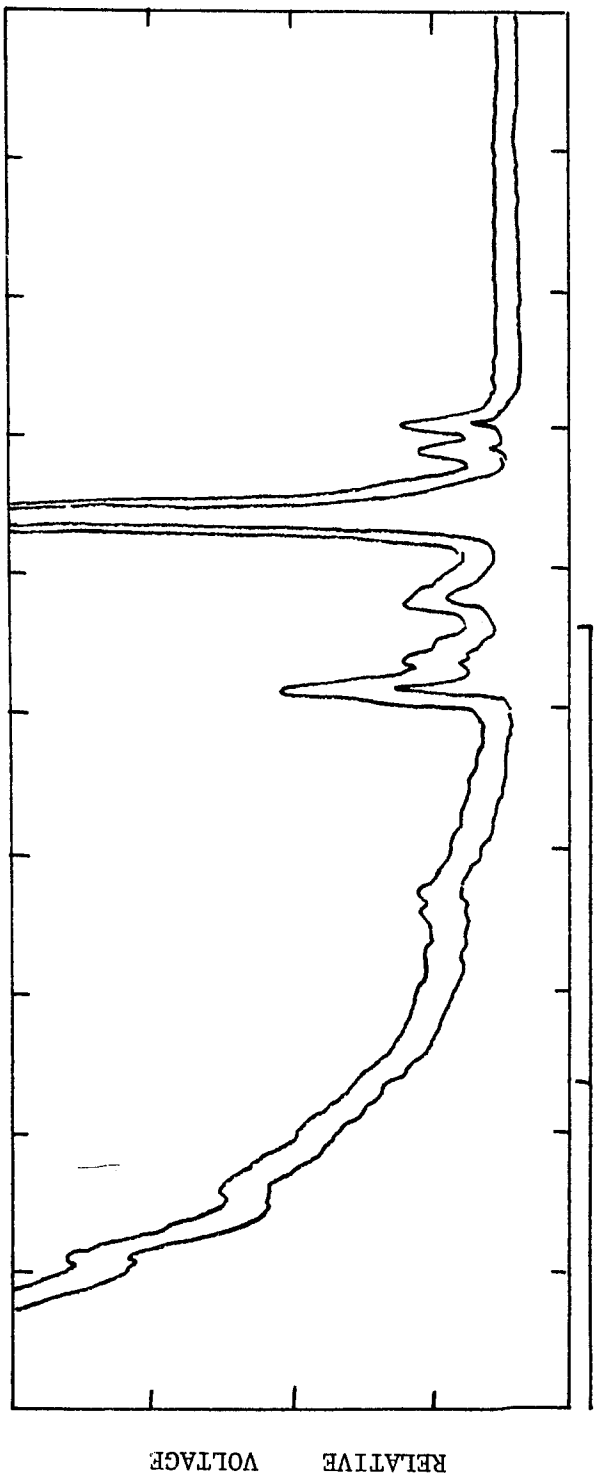

Fig. 30 Voltage across the photomultiplier load resistor versus altitude of scattering volume for backscatter from cirrostratus clouds on May 8, 1968 at 2:34 p.m.

the vertical structure of the cloud at horizontal displacements of 3039 feet. In view of the winds in the region of the cirrostratus, the resemblance of backscatter profiles taken at one minute intervals indicates that the vertical structure of the cirrostratus exhibited some temporal stability and spatial homogeniety. The average thickness of the individual layers agrees with Weickmann's data.

The backscatter records for cirrus clouds shown in Fig. 31 also exhibit the layered structure which has been found to be typical of cirrus type clouds. Although the cirrus usually consisted of thin layers, scattering layers as thick as two kilometers have been observed.

Figs. 32 and 33 are included because they show an interesting scattering phenomenon which could be important for cloud studies. The stable scattering layer evident in Fig. 32 near 6 km was observed over a period of one hour, and only minor changes were noted with the exception of the record shown in Fig. 33 in which cloud backscatter is evident. The magnitude and temporal behavior of the scattering layer would suggest that the scatterers were aerosol particles. The appearance of the cloud backscatter also suggests the presence of aerosol particles since particles in the size range 0.1 μ to 1 μ are particularly effective as cloud nucleating agents.

Other evidence also exists for the presence of appreciable concentrations of aerosol particles near 6 km. Rosen (1969) has measured the number density of aerosol particles above Wallops Island and found layers of particles at 0 - 5 km, 6.4 km and 9 - 25 km. The particle concentration at 6.4 km was 10 cm^{-3}. For a Junge distribution of parti-

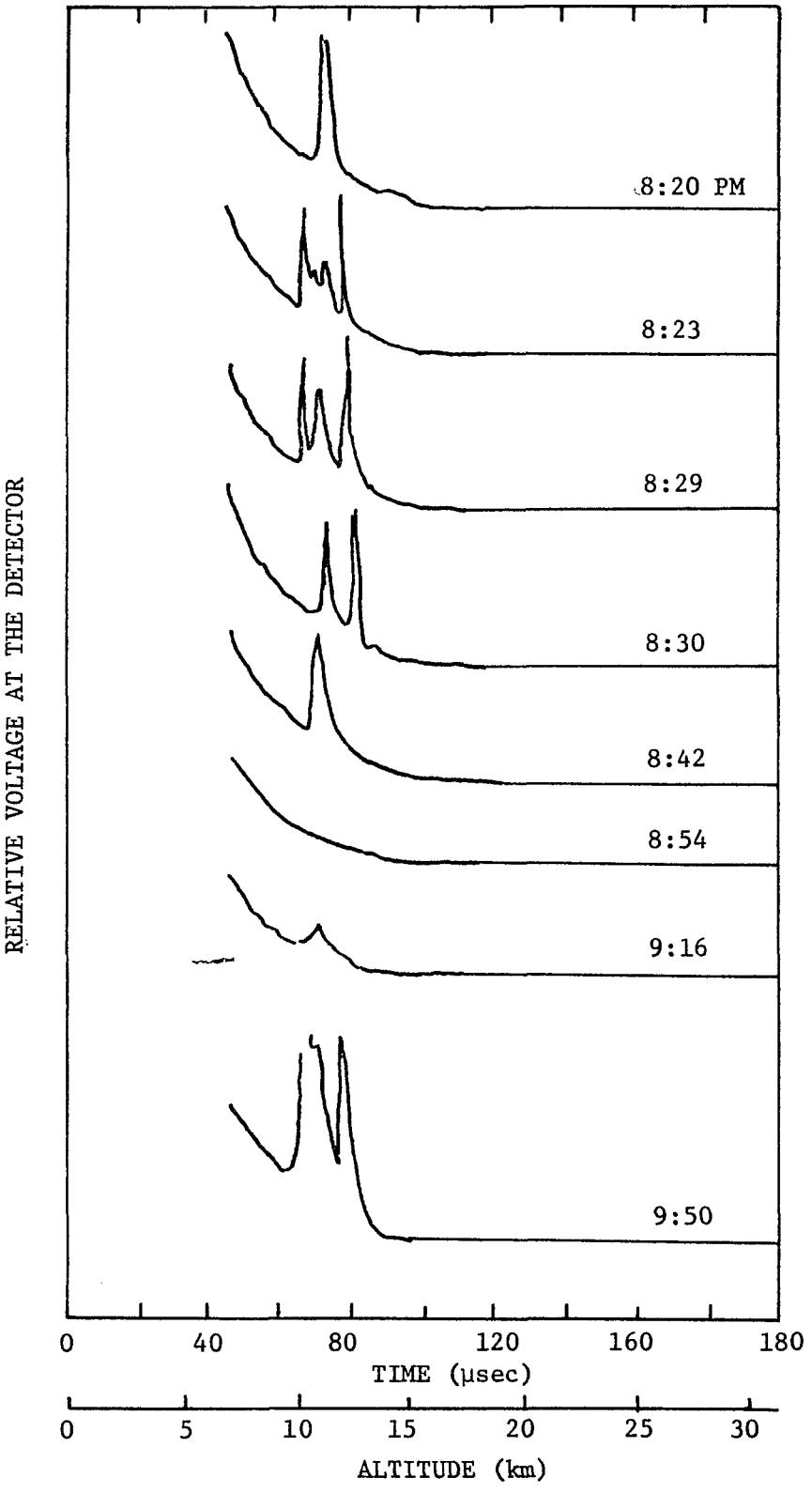

Fig. 31 Relative voltage at the detector versus altitude (time) for cirrus cloud backscatter.

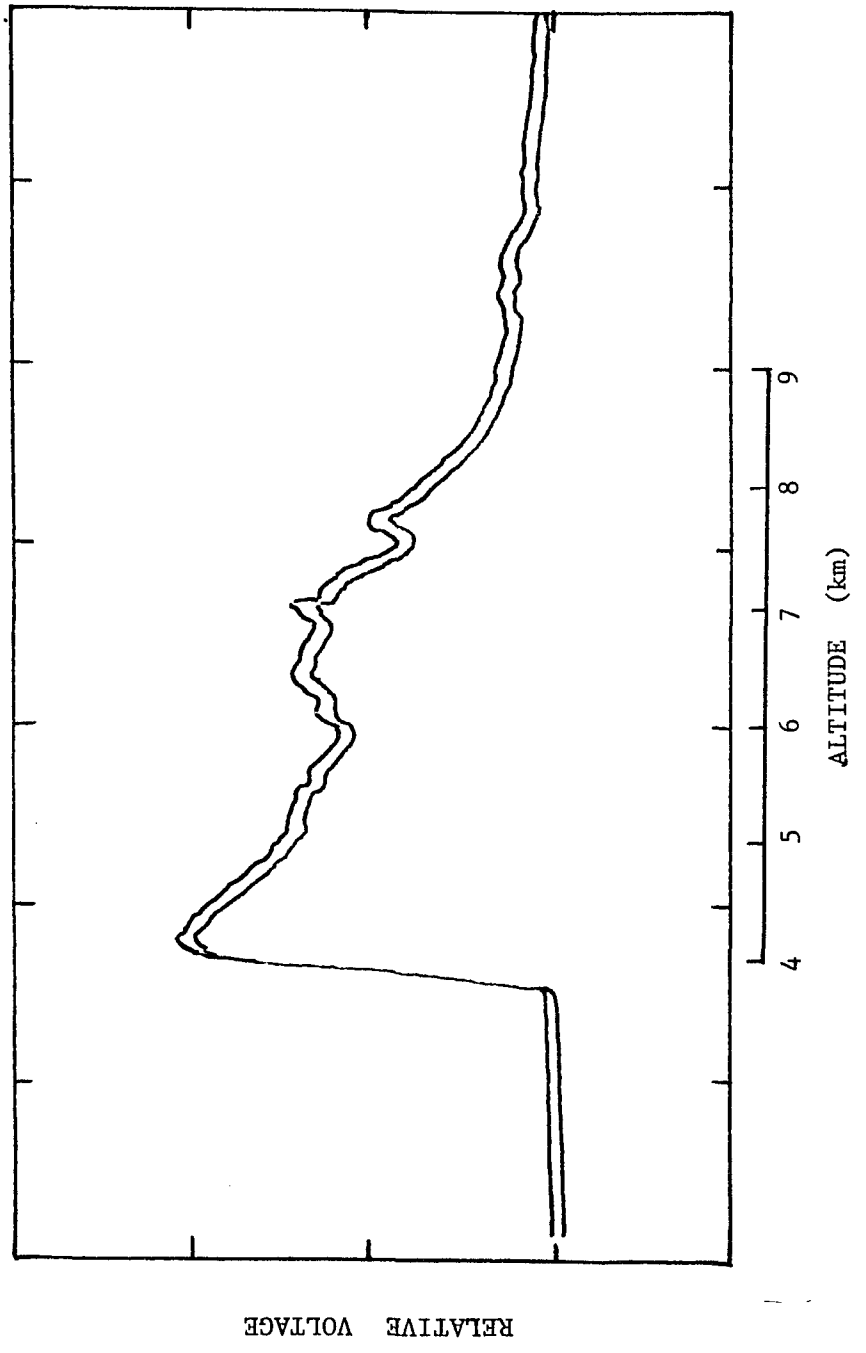

Fig. 32 Relative voltage across the photomultiplier load resistor versus altitude prior to appearance of cloud backscatter.

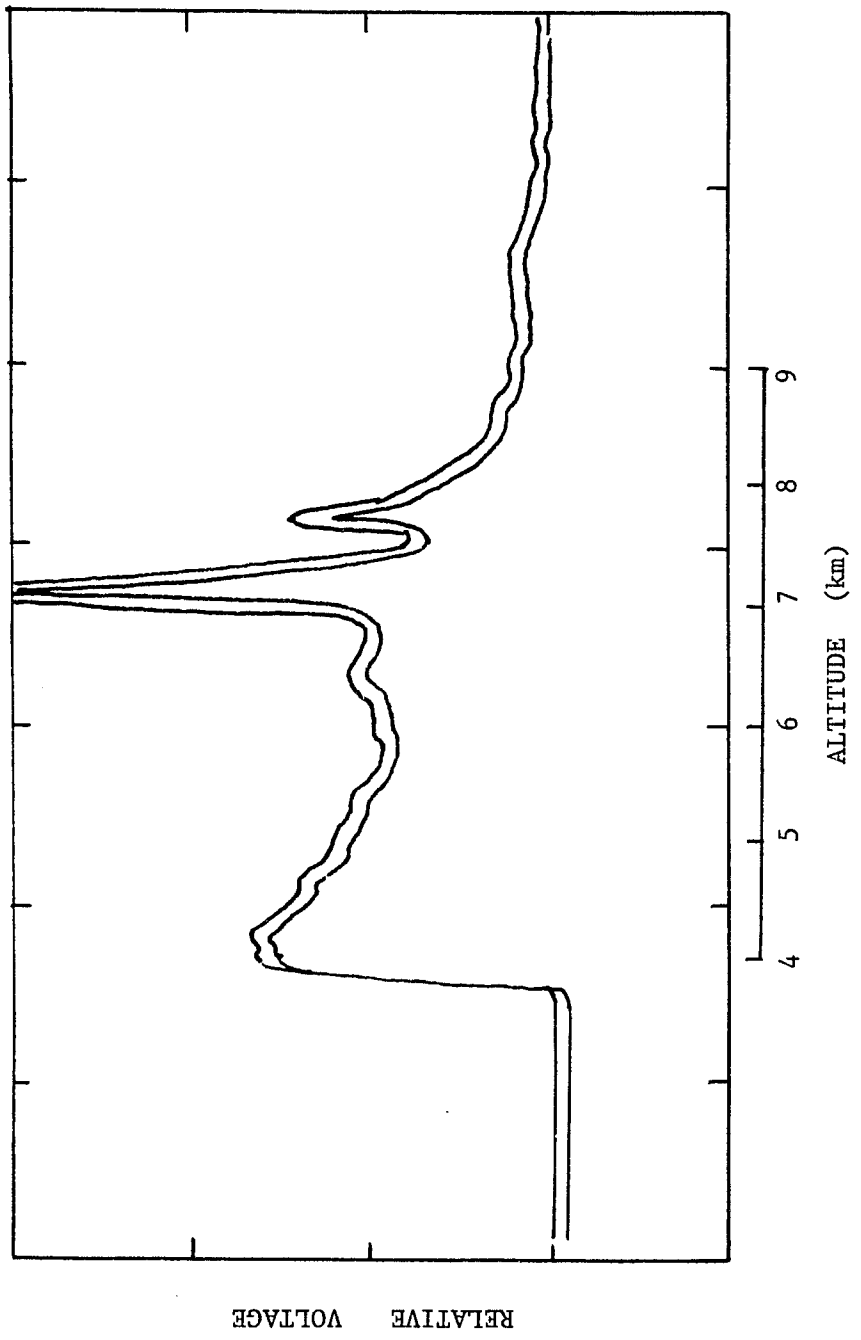

Fig. 33 Relative voltage across the photomultiplier load resistor versus altitude. Cloud backscatter is evident at 6 km.

cles ranging in size from .08 μ to 10 μ with a size distribution parameter $\nu = 3$, the average differential backscatter cross section per particle is 3.02×10^{-11} cm^2 sr^{-1} ($\lambda = 6943A$). The volume backscatter cross section for a concentration of 9 particles/cm^3 would equal 1/10 of the molecular volume backscatter cross section and produce a discernable enhancement in the backscattered signal.

It appears, therefore, that concentrations of aerosol particles of the order of those measured by Rosen at Wallops Island near 6 km could produce sufficient backscatter to explain the scattering feature in Figs. 32 and 33. It is also recognized that other explanations of the enhanced scattering at 6 km are possible, but it is felt that the correlation of Rosen's direct particle sampling data with the altitude of the scattering enhancement is particularly noteworthy.

VI. CONCLUSIONS

A sensitive and versatile optical radar system has been developed using the 31 inch RT-2 telescope at NASA, Wallops Island as a receiver. Optimization of the signal-to-noise ratio of the system has permitted the detection of laser backscatter from altitudes up to 80 km and operation of the system during daytime sky background conditions.

The development of interchangeable analog and digital receiver instrumentation has permitted the measurement of the backscattered signal over a range of five orders of magnitude, and measurements of the relative volume backscatter cross section of the atmosphere have been made over the complete range of 10 km to 80 km.

In the 10 - 25 km region, measurements of the relative volume backscatter cross section of the atmosphere above Wallops Island, Va. (38° N latitude) have shown general agreement with similar measurements performed by investigators at other locations (Massachusetts, New Mexico, West Indies). The agreement of the Wallops Island data with that of Fiocco, Clemesha, Goyer, and Watson emphasizes the temporal and spatial uniformity which appears to be characteristic of the lower stratospheric aerosol scattering. Fiocco and Grams studied the temporal characteristics of the "20 km layer" during 1964 and 1965, and all of the measurements of the relative volume backscatter cross section of the layer reported to date fall within the range of fluctuations observed by Fiocco and Grams.

It has been demonstrated that optical radar systems can accurately

detect aerosol layers in the stratosphere and measure their temporal and spatial variations in altitude, thickness, and scattering intensity. Attention should now be focussed on quantitative measurements of parameters such as aerosol number density, size distribution, and index of refraction.

It is impossible to draw any conclusions concerning the temporal or spatial behavior of the aerosol particles near the mesopause with the limited amount of laser backscatter data which is now available. The experiments have significance, however, in the following respects:

(1) The detection of scattering layers near the mesopause with existing optical radar systems indicates that studies of the temporal and spatial behavior of the aerosol content of the upper atmosphere should be feasible with optical radar systems employing high energy, high repetition rate lasers and fast data acquisition systems.

(2) The fact that all investigators using optical radar techniques have obtained a good fit of their data to a molecular scattering curve in the 30 - 60 km region strongly suggests that aerosol scattering is unimportant in this region. If this is correct, laser backscatter measurements could be used to monitor seasonal and diurnal changes of the molecular density in this region. Measurements of the transmissivity of the lower atmosphere would also be feasible.

(3) The correlation of the altitude range of the observed scattering layers (70 - 80 km) with other atmospheric

phenomena (noctilucent clouds, the sodium layer) provides support for continued systematic studies of laser backscatter from the upper atmosphere.

This research has demonstrated that the optical radar can be an effective meteorological tool for both daytime and nighttime cloud studies. Significant aerosol scattering and sporadic cloud backscatter has been observed at 6 km. Rosen (1969) also observed a relatively dense particle layer at 6 km above Wallops Island, Va. These measurements are particularly noteworthy because aerosol scattering is usually considered to be negligible with respect to molecular scattering in the 4 - 10 km region of the atmosphere. It is suggested that photographic observations of halos, coronae and Tyndall spectra be employed in conjunction with daytime backscatter studies of thin cloud formations. In some cases the average particle size could be inferred from such observations. Optical radar measurements of the backscattered intensity would then permit estimates to be made of the cloud particle density.

VI. APPENDICES

A. Computer Ray Trace Program

The signal-to-noise ratio of an optical radar system can be improved if auxiliary optics are used to reduce the laser beam divergence. Better collimation of the laser beam enables one to decrease the field of view of the receiver, thereby reducing the sky background noise without loss of signal (the transmission of the auxiliary optics is approximately 99 percent). This technique is essential for effective operation under daytime sky background conditions.

A computer ray tracing program was written and used to determine the design parameters for a laser beam collimator. The program was used to determine the effect of f number , magnification and laser wavelength on the residual spherical aberration of the collimator. All other aberrations can be neglected for this system if small f numbers are avoided.

The Galilean lens configuration was chosen for its simplicity and lack of a real primary focus (Q-switched lasers can ionize air when focussed). The design approach was based upon the partial concellation of the positive spherical aberration of the positive lens by the negative spherical aberration of the negative lens. A subprogram was written to calculate the longitudinal spherical aberration for a single lens, assuming incident parallel light. The in-

cident light was represented by five parallel rays. The computer was programmed to repeat the calculations, increasing the shape factor after tracing each set of five rays. The radii of the lens surfaces were calculated for each shape factor. Input data for this program included: the index of refraction of the optical material (PINDEX), the axial thickness of the lens (THICK), the initial shape factor (QFAC), the final shape factor (QMAX), the shape factor increment (QINC*QMAX), and the focal length (FOCAL). The calculations could be terminated at a specified shape factor (XLENS = 10.), or when the aberration reached a minimum (XLENS = 1.).

The magnification and length of the collimator are first specified, and the corresponding paraxial focal lengths for the positive and negative lenses over a range of shape factors. The radii r_1 and r_2 are chosen for the positive lens of minimum spherical aberration. The negative lens is then chosen such that the longitudinal spherical aberration of a marginal ray is equal and opposite to the marginal aberration of the positive lens.

The radii of all the lens surfaces are now known. With this information plus the lens separation distance, the main computer program traces the five rays through the complete two-element lens system. The program automatically adjusts the lens separation for negligible aberration of a marginal ray. With the lens separation fixed, the four additional rays are then traced through the system, and the angle between the emerging ray and the lens system axis is calculated for each ray.

The residual spherical aberration of a corrected collimator is compared with a collimator composed of equiconvex and equiconcave lenses in Fig. 11. The specifications of the 5:1 laser beam collimator used in this experiment are shown in Fig. 34.

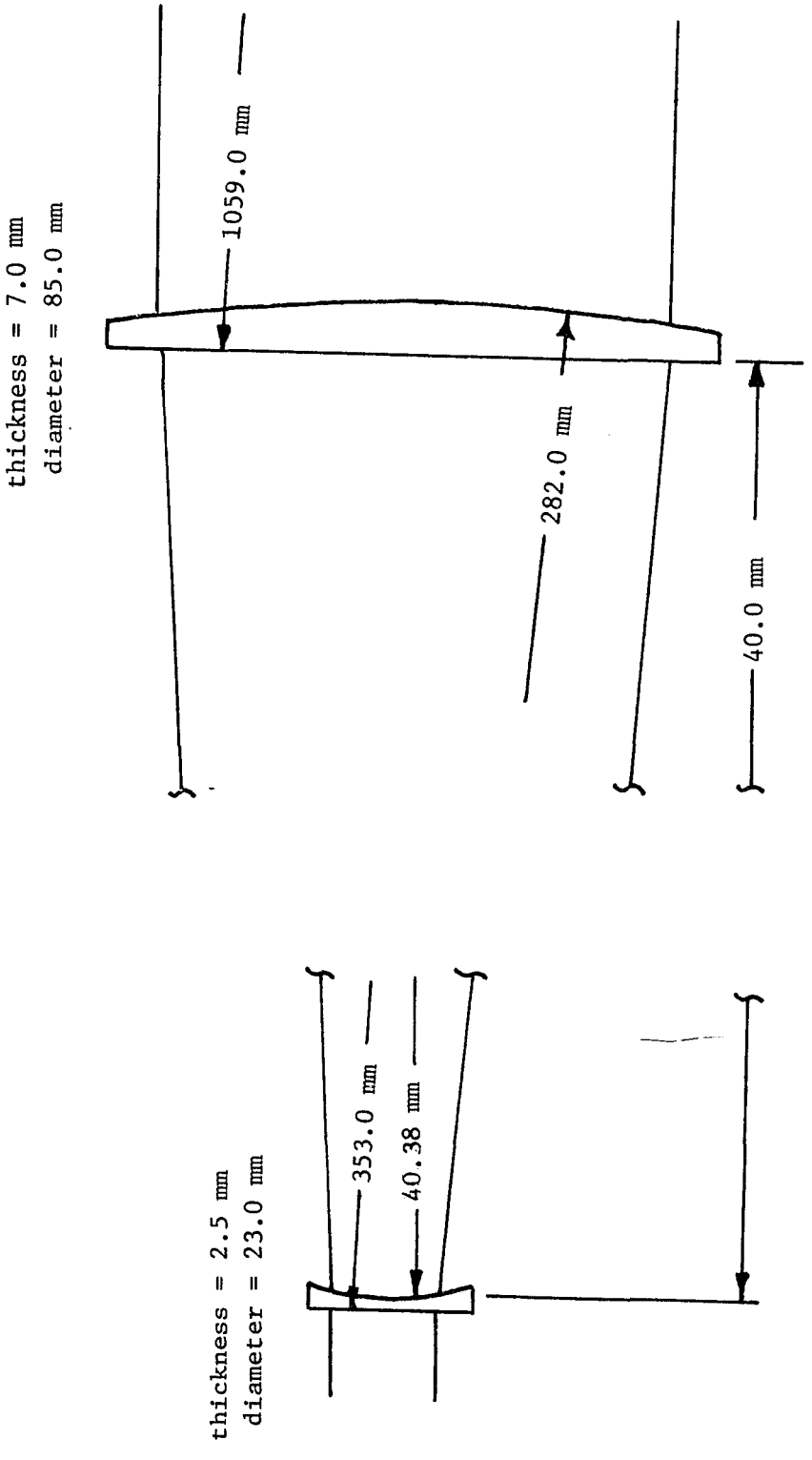

Fig. 34 Specifications of lenses of 5:1 laser beam collimator.

```
// EXEC FORTRAN
      DOUBLE PRECISION THETA1,FH,THETA2,FH2,SEP,S1,X1,X2,X3,S2,X4,X5,
     1 THETAR,DEV,TEST,XTHETA,ASIN,THETA3,FH3,THETA4,FH4
      DOUBLE PRECISION S16,S17,S5,S6,S8,S9,S11,S12,S14,S15
      COMMON S16,S17,FH2,THETA2,FH3,THETA3,FH4,THETA4,FH,THETA1,PINDEX,
     1HMAX
      ASIN(X)=DATAN(X/DSQRT(1.-X**2))
C
C          LENS 6 IS A MODIFICATION OF LENS 5 DP WHICH INCLUDES
C          LENS 2A AS A SUBROUTINE.   6ENS 2A IS USED FIRST TO
C          DETERMINE Q FOR THE NEG. LENS AND R1 AND R2 FOR THE
C          POSITIVE.   LENS 6 WILL THEN CALCULATE THE RESIDUAL
C          SPHERICAL ABERRATION OF THE TWO-ELEMENT LENS SYSTEM
C          A COMMON STATEMENT IS USED TO CARRY THE DATA FROM LENS 2A
C          TO LENS 5.
C
C
C
C          SUBROUTINE INPUT DATA***
C          AIR INDEX,H(MAX),NEG LENS THICKNESS,LENS INDEX,QINC, QMAX,
C          (QINC*QMAX=SHAPE FACTOR INCREMENT), NEG LENS FOCAL LENGTH,
C          LOWER Q LIMIT, MODEOF OPERATION.
C
C          MAIN INPUT***
C          R1,R2, POS. LENS THICKNESS, LENS SEPARATION.
C
C
C
      CALL TWOA
C
      J=1
      K=1
      M=1
      N=1
      X=.00005
  100 READ(1,1)R1,R2,THICK,SEP
C
C           FH IS THE FOCAL LENGTH OF THE FIRST ELEMENT FOR A
C           PARTICULAR H.  THETA1 IS THE ANGLE OF INTERCEPTION OF A
C           FOCUSSED RAY WITH THE AXIS.  THE INPUT VARIABLE SEP
C           REFERS TO THE ALGEBRAIC SUM OF THE PARAXIAL FOCAL LENGTHS
C           REFERENCE    JENKINS & WHITE
C
      H=HMAX
  200 WRITE(3,2)
  300 WRITE(3,3)THETA1,PINDEX,R1,R2,THICK,FH,HMAX,SEP,THETA3,FH3,
     1THETA2,FH2,THETA4,FH4
  325 WRITE(3,5)
  354 GO TO 360
  355 SEP=SEP+X*SEP
C
C           SEP IS THE SEPERATION OF THE ADJACENT LENS SURFACES
```

```
C
C           BEGIN RAY TRACE CALC FOR FIRST SURFACE
C
  360 S1=SEP+(-FH)
      X1=((R1+S1)/R1)*DSIN(THETA1)
      X2=(1./PINDEX)*X1
      XTHETA=ASIN(X2)+THETA1-ASIN(X1)
      X3=DSIN(XTHETA)
      S2=(R1*X2/X3)-R1
C
C           BEGIN RAY TRACE CALC FOR SECOND SURFACE
C
      S2=S2+THICK
      X4=((S2+R2)/(-R2))*X3
      X5=(PINDEX/1.)*X4
      THETAR=ASIN(X4)+XTHETA
      DEV=(THETAR-ASIN(X5))*1000.
C
      IF(N-1000)363,362,362
  362 WRITE(3,4)H,DEV,SEP
  363 CONTINUE
C
      IF(N-3)365,390,390
C
C           THIS IF STATEMENT BYPASSES THE TEST WHEN THE PROPER SIGN
C           HAS BEEN DETERMINED FOR X
C
  365 GO TO (370,380,390), N
C
C           THE COMPUTED GO TO CAUSES A COMPARISON OF THE FIRST AND
C           SECOND PASSES TO DETERMINE SIGN OF X
C
  370 TEST=DEV
      N=N+1
      GO TO 355
  380 N=N+1
      IF(DABS(TEST)-DABS(DEV))385,355,355
  385 X=-X
      GO TO 355
  390 IF(N-1000)395,600,650
  395 IF(DABS(DEV)-.1)400,400,355
C
C           THIS IF STATEMENT INCREMENTS THE LENS SEPARATION BY A
C           SMALLER NUMBER (1/10) WHEN THE DEVIATION ANGLE BECOMES
C           LESS THAN 0.1 MILLIRADIAN
C
  400 M=M+1
      IF(M-2)356,356,357
  356 X=.1*X
      GO TO 355
  357 WRITE(3,4)H,DEV,SEP
  358 IF(DABS(DEV)-.001)500,500,510
  510 IF(DEV-0.0)355,355,500
C
C           THIS IF STATEMENT DETERMINES THE LENS SEPARATION FOR
C           MARGINAL ZONE CORRECTION
```

```
C
  500 WRITE(3,6)SEP
C
      H=.707*HMAX
      THETA1=THETA2
      FH=FH2
      N=1000
      GO TO 360
C
  600 H=.5*HMAX
      THETA1=THETA3
      FH=FH3
      N=1500
      GO TO 360
C
  650 K=K+1
      GO TO (670,660,670), K
  660 H=.2*HMAX
      THETA1=THETA4
      FH=FH4
      N=1500
      GO TO 360
C
    1 FORMAT(F20.8,F20.8,F20.8,D20.8)
    2 FORMAT('0',T3,'THETA1',T14,'PINDEX',T25,'R1',T36,'R2',T47,'THICK'
     1 ,T58,'FH',T69,'H',T80,'SEP',T91,'N',T102,'X',T112,'THETA2',T
     1 121,'FH2')
    3 FORMAT(D20.8,F20.8,F20.8,F20.8,F20.8,D20.8//F20.8,D20.8,D20.8,
     1D20.8,D20.8,D20.8/D20.8,D20.8//)
    4 FORMAT(10XF10.5,D20.8,D20.8)
    5 FORMAT('0',T18,'H',T31,'DEVIATION')
    6 FORMAT('0',T12,'THE SEPARATION FOR MARGINAL ZONE CORRECTION
     1 IS,'D20.8)
C
  670 END
/*
// EXEC FORTRAN
      SUBROUTINE TWOA
      DOUBLE PRECISION S16,S17,S5,S6,S8,S9,S11,S12,S14,S15
      DOUBLE PRECISION DIFF(100),ASIN,Q,P,PS1,PS2,ARG,THETA,P2S2,
     1 PAR(100),DIFF1,DIFF2,H,DIF(100),DIFF3
      COMMON S16,S17,S5,S6,S8,S9,S11,S12,S14,S15,PINDEX,HMAX
C
C           RAY TRACE PROGRAM FOR SHERICAL ABERRATION
C           PARALLEL RAYS ARE TRACED THROUGH THE LENS, AND SUCCESSIVE
C           CALCULATIONS CAN BE MADE WITH INCREMENTED SHAPE FACTOR
C           (QFAC(M)).  QFAC(M) CAN BE INCREMENTED BETWEEN TWO LIMITS
C           (QFAC(2) TO QMAX), OR THE PROGRAM CAN BE MADE TO STOP WHEN
C           THE ABERRATION REACHES A MINIMUM.
C
C           FIVE RAYS ARE TRACED DENOTED BY HMAX, .00001*HMAX, .707*HMAX,
C           .5*HMAX, AND .2*HMAX.
C
C           OUTPUT CONSISTS OF FOCAL LENGTH, LONGITUDINAL SPHERICAL
C           ABERRATION,   AND THE ANGLE OF INTERSECTION OF EACH RAY
```

```
C          WITH THE AXIS. RADII OF THE SURFACES AND THE CORRESPONDING
C          SHAPE FACTORS ARE ALSO PRINTED OUT.
C
C          TWO MODES OF OPERATION ARE AVAILABLE DEPENDING ON THE VALUE
C          OF XLENS.
C             1)INCREMENT QFAC(M) FROM QFAC(2) TO QMAX IN STEPS OF
C               QINC*QMAX.
C             2)SAME AS 1), BUT STOP WHEN ABERRATION MINIMIZED.  SET
C               XLENS = 1..
C
C          DEFINITION OF SYMBOLS:
C             VINDEX = INDEX OF MEDIUM
C             PINDEX = INDEX OF OPTICAL MATERIAL
C             TMICK = AXIAL THICKNESS OF LENS
C             FOCAL = PARAXIAL FOCAL LENGTH (.00001*HMAX)
C             H = DISTANCE OF PARALLEL INPUT RAY ABOVE AXIS.
C             R1 = FIRST LENS RADIUS
C             R2 = SECOND LENS RADIUS
C
      DIMENSION R1(100), R2(100), QFAC(100)
      ASIN(X)=DATAN(X/DSQRT(1.-X**2))
      M=2
      DIFF(1)=1000.
  100 READ(1,12)UINDEX,HMAX,THICK,PINDEX,XINC,QINC,QMAX,FOCAL,QFAC(2)
     1 ,XLENS
      WRITE(3,11)
      WRITE(3,14)UINDEX,HMAX,THICK,PINDEX,XINC,QINC,QMAX,FOCAL,QFAC(2)
     1 ,XLENS
  625 WRITE(3,13)QFAC(M)
      R1(M)=2.*FOCAL*(PINDEX-1.)/(QFAC(M)+1.)
      R2(M)=2.*FOCAL*(PINDEX-1.)/(QFAC(M)-1.)
  125 WRITE(3,10)R1(M),R2(M)
C
C          BEGIN CALCULATION OF PARAXIAL FOCAL LENGTH
C
      N=1
      H=.00001*HMAX
  600 WRITE(3,7)
  250 Q=UINDEX*H/(PINDEX*R1(M))
      P=DSIN(ASIN(Q)-ASIN(H/R1(M)))
      PS1=-(R1(M)*Q/P)+R1(M)
      PS2=PS1-THICK
      PS2=-PS2
      ARG=((PINDEX/UINDEX)*((R2(M)+PS2)/R2(M))*P)
      THETA=(ASIN(ARG)+ASIN(P)-ASIN((R2(M)+PS2)*P/R2(M)))
      P2S2=-((R2(M)*ARG)/(DSIN(THETA)))+R2(M)
      GO TO (310,320,322,325,330), N
  310 PAR(M)=P2S2
      DIFF1=PAR(M)-P2S2
  275 WRITE(3,15)H,PAR(M),DIFF1,THETA
      S16=PAR(M)
      S17=THETA
      H=.707*HMAX
      N=N+1
      GO TO 250
```

```
  320 DIFF2=PAR(M)-P2S2
      WRITE(3,5)H,P2S2,DIFF2,THETA
      S5=P2S2
      S6=THETA
      H=.5*HMAX
      N=N+1
      GO TO 250
  322 DIFF3=PAR(M)-P2S2
      WRITE(3,5)H,P2S2,DIFF3,THETA
      S8=P2S2
      S9=THETA
      H=.2*HMAX
      N=N+1
      GO TO 250
  325 DIF(M)=PAR(M)-P2S2
      WRITE(3,5)H,P2S2,DIF(M),THETA
      S11=P2S2
      S12=THETA
      H=HMAX
      N=N+1
      GO TO 250
  330 DIFF(M)=PAR(M)-P2S2
      WRITE(3,5)H,P2S2,DIFF(M),THETA
      S14=P2S2
      S15=THETA
      IF(XLENS-10.)626,627,627
  626 IF(DABS(DIFF(M))-DABS(DIFF(M-1)))628,628,710
  627 IF(DABS(QFAC(M))-DABS(QMAX+QINC*QMAX))628,750,750
  628 M=M+1
  500 QFAC(M)=QFAC(M-1)+(QINC*QMAX)
      GO TO 625
  710 WRITE(3,16)DIFF(M-1),R1(M-1),R2(M-1),QFAC(M-1)
C
    5 FORMAT(D20.6,10XD20.8,D20.8,D20.8)
    7 FORMAT(16X5HH(CM)15X5HFOCAL1X6HLENGTH1X4H(CM)9X10HDIFFERENCE
     1 9X10HTHETA(RAD))
   10 FORMAT(' R1 AND R2 ARE, RESP.,',2XE12.5,2X,'AND',2XE12.5/)
   11 FORMAT(T1,'0 UINDEX',T15,'HMAX',T25,'THICK',T33,'PINDEX',
     1  T45,'XINC',T55,'QINC',T65,'QMAX',T75,'FOCAL',T85,'QFAC')
   12 FORMAT(8F10.5)
   13 FORMAT('0THE SHAPE FACTOR NOW EQUALS',2XF8.4)
   14 FORMAT(9F10.5)
   15 FORMAT(D20.6,10XD20.8,D20.8,D20.8)
   16 FORMAT('0',D15.8,10XE12.5,10XE12.5,10XF8.4)
C
  750 END
```

B. Beam Crossover Program

Fig. 35 shows the geometry for the optical radar transmitter and receiver beams. A_a is the cross sectional area which determines the size of the scattering volume.

$$\Delta V = \frac{\pi}{8}(z\Theta_L)^2 c\gamma$$

where Θ_L is the laser beam divergence (full-angle), c is the speed of light, γ is the laser pulse duration and z is the altitude. Interpretation of the backscattered signal from low altitudes requires a knowledge of the effect of the initial crossover of the laser beam with the receiver field of view on the size of the scattering volume. This can be determined if the area of intersection of the receiver and laser beams is known as a function of altitude. A computer program was written to calculate this area for an arbitrary laser radar system where the laser and receiver axes are separated. Fig. 36 defines the symbols used in the program, and the input parameters are as follows:

DISP	= The displacement of the laser and receiver axes
DIA	= The receiver diameter
THETAL	= The laser beam divergence half-angle
ANGLE	= The laser beam misalignment angle
ZINC (1)	= The initial altitude increment

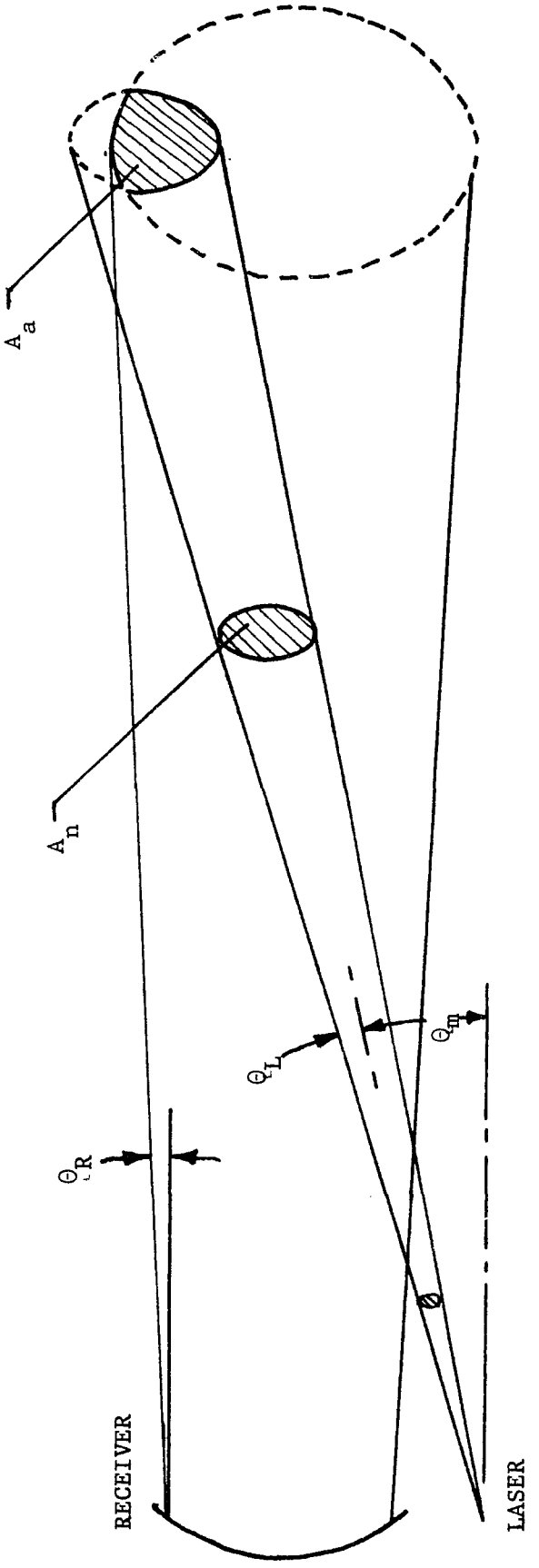

Fig. 35 Beam crossover geometry. Θ_m = misalignment angle, A_n = normal scattering area, and A_a = actual scattering area.

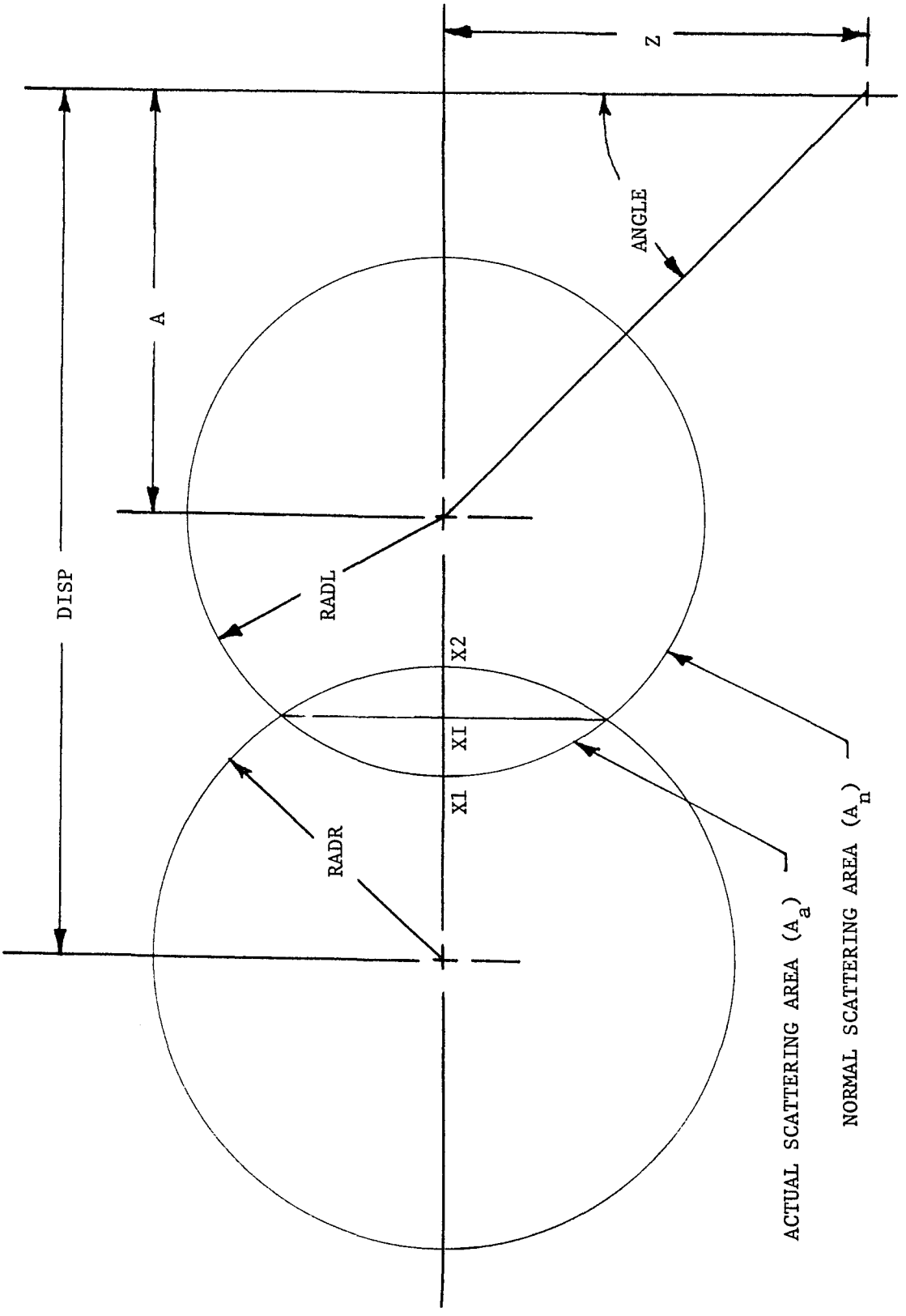

Fig. 36 Definition of variables used in beam crossover computer program.

THETAR = The receiver field of view half-angle

ZMAX = Maximum altitude.

The output data was in the form of the fractional scattering area (actual scattering area/normal scattering area) for altitudes from z = 0 to z = ZMAX. The normal scattering area is the cross sectional area of the laser beam. Fig. 37 shows the percentage normal scattering area for three different optical configurations in the region of the low altitude crossover. A high altitude effect caused by a misalignment of the laser beam is shown in Fig. 38. The results cannot be used for a quantitative interpretation of data in the crossover region because the assumption of uniform intensity across the laser beam is unrealistic. The results do give, however, a useful indication of the qualitative effects of beam misalignment and the altitude of beam crossover.

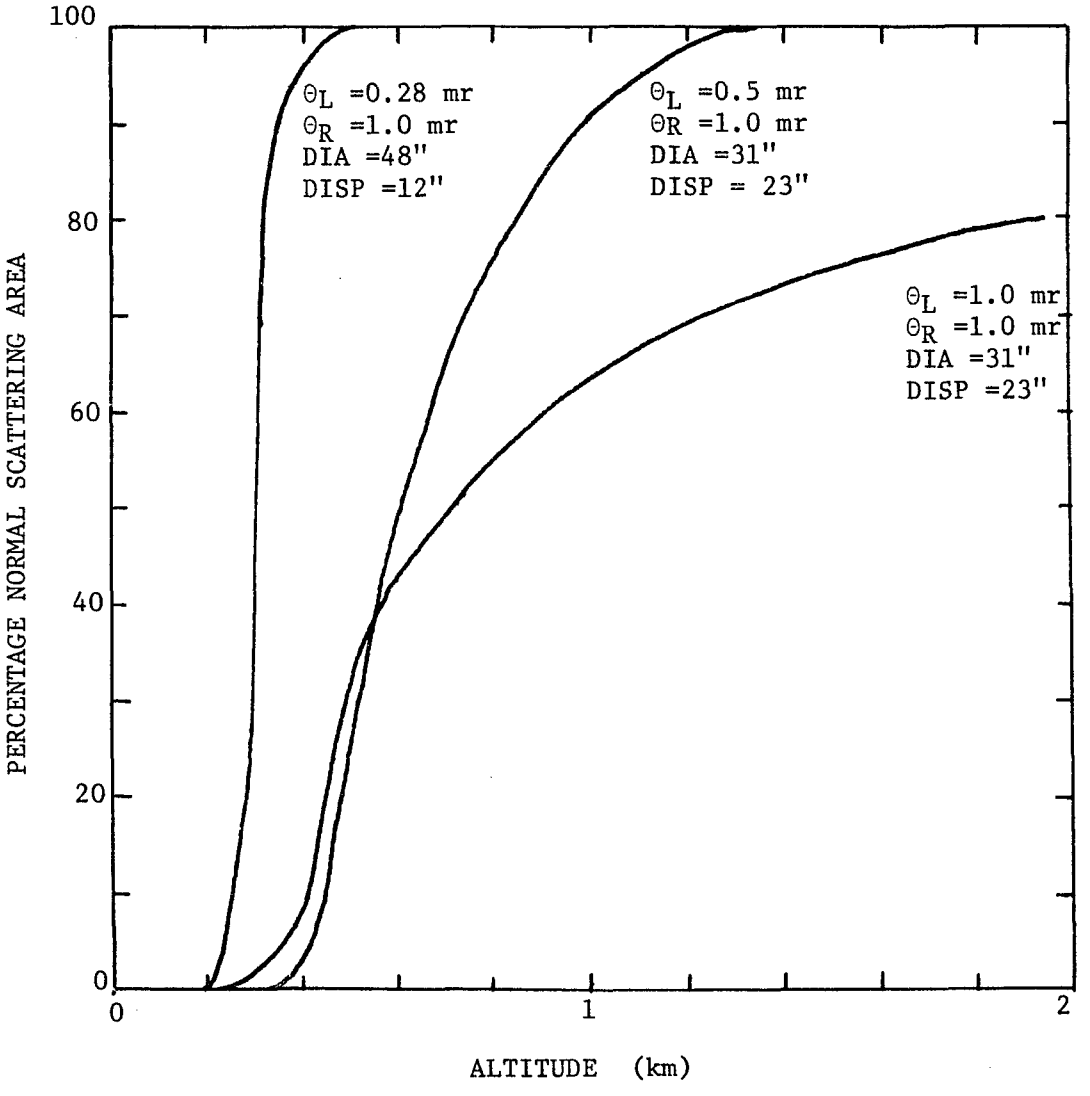

Fig. 37 Percentage normal scattering area versus altitude for three optics configurations.

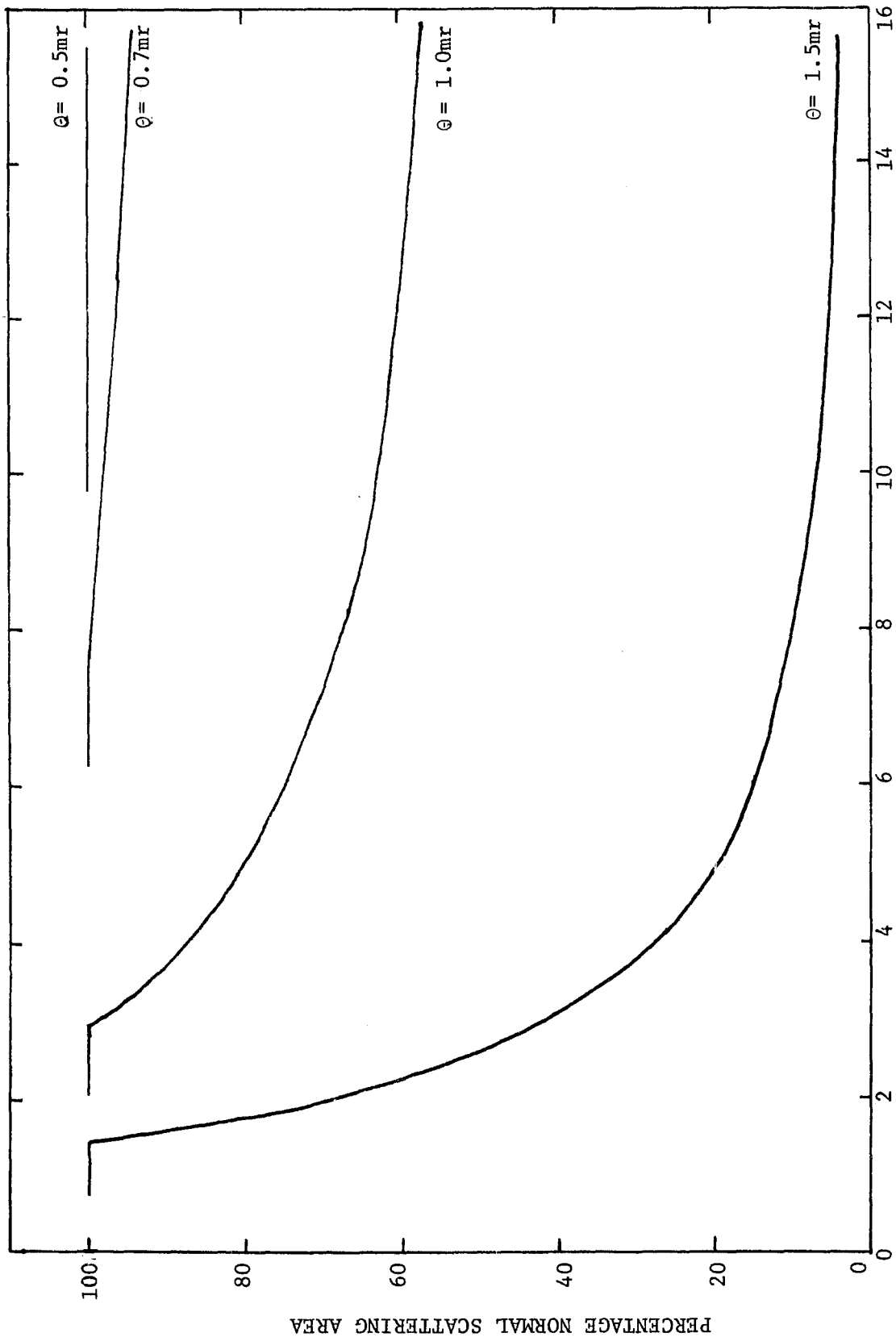

Fig. 38 The percentage normal scattering area versus altitude for Θ_L=0.5 mr, Θ_R=1.0 mr, and laser misalignment angle Θ =0.5, 0.7, 1.0, and 1.5 mr. The initial beam overlap is similar for all four curves and is not shown.

```
// EXEC FORTRAN
C     BEAM CROSSOVER PROGRAM
C
C     THE RATIO OF THE ACTUAL SCATTERING AREA TO THE NORMAL SCATTERING
C     AREA IS COMPUTED AS THE ALTITUDE IS INCREMENTED.  THE PROGRAM
C     WILL HANDLE A GENERAL BI-STATIC LASER RADAR, EITHER ALIGNED
C     OR INTENTIONALLY MISALIGNED.
C
      DOUBLE PRECISION DISP, DIA, THETAL, THETAR, ANGLE, Z, A, TA,
     1TDISP, RADL, RADR, REF, FRAC, X1, X2, XI, DELTAX, AREA(20),
     1X(20), Y(20), AREA1, XAREA(20), XP(20), YP(20), AREA2,
     1TAREA, ZINC(2), ZMAX
      DIMENSION Q(2)
      Q(1)=-1.
      Q(2)=1.
      K=1
  100 READ(1,1)DISP,DIA,THETAL,THETAR,ANGLE,ZINC(1),ZMAX
  125 WRITE(3,2)DISP,DIA,THETAL,THETAR,ANGLE,ZINC(1),ZMAX
      ZINC(2)=5.*ZINC(1)
      Z=ZINC(1)
  150 A=ANGLE*Z
      TA=A+1000.
      TDISP=DISP+1000.
      RADL=(Z/DCOS(ANGLE))*THETAL
      RADR=(DIA/2.)+(Z*THETAR)
      REF=3.14*(RADL**2)
      IF((RADL+A)-(DISP-RADR))155,175,175
  155 FRAC=.0
  160 WRITE(3,5)Z,REF,FRAC
      Z=Z+ZINC(K)
      GO TO 150
  175 X1=TA+RADL
      X2=TDISP-RADR
C 177 WRITE(3,7)RADL,TDISP,RADR,TA
C   7 FORMAT(4D20.6)
  180 XI=((RADR**2)-(RADL**2)-(TDISP**2)+TA*TA)/(-2.*TDISP+2.*TA)
      DELTAX=.1*DABS(X1-XI)*Q(K)
  190 WRITE(3,8)DELTAX,X1,XI,X2,RADR,RADL
    8 FORMAT(6D14.6)
      AREA(1)=0.0
      X(1)=X1
  200 DO 300 I=2,11
      X(I)=X(I-1)+DELTAX
      Y(I)=DSQRT((RADL**2)-(X(I)-TA)**2)
      AREA(I)=DABS(DELTAX)*Y(I)+AREA(I-1)
C     WRITE(3,9)Y(I),AREA(I),X(I)
  300 CONTINUE
C   9 FORMAT (3D14.6)
      AREA1=2.*AREA(I)
C 350 WRITE(3,5)Z,REF,AREA1
      DELTAX=.1*DABS(XI-X2)*Q(K)
  400 DO 500 J=2,10
```

```
      XAREA(1)=0.0
      XP(1)=XI
      XP(J)=XP(J-1)+DELTAX
      YP(J)=DSQRT((RADR**2)-(XP(J)-TDISP)**2)
      XAREA(J)=DABS(DELTAX)*YP(J)+XAREA(J-1)
C     WRITE(3,10)YP(J),XAREA(J),XP(J)
C  10 FORMAT('                    ',3D14.6)
 500  CONTINUE
      REF=3.14*(RADL**2)
      AREA2=2.*XAREA(J)
      TAREA=AREA1+AREA2
      FRAC=TAREA/REF
      WRITE(3,6)Z,REF,FRAC
      IF(Z-ZMAX)510,900,900
 510  Z=Z+ZINC(K)
      GO TO (525,550),K
 525  RADR=(DIA/2.)+(Z*THETAR)
      A=ANGLE*Z
      TA=A+1000.
      RADL=(Z/DCOS(ANGLE))*THETAL
      IF((A-RADL)-(DISP-RADR))150,600,600
 550  RADR=(DIA/2.)+(Z*THETAR)
      A=ANGLE*Z
      TA=A+1000.
      RADL=(Z/DCOS(ANGLE))*THETAL
      X2=TDISP+RADR
      X1=TA-RADL
      IF((A-RADL)-(DISP+RADR))180,800,800
 600  A=ANGLE*Z
      RADL=(Z/DCOS(ANGLE))*THETAL
      RADR=(DIA/2.)+(Z*THETAR)
      REF=3.14*(RADL**2)
      FRAC=1.
      WRITE(3,5)Z,REF,FRAC
      Z=Z+ZINC(K)
      RADL=(Z/DCOS(ANGLE))*THETAL
      RADR=(DIA/2.)+(Z*THETAR)
      IF((RADL+A)-(DISP+RADR))650,700,700
 650  IF(Z-ZMAX)660,900,900
 660  GO TO 600
 700  A=ANGLE*Z
      TA=A+1000.
      X1=TA-RADL
      X2=TDISP+RADR
      RADL=(Z/DCOS(ANGLE))*THETAL
      RADR=(DIA/2.)+(Z*THETAR)
      REF=3.14*(RADL**2)
      K=2
      GO TO 180
```

```
800 A=ANGLE*Z
    RADL=(Z/DCOS(ANGLE))*THETAL
    RADR=(DIA/2.)+(Z*THETAR)
    REF=3.14*(RADL**2)
    FRAC=.0
    WRITE(3,5)Z,REF,FRAC
    IF(Z-ZMAX)850,900,900
850 Z=Z+ZINC(K)
    GO TO 800
  1 FORMAT(5D14.8)
  2 FORMAT(7D15.8)
  5 FORMAT(D10.3,D20.8,2XD20.8)
  6 FORMAT(' ',D10.3,D20.8,'ACTUAL AREA/NORMAL AREA IS',D20.8)
900 END
```

C. Data Reduction Program

A computer program was written to facilitate the plotting and error analysis of the single photoelectron counting data. The output data from the counter memory system is in the form of a column of three digit numbers where each column represents the number of counts received in an 11 μsec time interval. This data was read into the computer from punched cards as an array where each column represented one laser shot. The desired quantities were z^2S and the end points of the error bars associated with S, where S is the total counts for each altitude interval and z is the altitude. The standard deviation of the number of signal counts is given by

$$\delta = (S+C_B)^{\frac{1}{2}}$$

where S is the number of signal counts and C_B is the number of background counts. The computer output was in the form of $z^2(S+\delta)$, z^2S, and $z^2(S-\delta)$ for each altitude interval.

```
// EXEC FORTRAN
      DIMENSION X(130,25),          XDELTA(130), SUMC(130), SUM(130),
     1 PT(130), TPT(130), BPT(130)
   10 READ(1,3) N, BACK, ZINI
    3 FORMAT(I5,F10.0,F10.0)
      READ(1,2)((X(I,J),I=1,128),J=1,N)
    2 FORMAT(16F5.0)
      DO 15 I=1,130
   15 SUM(I)=0.0
      Z=ZINI
      DO 50 I=1,112
      DO 30 J=1,N
      SUM(I)=SUM(I)+X(I,J)
   30 CONTINUE
      WRITE(3,5) Z, SUM(I)
    5 FORMAT(F8.2,10XF8.2)
      XDELTA(I)=SQRT(SUM(I))
      SUMC(I)=SUM(I)-BACK
      PT(I)=SUMC(I)*Z**2
      TPT(I)=(SUMC(I)+XDELTA(I))*Z**2
      BPT(I)=(SUMC(I)-XDELTA(I))*Z**2
   40 WRITE(3,4) Z, TPT(I), PT(I), BPT(I)
    4 FORMAT(F9.2,5XE20.8,5XE20.8,5XE20.8)
      Z=Z-1.65
   50 CONTINUE
   70 END
```

VII. REFERENCES

Alexander, W. M. and H. E. LaGow, 1960: Recent direct measurements of cosmic dust in the vicinity of the earth using satellites. Space Research, H. Kallmann-Bijl, ed., Amsterdam, North-Holland Publ. Co., 1033-1041.

Alexander, W. M., C. W. McCracken, L. Secretan and O. E. Berg, 1963: Review of direct measurements of interplanetary dust from satellites and probes. Space Research III, W. Priester, ed., Amsterdam, North-Holland Publ. Co., 891-917.

Bain, W. C. and M. C. W. Sandford, 1966: Backscattering from the upper atmosphere (70-160 km) detected by optical radar. Nature, 210, 826.

Bain, W. C. and M. C. W. Sandford, 1966a: Light scatter from a laser beam at heights above 40 km. J. Atmos. Terr. Phys., 28, 543-552.

Bigg, E. K., 1956: Detection of atmospheric dust and temperature inversions by twilight scattering. Nature, 177, 77-79.

Bowen, E. G., 1953: The influence of meteoritic dust on rainfall. Austral. J. Phys., 6, 490-497.

Broadfoot, A. L. and K. R. Kendall, 1968: The airglow spectrum, 3100-10,000 A. J. Geophys. Res., 73, 426-428.

Bullrich, K. 1964: Scattered radiation in the atmosphere and the natural aerosol. Advances in Geophysics No. 10, New York, Academic Press, 99.

Cadle, R. D., 1966: Particles in the atmosphere and space. New York, Reinhold Publ. Co.

Carrier, L. W., G. A. Cato and K. J. von Essen, 1967: The backscattering and extinction of visible and infrared radiation by selected major cloud models. Appl. Opt., 6, 1209-1216.

Chagnon, C. W. and C. E. Junge, 1961: The vertical distribution of sub-micron particles in the stratosphere. J. Meteor., 18, 746.

Chu, Chiao-Min and S. W. Churchill, 1955: Representation of the angular distribution of radiation scattered by a spherical particle. J. Opt. Soc. Amer., 45, 958-962.

Clemesha, B. R., et al., 1966: Laser probing the lower atmosphere. Nature, 209, 184-185.

Collis, R. T. H. and M. G. H. Ligda, 1966: Note on lidar observations of particulate matter in the stratosphere. J. Atmos. Sci., 23, 255-257.

Davari, N. B., 1964: The dust concentration in the upper layers of the earth's atmosphere. Geomagnetism and Aeronomy, USSR Acad. Sci., 4, 886-892.

Dubin, M., 1960: Meteoritic dust measured from Explorer I. Planet. Space Sci., 2, 121-129.

Dubin, M. and C. W. McCracken, 1962: Measurements of distributions of interplanetary dust. Astron. J., 67, 248-256.

Elterman, L., 1954: Seasonal trends of temperature, density and pressure in the stratosphere obtained with the searchlight probing technique. Air Force Cambridge Research Center, Cambridge, Mass., Geophysical Research Paper No. 29.

Elterman, L., 1966: Aerosol measurements in the troposphere and stratosphere. Appl. Opt., 5, 1769-1775.

Elterman, L. and A. B. Campbell, 1964: Atmospheric aerosol observations with searchlight probing. J. Atmos. Sci., 21, 457-458.

Fiocco, G. and G. Colombo, 1964: Optical radar results and meteoric fragmentation. J. Geophys. Res., 69, 1795-1803.

Fiocco, G. and G. Grams, 1964: Observations of the aerosol layer at 20 km by optical radar. J. Atmos. Sci., 21, 323-324.

Fiocco, G. and G. Grams, 1966: Observations of the upper atmosphere by optical radar in Alaska and Sweden during the summer 1964. Tellus, XVIII, 34-38, (Available from Defense Documentation Center, AD 643 006).

Fiocco, G. and L. D. Smullin, 1963: Detection of scattering layers in the upper atmosphere (60-140 km) by optical radar. Nature 199, 1275.

Friedland, S. S., J. Katzenstein and M. R. Zatzick, 1956: Pulsed searchlighting the atmosphere. J. Geophys. Res., 61, 415-434.

Friend, J. P., 1966: Properties of the stratospheric aerosol. Tellus, XVIII, 465-473.

Gadsden, M., 1966: Sodium in the upper atmosphere: meteoric origin. J. Atmos. Terr. Phys., 30, 151-161.

Giese, R. H., 1959: Lichtstreuung an spharischen metallpartikeln, Z. Naturforsch., 14, 12.

Goyer, G. G. and R. D. Watson, 1968: Laser techniques for observing the upper atmosphere. Bull. Amer. Meteor. Soc., 49, 890-895.

Grams, G. and G. Fiocco, 1967: Stratospheric aerosol layer during 1964 and 1965. J. Geophys. Res., 72. 3523-3542.

Greenman, N. N. and C. B. Gilpin, 1965: Electron diffraction control studies of Venus Flytrap particles. Proc. of the Symposium on Meteor Orbits and Dust, Smithsonian Contr. Astrophys., 11, 285-291.

Gruner, P. and H. Kleinert, 1927: Die dammerungserscheinungen, Probleme der Kosmischen Physik, 10, Henri Grand, Hamburg.

Hall, Jr., F. F., 1968: A physical model of cirrus 8-13-μ infrared radiance. Appl. Opt., 7, 2264-2269.

Junge, C. E., 1961: Vertical profiles of condensation nuclei in the stratosphere. J. Meteor., 18, 501.

Junge, C. E. and J. E. Manson, 1961: Stratospheric aerosol studies. J. Geophys. Res., 66, 2163.

Kent, G. S., B. R. Clemesha and R. W. Wright, 1967: High altitude atmospheric scattering of light from a laser beam. J. Atmos. Terr. Phys., 29, 169-181.

Kent, G. S., B. R. Clemesha and R. W. Wright, 1967a: Laser radar for atmospheric studies. J. Appl. Meteor., 6, 386-395.

McCormick, M. P., 1967: Laser backscatter measurements of the lower atmosphere. Ph.D. thesis, College of William and Mary (available from University Microfilms, Inc., Ann Arbor, Mich., # 68-810).

McCormick, M. P., J. D. Lawrence, Jr. and F. R. Crownfield, Jr., 1968: Mie total and differential backscattering cross sections at laser wavelengths for Junge aerosol models. Appl. Opt., 7, 2424-2425.

McCormick, P. D., 1968: Optical radar measurements of atmospheric backscattering. Ph.D. thesis, University of Maryland (available from University Microfilms, Inc., Ann Arbor, Mich., # 69-2230).

McCormick, P. D., S. K. Poultney, U. Van Wijk, C. O. Alley, R. T. Bettinger and J. A. Perschy, 1966: Backscattering from the

upper atmosphere (75-160 km) detected by optical radar. Nature, 209, 798-799.

Mie, G. 1908: Beitrage zur optik truber medien speziell Kollidaler metallosungen. Ann. Physik, 25, 377.

Mikirov, A., 1963: Average particle size at heights of 70 to 450 km. Space Research III, W. Priester, ed., Amsterdam, North-Holland Publ. Co., 155.

Newkirk, Jr., G. and J. A. Eddy, 1964: Light scattering by particles in the upper atmosphere. J. Atmos. Sci., 21, 35-59.

Penndorf, R., 1961: Research on aerosol scattering in the infrared, Sci. Rept. 5, Atlas of scattering diagrams for n = 1.33, AFCRL - 1044, Tech. Rept. RAD-TR-61-32.

Penndorf, R., 1962: Research on aerosol scattering in the infrared, Sci. Rept. 10, Atlas of scattering diagrams for n = 1.5, AFCRL - 62-1131, Tech. Rept. RAD-TR-63-9.

Ratcliffe, J. A., 1960: Physics of the upper atmosphere. New York, Academic Press.

Rosen, J. M., 1964: The vertical distribution of dust to 30 km. J. Geophys. Res., 69, 4673-4676.

Rosen, J. M. 1966: Correlation of dust and ozone in the stratosphere. Nature, 209, 1342-1342.

Rosen, J. M., 1967: Simultaneous dust and ozone soundings over North and Central America, (Available from Defense Documentation Center, AD 658 546).

Rosen, J. M., 1969: Private communication.

Rosen, J. M. and E. P. Ney, 1965: Vertical distribution of dust in the stratosphere. Proc. of the Symposium on Meteor Orbits and Dust, Smithsonian Contr. Astrophys., 11, 345-347.

Rosenberg, G. V., 1960: Light scattering in the earth's atmosphere. Soviet Physics Uspekhi, 3, 346.

Sandford, M. C. W., 1967: Laser scatter measurements in the mesosphere and above. J. Atmos. Terr. Phys., 29, 1657-1662.

Sandford, M. C. W., 1967a: Optical radar performance in atmospheric scattering. J. Atmos. Terr. Phys., 29, 1651-1656.

Soberman, R. K., 1965: Extraterrestrial dust concentrations in the upper atmosphere. Proc. of the Symposium on Meteor Orbits and Dust, Smithsonian Contr. Astrophys., 11, 323-331.

Synge, E. H., 1930: A method of investigating the higher atmosphere. Phil. Mag., 9, 1014.

Twomey, S., and G. T. Severynse, 1964: Size distributions of natural aerosols below 0.1 micron. J. Atmos. Sci., 21, 558-564.

U. S. Standard Atmosphere, 1962. Washington, D. C., U. S. Government Printing Office.

U. S. Standard Atmosphere Supplements, 1966. Washington, D. C., U. S. Government Printing Office.

Van de Hulst, H. C., 1957: Light scattering by small particles. New York, John Wiley and Sons, Inc.

de Vaucouleurs, G., 1951: Ann. Phys., 6, 211.

Volz, F. E. and R. M. Goody, 1962: The intensity of the twilight and upper atmospheric dust. J. Atmos. Sci., 19, 385-406.

Weickmann, H., 1949: Ber. Deut. Wetter. U. S. Zone 6, 61.

Whipple, F.L., 1961: The dust cloud about the earth. Nature, 189, 127-128.